Fakultät für Medizin

Klinik und Poliklinik für Chirurgie

Transcriptional and functional characterization of the first neuro-invasive, genetically engineered mouse model of pancreatic cancer

Dr. med. Ihsan Ekin Demir

Vollständiger Abdruck der von der Fakultät für Medizin der Technischen Universität München zur Erlangung des akademischen Grades eines

Doctor of Philosophy (Ph.D.)

genehmigten Dissertation.

Vorsitzender: Univ.-Prof. Dr. Roland M. Schmid

Betreuer: Priv.-Doz. Dr. Güralp O. Ceyhan

Prüfer der Dissertation:

1. apl. Prof. Dr. Hana Algül

2. Univ.-Prof. Dr. Mathias Heikenwälder

3. Prof. Dr. Karl-Herbert Schäfer

Die Dissertation wurde am 01.07.2015 bei der Fakultät für Medizin der Technischen Universität München eingereicht und durch die Fakultät für Medizin am 08.12.2015 angenommen.

Dedicated to all the patients whom we could not save in the past years.

I wanted very much to learn to draw, for a reason that I kept to myself: I wanted to convey an emotion I have about the beauty of the world. *It's difficult to describe because it's an emotion. It's analogous to the feeling one has in religion that has to do with a god that controls everything in the whole universe: there's a generality aspect that you feel when you think about how things that appear so different and behave so differently are all run "behind the scenes" by the same organization, the same physical laws. It's an appreciation of the mathematical beauty of nature, of how she works inside; a realization that the phenomena we see result from the complexity of the inner workings between atoms; a feeling of how dramatic and wonderful it is.* ***It's a feeling of awe — of scientific awe — which I felt could be communicated through a drawing to someone who had also had this emotion. It could remind him, for a moment, of this feeling about the glories of the universe.***

Richard Feynman

from: Surely You're Joking, Mr. Feynman! (1985), Part 5: "The World of One Physicist", "But Is It Art?", p. 261.

Table of Contents

Declaration on publication

Part of the results presented in this dissertation have been published as follows:

Demir IE, Boldis A, Pfitzinger PL, Teller S, Brunner E, Klose N, Kehl T, Maak M, Lesina M, Laschinger M, Janssen KP, Algül H, Friess H, Ceyhan GO.

Investigation of Schwann cells at neoplastic cell sites before the onset of cancer invasion.

J Natl Cancer Inst. 2014 Aug 8;106(8). pii: dju184. doi: 10.1093/jnci/dju184. Print 2014 Aug.

Introduction

Pancreatic cancer: clinical impact and management

Pancreatic ductal adenocarcinoma (PDAC), or commonly termed as “pancreatic cancer” (PCa), is widely perceived as one of the most lethal human malignancies and described by many newly diagnosed patients as a “sentence to death”. Apart from its frequent current coverage in popular media, what accounts for this dramatic perception of PDAC is its high lethality, the (near-)impossibility of early diagnosis, and its despite-all-relentless-efforts unchanging dismal prognosis. The number of annual deaths due to PDAC continues to equal the number of annual new PDAC cases (~40,000 in the USA), and the 5-year overall survival rate is reported to be around 3-5%, with only 20% of patients diagnosed at a surgically resectable, i.e. potentially curable stage (Hidalgo, 2010) (Figure 1). PDAC continues to rank fourth among the cancer-associated deaths in the USA, and a discomforting observation that emerged out of retrospective studies is that the increase in PDAC incidence (44%) in the past 10 years even surpasses the increase in overall cancer incidence (21%) in the USA (Siegel et al., 2014).

No single symptom can be regarded as specific for PDAC, but the most common symptoms include abdominal pain, jaundice, weight loss and new-onset diabetes mellitus (DiMagno et al., 1999). From these, abdominal pain was reported to be the most frequent symptom (80% of cases) and to be present in the majority (80-85%) of patients with unresectable or locally advanced tumors (DiMagno et al., 1999) (Figure 1). Consequently, efforts toward palliation of PDAC-associated pain include both medication-based and interventional strategies, but the success of such procedures like endoscopic or percutaneous celiac plexus blockade seems to be short-lived and limited (Wong et al., 2004; McGreevy et al., 2013).

The diagnosis of PDAC is currently made by a combination of modern imaging and endoscopic procedures. Triple-phase multidetector computed tomography (MD-CT), contrast-enhanced magnetic resonance imaging (MRI) in combination with MR-cholangio-pancreatography (MRCP), or endoscopic ultrasonography (EUS) represent three modalities with comparable diagnostic strength, and their different combinations with nuclear imaging, e.g. 18F-Desoxyglucose (FDG) positron emission tomography (PET) are currently tested for their ability to improve diagnostic accuracy (Ergul et al., 2014). There are further intensive efforts to identify novel biomarkers of PDAC, since the only and currently most widely used serum marker is carbohydrate antigen 19-9 (CA19-9), with a sensitivity and specificity of 79–81% and 82–90% respectively for the diagnosis of symptomatic PDAC (Ballehaninna et al., 2011) (Figure 1). Remarkably, CA19-9 has been repeatedly shown to predict the therapy response and prognosis after neoadjuvant therapy or in advanced disease (Bauer et al., 2013; Kobayashi et al., 2014).

In cases without diagnostic evidence for metastases or for a locally advanced disease with infiltration of peripancreatic major arteries, the immediate therapeutic measure is surgical exploration with the intention to resect the primary tumor (DiMagno et al., 1999). Depending on the localization of the tumor, the type of operation would be classical or pylorus-preserving (pp) pancreaticoduodenectomy (Whipple's operation) for pancreatic head tumors, total pancreatectomy for tumors of the body, and distal pancreatectomy for tail tumors. Despite advances in imaging, 10-15% of patients without preoperative evidence for metastatic disease are found to bear hepatic or peritoneal metastases intraoperatively (Warshaw et al., 1990; DiMagno et al., 1999). The surgical management of PDAC has made significant advances in the past decade, owing to the increasing number of randomized

controlled trials and large retrospective analyses. After surgical resection, the 5-year survival rate for PDAC was reported to be around 20-25%, corresponding to a median survival of 15 to 23 months (Neoptolemos et al., 2010; Lopez et al., 2014). Seeing this modest increase in long-term survival, surgeons intensively weighed the benefits and risks of extended resections within clinical trials to determine the rational boundaries of PDAC surgery. Currently, increasing age or tumor size *per se* is not considered as contraindication to surgery for resectable tumors. Similarly, evidence of invasion of veins (like portal or superior mesenteric vein) or neighboring (not distant) organs does not count as contraindications (Hartwig et al., 2009; Hartwig et al., 2014; Kanda et al., 2014), whereas visible infiltration of peripancreatic arteries (e.g. superior mesenteric artery, celiac trunk) is increasingly declared as contraindications, not due to technical reasons, but due to the more frequently observed postoperative complications and due to the absence of prognostic improvement (Bockhorn et al., 2014). These technical considerations, but also the propensity of PDAC to grow along the vessels and nerves around the pancreas, have sparked numerous recent studies that tested the effect of neoadjuvant, i.e. preoperative, chemotherapy or chemoradiotherapy in locally advanced, non-metastatic PDAC. The collective results from such studies that demonstrated encouraging results for novel regimens such as FOLFIRINOX (combination of 5-fluorouracil, leucovorin, irinotecan, and oxaliplatin) (Conroy et al., 2011) suggest that the resection and survival rates achieved after such a neoadjuvant approach very much resemble those after primary tumor resection (Gillen et al., 2010) (Figure 1). Therefore, the current trend in the preoperative management of locally advanced PDAC is toward comparison of different neoadjuvant radio-/chemotherapy regimens within randomized controlled trials (Katz et al., 2013). For the postoperative (adjuvant) therapy, based on the survival benefit that was shown in large multicenter

European trials (20 months with versus 14 months median survival without), adjuvant chemotherapy with nucleoside analogues 5-fluorouracil or gemcitabine is standard treatment (Neoptolemos et al., 2001).

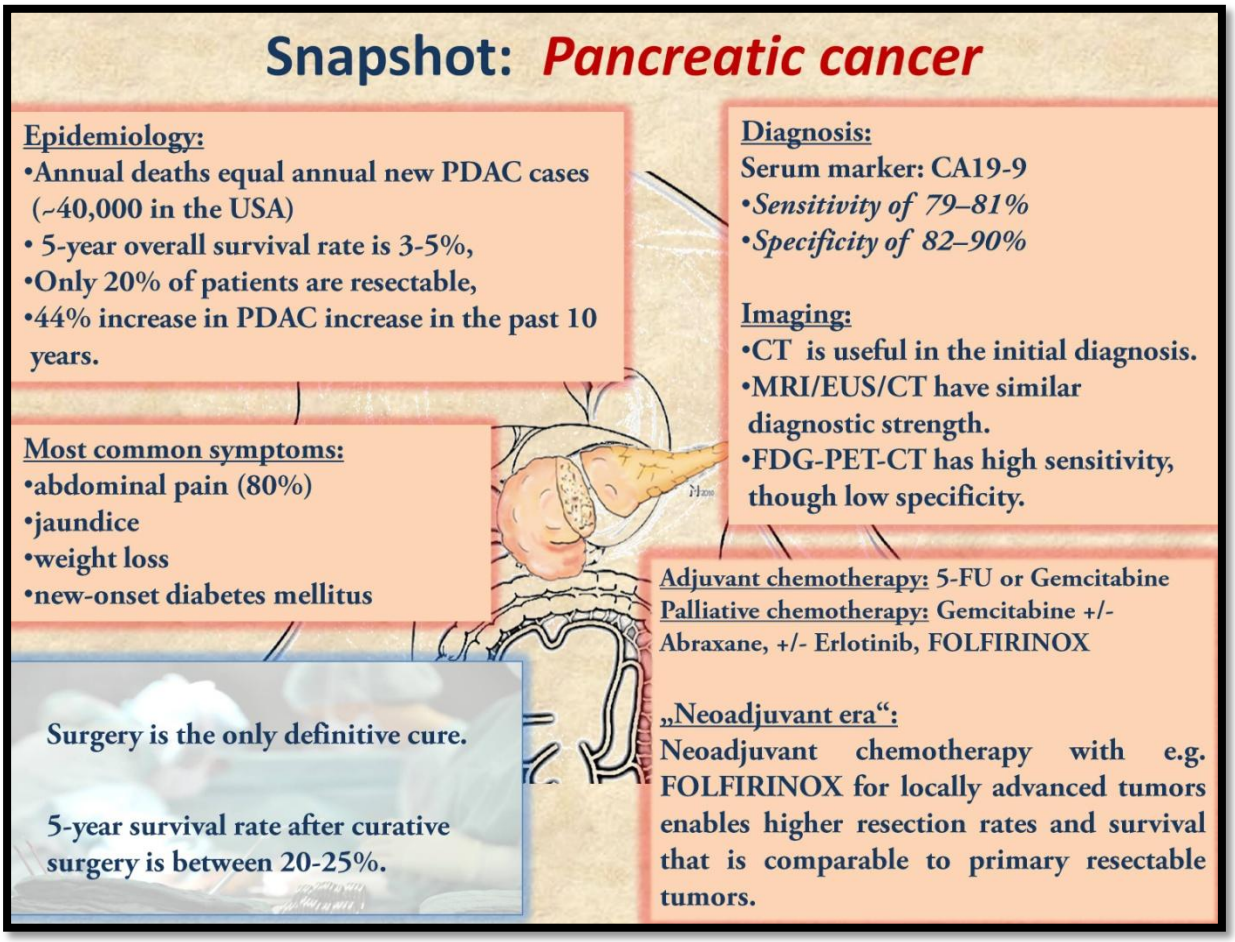

Figure 1. The defining features of human pancreatic cancer (PDAC) from a clinical perspective. CA19-9: carbohydrate antigen 19-9. EUS: endosonography.

Genetics of pancreatic cancer

Like every other cancer, PDAC is characterized by genomic instability, and the evolution of the disease is dictated by either inherited or acquired mutations. In the progression model of PDAC, there is an accumulation of mutations in common genes, which gradually increase in number during the transition from the low-grade pancreatic intraepithelial neoplasia (PanIN) to higher grade PanIN lesions and overt

cancer (Figure 2) (Makohon-Moore et al., 2013). Among the acquired mutations that give rise to sporadic PDAC, the four genes that harbor the highest frequency of mutations are

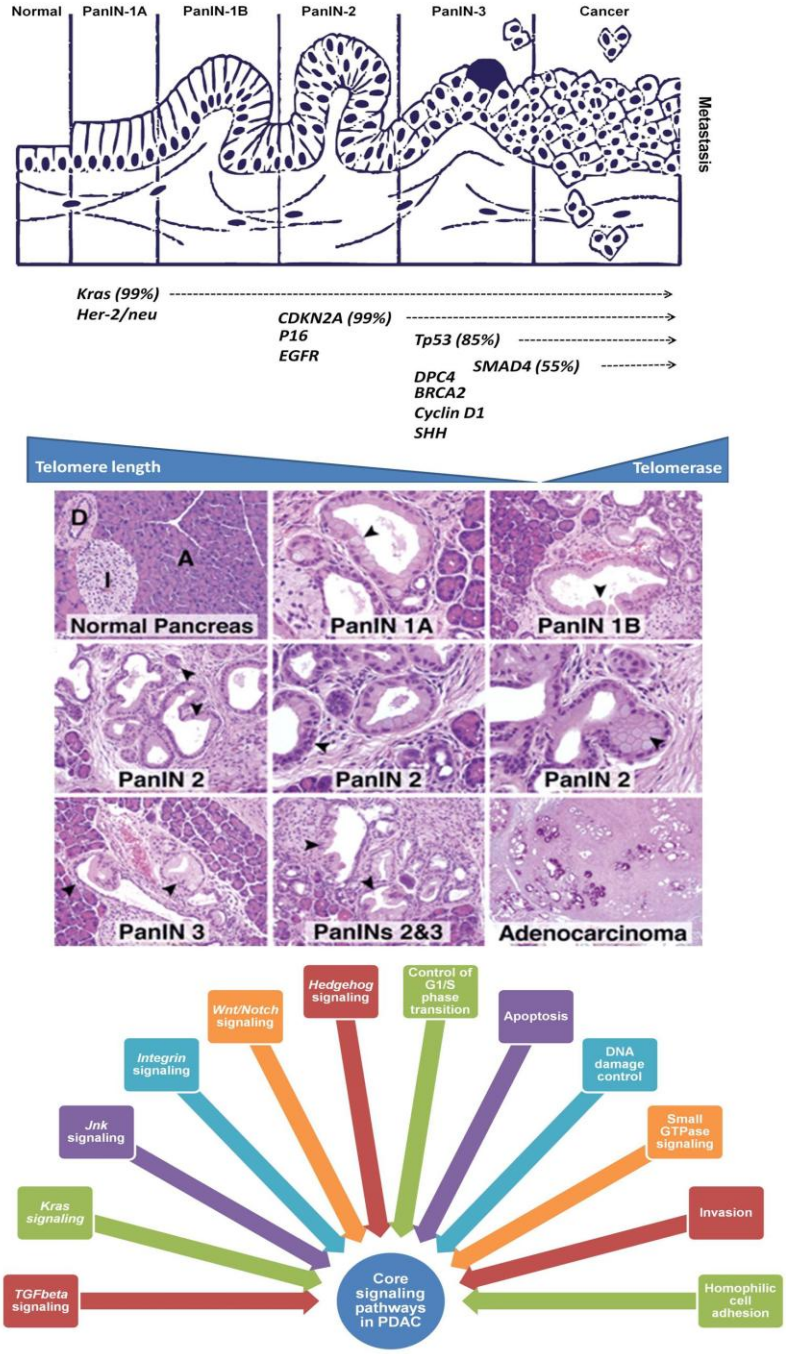

Figure 2. PanIN progression model of PDAC and its relation to genetic alterations. *Upper panel:* Emergence of invasive PDAC from the normal epithelium over PanIN lesions relies on sequential accumulatlon of mutations in PDAC-driving genes. The frequency of the respectable mutations is indicated within parentheses. *Middle panel:* Oncogenic *Kras*-based GEMM of PDAC exhibit all the PanIN stages that are typical for human PDAC. Arrowheads point to the PanIN lesions (from: http://www.jimmunol.org/content/181/5/3116/F2.expansion.html, (Tinder et al., 2008). *Lower panel:* A comprehensive analysis of PDAC-associated genetic alterations by Jones et al. identified the core signaling pathways that were detected to be altered in human PDAC (Jones et al., 2008). Genes belonging to these families represent important targets for developing genetic therapies for GEMM.

Kras, CDKN2A (p16, cyclin-dependent kinase inhibitor 2A gene), Trp53 and SMAD4 (Iacobuzio-Donahue et al., 2012) (Table 1). These four genes are accordingly termed the “driver genes” of PDAC. The most common mutations in PDAC involve point

	Genes	Full name	Known function(s)	Location	Effect	Prevalence	Other cancers	Inherited syndrome	Est. rel. risk
Somatic DRIVER MUTATIONS	*KRAS*	v-Ki-ras2 Kirsten rat sarcoma viral oncogene homolog	GDP/GTP binding proteins, proliferation, survival, others	12p12.1	Act	90-95%	Bladder, breast, leukemia, and lung	Cardiofaciocutaneous syndrome	
	CDKN2A (p16)	Cyclin-dependent kinase inhibitor 2A	Cell cycle	9p21.3	In	90%	Melanoma	FAMMM	20-34x
	TP53	Tumor protein p53	Cell cycle, apoptosis, DNA repair, others	17p13.1	In	75%	Breast, colorectal, hepatocellular, others	Li-Fraumeni syndrome	
	SMAD4/DPC4	SMAD family member 4	TGF-β signaling, BMP signaling, development, proliferation, others	18q21.2	In	55%	Colorectal	Juvenile polyposis syndrome, Myhre syndrome	
Somatic mutations	*TGFBR1,2*	Transforming growth factor, beta receptor 1, 2	TGF-β signaling, development, proliferation, others	9q22.33, 3p24.1	In	5-10%	Colorectal, esophageal	Loeys-Dietz syndrome	
	ACVR1B	Activin A receptor, type IB	TGF-β signaling, development, proliferation, others	12q13.13	In	5-10%	Unknown	Unknown	
	MKK4	Mitogen-activated protein kinase kinase 4	Cell stress, JNK signaling	17p12	In	5-10%	Unknown	Unknown	
	MLL3	Myeloid/lymphoid or mixed-lineage leukemia 3	Chromatin remodeling, transcription	7q36.1	In	<10%	Breast, colorectal, and leukemia		
	ARID1A/B	AT-rich interaction domain-containing protein 1A/B	Chromatin remodeling, transcription	1p36.11, 6q25.3	In	<10%	Breast, ovary and liver	Coffin-Siris syndrome	
	PBRM1	Polybromo 1	Chromatin remodeling, transcription	3p21.1	In	<10%	Kidney		
	SMARCA4	Swi/Snf-related, matrix associated, actin-dependent regulator of chromatin, subfamily A, member 4	Chromatin remodeling, transcription	19p13.2	In	<10%	Lung	Coffin-Siris syndrome, rhaboid tumor predisposition syndrome	
Familial /inherited / germline mutations	*BRCA1, BRCA2*	Breast cancer 1, early onset, breast cancer 2, early onset	DNA repair, cell cycle, genome stability	17q21.31, 13q13.1	In	<10%	Breast, ovary and prostate	Breast cancer	3.5-10x, 2x
	PALB2, ATM, others	Partner and localizer of BRCA2, Ataxia telangiectasia mutated	DNA repair, cell cycle, genome stability	7q34	In	<10%	Unknown	Familial pancreatic cancer[¥]	32x (overall)
	PRSS1	Protease, serine, 1 (trypsin 1)	Cell metabolism and signaling	19p13.3	In	<10%	None	Familial pancreatitis	50-80x
	STK11/LKB1	Serine/threonine kinase 11	p53 signaling, DNA repair, apoptosis	3p22.2, 2p21	In	<10%	Breast, colorectal, gastroesophageal, and small bowel	Peutz-Jeghers syndrome	132x
	hMLH1, hMSH2, others	MutL Homolog 1, colon cancer, nonpolyposis type 2 (I), mutS homolog 2, colon cancer, nonpolyposis type 1 (I)	DNA mismatch repair	9q22.32, 9p13.3	In	<10%	Biliary tract, brain, colorectal, endometrial, ovarian, stomach, ureter and renal pelvis	HNPCC	
	FANC-C, FANC-G	Fanconi anemia, complementation group C, Fanconi anemia, complementation group G	DNA stability and repair	9q22, 9p13	In	<10%	Unknown	Young-age-onset pancreatic cancer	

Table 1. Overview of the sporadic and inherited genetic mutations that are inherent to human PDAC. Act: activation, In: inactivating. Est. rel. risk; estimated relative risk. Adapted from: (Makohon-Moore et al., 2013).

mutations of the Kras (v-Ki-ras2 Kirsten rat sarcoma viral oncogene homolog) at the codons 12, 13, or 61 (Makohon-Moore et al., 2013). As a result, the coded GTPase is constitutively active and leads to the activation of downstream effectors of receptor

tyrosine kinases like the RAF–mitogen-activated protein kinase (MAPK) pathway and the phosphoinositide 3-kinase pathway (Makohon-Moore et al., 2013). Kras mutations have been reported to be present in around 95% of PDAC cases, in 35% of PanIN-1 lesions (Delpu et al., 2011) and in 75% of PanIN-3 lesions (Delpu et al., 2011). CDKN2A as a cyclin-dependent kinase inhibitor controls the G1-S transition in the cell cycle; its loss results in uncontrolled cell cycle progression (Makohon-Moore et al., 2013). Mutations of CDKN2A lead to its inactivation and occur as part of allelic loss, homozygous deletion, or hypermethylation (Makohon-Moore et al., 2013). Mutations of the tumor protein p53 (Trp53) occur in up to 75% of PDAC cases, usually as a point mutation or small intragenic deletion (Barton et al., 1991; Redston et al., 1994). Furthermore, mutations in SMAD4 (DPC4, SMAD family member 4 gene) gene, which encodes a transcription factor related to transforming growth factor-β (TGF-β) and bone morphogenetic protein (BMP) signaling, are a late event during PanIN progression and are typically found from PanIN-3-stage onwards (Makohon-Moore et al., 2013). SMAD4 mutations are found in ca. 55% of PDAC cases (Hahn et al., 1996). Further genes that are found to be mutated in lower frequencies (i.e. <10% of cases) are listed on Table 1. Beyond acquired somatic mutations, there is a group of genes that harbor low-frequency “germline” mutations and are therefore associated with familial PDAC. Patients with Peutz-Jeghers syndrome carry germline mutations in the liver kinase B1 gene (LKB19) and have greater than 100-fold risk of developing PDAC (Hruban et al., 2010). Although best characterized in the context of increased risk for ovarian and breast cancer, BRCA2 mutations are also associated with a 3.5 to 10-fold increased risk for PDAC (Goggins et al., 1996). Furthermore, mutations in the ATM (Ataxia teleangiectasia mutated) gene have been described in subsets of familial PDAC cases (Roberts et al., 2012).

In an effort to comprehensively characterize PDAC-associated genetic alterations, Jones et al. sequenced 23,219 transcripts, representing 20,661 protein-coding genes, in 24 PDAC samples and searched for homozygous deletions and amplifications in the tumor DNA by using microarrays containing probes for single-nucleotide polymorphisms (SNP) (Jones et al., 2008). Here, they found that PDAC contains an average of 63 genetic alterations, and the majority of these were point mutations (Jones et al., 2008). In this study, they could detect previously unknown mutations in genes associated with chromatin remodeling (*ARID1A* and *MLL3*). In a subsequent study of the same group, they performed whole-exome sequencing of germline DNA to differentiate between somatic and germline mutations in PDAC. Here, they could identify a germline *PALB2* gene mutation coupled with a second hit to the *PALB2* gene in the cancer DNA (Jones et al., 2009). In a validation set of 96 familial PDAC patients, they detected three additional germline *PALB2* mutations. Importantly, this subset of PDAC patients was postulated to be more sensitive to chemotherapy with mitomycin C (Jones et al., 2009). One important contribution of the studies by Jones et al. was the classification of gene alterations in PDAC into 12 different core signaling pathways including those related to apoptosis, DNA damage control, GTPase signaling, invasion, cell adhesion, integrin signaling, etc. (Figure 2) (Jones et al., 2008). In a more comprehensive whole-exome sequencing study in combination with copy number analysis in 99 PDAC cases, Biankin et al. could additionally identify many genetic alterations in genes encoding axon guidance molecules such as Slit and Robo (Biankin et al., 2012). Recently, *in vivo* mutagenesis screens revealed several PDAC candidate genes in murine PDAC that will be of interest for further analyses in human PDAC (Rad et al., 2015). In this context, Mann et al. performed Sleeping-beauty-transposon based mutagenesis in combination with mutant Kras in a mouse model of PDAC to induce metastatic PDAC (Mann et al.,

2012). This way, they could identify 543 candidate cancer genes (CCGs), from which 75 (like Mll3 and Ptk2) belonged to known mutations in human PDAC (Mann et al., 2012). From the identified mutations, 10% were involved in chromatin remodeling (such as Arid4b, Kdm6a, and Nsd3 mutations), and mutations in the Ctnnd1, Fbxo11, and Vgll4 genes were also significantly associated with poor patient survival. Therefore, the application of next generation sequencing together with in vivo mutagenesis screens have enabled the rapid identification of genetic alterations both in sporadic and familial PDAC (Mann et al., 2012). These genetic alterations reveal the presence of common genetic alterations in a large portion of PDAC cases that can be remodeled in murine PDAC models. On the other hand, owing to these sequencing and mutagenesis technologies, altered common pathways that can be effectively targeted are identified and can be further evaluated in translational studies.

Genetically engineered mouse models of PDAC

The knowledge on the driver genes and accumulating mutations during the progression of PDAC precursor lesions, i.e. via the emergence of acinar-ductal-metaplasia (ADM) and the progression of PanIN lesions, sparked efforts to simulate pancreatic carcinogenesis in genetically engineered mouse models (GEMM) of PDAC. As a basic principle, these models are grounded on 1) the transgenic expression of trophic factors under the control of pancreas-specific gene promoters, or 2) on the activation of the most common mutation in PDAC, the mutated oncogenic Kras, in cyclic recombinase/Cre-loxP-based recombination models via the expression of the Cre under the control of pancreas-specific promoters (Figure 3). Furthermore, another distinguishing feature of these models lies in the start of the

expression of mutant Kras either in the prenatal, or in the postnatal period within “inducible” models.

In the earliest and only purely transgenic model of PDAC, Sandgren et al. described mice that express the epidermal growth factor receptor (EGFR) ligand transforming growth factor alpha (TGFalpha) under the control of the acinar elastase promoter (Ela-TGFalpha mice) (Sandgren et al., 1990) (Table 2). These mice developed widespread ADM and carcinoma in situ. In a later study, Wagner et al. showed that these ADM lesions (termed tubular complexes in the original study) had increased ERK-phosphorylation and exhibited higher levels of GTP-loaded active Ras in the pancreas, suggesting enhanced Ras/Erk1/2 signaling in these preneoplastic cells (Wagner et al., 2001). Although these cells had higher levels of cyclin D1 and cyclin-dependent-kinase 4 (Cdk4), they did not incorporate BrdU, suggesting increased progression of these cells through the G1, but not S phase of the cell cycle. In parallel to this oncogenic signaling, these cells exhibited elevated expression of the cell cycle inhibitory, tumor-suppressive molecules $p21^{Cip1}$ and p53, but not of $p16^{Ink4a}$ and $p19^{Arf}$ (Wagner et al., 2001). In the subsequent step, when Ela-TGFalpha mice were crossed to $p53^{-/-}$ mice, the investigators observed a rapid progression to invasive cancer (Wagner et al., 2001): Whereas only 29% of Ela-TGFalpha transgenic mice developed PDAC with a mean tumor-free survival of 410 days, Ela-TGFalpha;$p53^{+/-}$ mice had a 77.3% PDAC incidence and a decreased mean tumor-free survival of 220 days, and Ela-TGFalpha/$p53^{-/-}$ mice (termed “TPC” mice) developed PDAC within 120 days after birth with a 100% penetrance (Wagner et al., 2001). In a significant portion of the heterozygous Ela-TGFalpha;$p53^{+/-}$ mice, the wild-type p53 allele was segregated in all mice that eventually developed PDAC, and these mice also exhibited homozygous deletions of the Ink4a/Arf and Smad4 genes (Wagner et al., 2001). Despite the merely transgenic trait of this model, the

Ela-TGFalpha mouse model of PDAC, especially when crossed to p53-null mice, successfully reproduced the increased Ras activity, cell cyle progression, the ductal metaplasia, and the emergence of invasive cancer seen in PDAC (Wagner et al., 2001).

The following and current generation of GEMM of PDAC has its origins in the studies that created heterozygous knock-in allele of a conditional mutated Kras insert ($Kras^{G12D}$) silenced by a floxed STOP transcriptional cassette (LSL-$Kras^{G12D}$) at the endogenous locus (Figure 3). When these mice were crossed to mice expressing Cre under the control of the promoters of pancreas-specific genes that arise around the embryonic day 8 to 9 (i.e. Pdx1/Ipf1 or p48/Ptf1), the mutated active oncogene exerts its effects after Cre-mediated excision of the STOP cassette (Figure 3). The obtained mouse model, i.e. Pdx1-Cre;LSL-$Kras^{G12D}$ or p48-Cre;LSL-$Kras^{G12D}$, ("KC" mice) was the first GEMM that was reported to develop the full spectrum of PanIN lesions of all grades (Table 2) (Hingorani et al., 2003). Looking at the temporal development, the proportion of non-neoplastic normal ducts was >80% at 2.25 months, around 68% at 4.5 months and less than 18% at 7-10 months of age. At this advanced age, the majority of PanINs were low-grade (1A and 1B) lesions (65%), but there was a considerable portion of grade 2 lesions (16%) and few PanIN-3 lesions (Hingorani et al., 2003). At molecular level, PanINs were observed to upregulate Notch signaling, the cytoplasmic expression of Hes1, cyclooxygenase-2 and matrix metalloproteinase-7 (MMP-7). In the first study that described this model the authors also observed progression of PanINs to invasive, metastastic cancer in 2 out of 29 animals (one Pdx-1-Cre;LSL-$Kras^{G12D}$ at the age of 6.25 months, one Ptf1a/p48-Cre;LSL-$Kras^{G12D}$ mouse at the age of 8.25 months) (Hingorani et al., 2003). A large number of studies could demonstrate the rapid progression from PanIN to PDAC in additional GEMM in which the KC mice were crossed to mice lacking important tumor suppressors that

are found to be deleted in sporadic PDAC (e.g. 1) Ink4A/Arf$^{lox/lox}$, 2) Tp53$^{\Delta/\Delta}$ or Trp53$^{R172H/+}$ (Ptf1a/p48-Cre;LSL-Kras^{G12D};Tp53$^{\Delta/\Delta}$ or Trp53$^{R172H/+}$, termed “KPC”, 3) Smad4, 4) TGFbetaIIR) or in familial PDAC (BRCA$^{Tr/delta11}$, Lkb1 $^{lox/lox}$) (Table 3) (Herreros-Villanueva et al., 2012; Guerra et al., 2013).

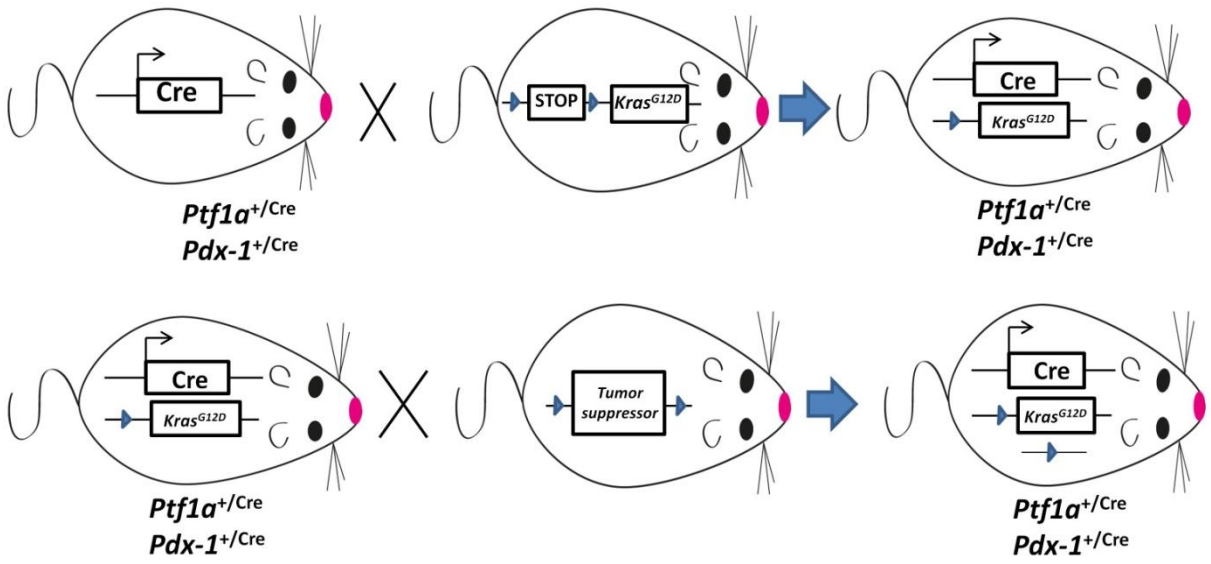

Figure 3. Schematic representation of Cre/loxP-based recombination for generation of GEMM of PDAC. Mice expressing cyclic recombinase (Cre) under the control of pancreas-specific promoters like *Ptf1a* or *Pdx1* are crossed to mice bearing a mutated *Kras* allele that contains an upstream, loxP (blue triangles)-flanked STOP cassette. Cre mediates excision of the STOP cassette, resulting in pancreas-specific expression of the mutated *Kras* allele (upper row). Crossing these mice to other strains bearing loxP-flanked tumor suppressor knockin alleles results in mice that rapidly progress to invasive PDAC (lower row).

In the ten years following the study by Hingorani and colleagues on the generation of the KC mice, researchers made use of different promoters to induce PanINs or PDAC. Depending on the time point of Kras^{G12D} activation and temporal induction of the promoter, these models could largely reproduce PanIN generation and progression at varying extent. To reach temporal induction, researchers made use of either tamoxifen-inducible Cre (Cre^{ERT2}) or of tetracycline-inducible (Tet-On/Tet-Off) promoters (Guerra et al., 2013). For example, ablation of Notch1 signaling in Pdx1-Cre;LSL-Kras^{G12D};Notch1$^{lox/lox}$ mice (Hanlon et al., 2010), or Cre-inducible expression of the dominant active form of the GLI2 transcription factor (*CLEG2* transgene), a downstream mediator of the Hedgehog signaling pathway,

were shown to accelerate PanIN development (Pasca di Magliano et al., 2006). Furthermore, targeting of Cre-expression to Mist1-expressing acinar cells (Habbe et al., 2008) or to Nestin-expressing progenitor-like cells in the pancreas also resulted in PanIN development (Carriere et al., 2007).

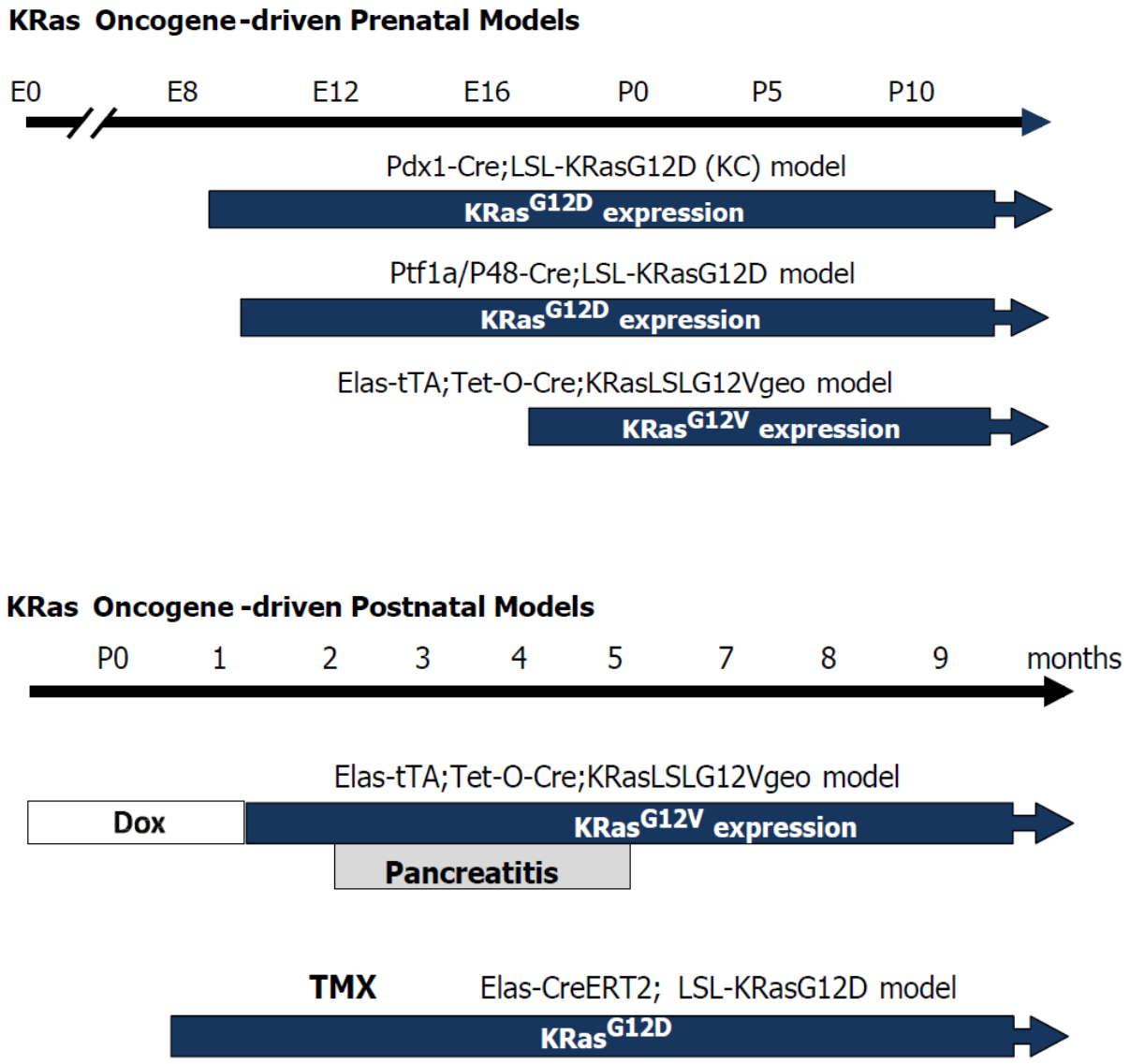

Figure 4. The schematic principle of pre- and postnatal oncogenic Kras induction in GEMM of PDAC. Upper panel: the timing of knocked oncogenic Kras expression in embryonic mouse models of PDAC. Lower panel: Strategies of mutated Kras induction in postnatal models of PDAC. In the Elas-tTA; Tet-O-Cre; $KRas^{LSLG12Vgeo}$ strain, the pregnant mothers and their offspring are exposed to doxycycline (Dox) in the drinking water to inhibit the expression of the KRasG12V oncogene until the age of 8 weeks. These mice do not develop any lesions unless pancreatitis is induced. In the $Elas\text{-}Cre^{ERT2}$; $LSL\text{-}KRas^{G12D}$ model, expression of the endogenous $KRas^{G12D}$ oncogene is induced after exposure to tamoxifen (TMX) that selectively activates the inducible CreERT2 recombinase. E: embryonic, P: postnatal. Adapted from Guerra & Barbacid, Molecular Oncology 2013. (Guerra et al., 2013).

In a tetracycline-inducible system, Guerra et al. observed 90% incidence of PanIN lesions in K-*Ras*$^{+/LSLG12Vgeo}$;*Elas*-tTA/*tetO*-Cre mice in which the tetracycline transactivator binds to the operator sequence upstream of the CMV promoter that drives Cre expression. Addition of tetracycline or derivatives (such as doxycycline) to the drinking water of these animals thus drives Cre expression and excision of the STOP cassette upstream of the mutated Kras allele (Guerra et al., 2007; Guerra et al., 2011) (Figure 4).

An important contribution to our understanding of PanIN and PDAC development in GEMM was the activation of oncogenic Kras in postnatal models. The above mentioned tetracycline-inducible model offered the unique advantage to study the impact of postnatal oncogenic Kras activation on PanIN generation, since human PDAC as an adult disease does not arise from the expression of oncogenic Kras in all acinar cells in the embryonic phase. Here, expression of oncogenic Kras after the age of 60 days, even in the presence of inactivated tumor suppressors like Tp53 or Ink4A/Arf did not lead to PanIN or PDAC development (Guerra et al., 2007). However, when these mice were simultaneously subject to cerulein-induced pancreatitis, they developed PanINs and PDAC with a 100% penetrance (Guerra et al., 2007). In another study, though, by using a tamoxifen-inducible Cre under the control of Elastase- or Mist1-promoter, Habbe et al. observed PanIN formation, but no PDAC in mice at the age of 6 weeks (Table 2) (Habbe et al., 2008). As a common observation, tumor incidence, ADM and PanIN formation decreased with increasing age of mice at the time of induction. In a study on the potential cellular origins of PDAC, expression of KrasG12D in Pdx1-positive cells in the adult mouse, which are a subpopulation of the endocrine (Beta cells) of the pancreas, was shown to give rise to PanIN lesions, yet with decreasing incidence as the age of mice increased (Gidekel Friedlander et al., 2009). Interestingly, although insulin-positive (Rip-

CreER^{TM}) cells were refractory to KrasG12D-dependent transformation even in the absence of p53, additional presence of chronic pancreatitis in these mice induced PanIN and PDAC formation (Gidekel Friedlander et al., 2009). These findings suggested that although insulin-containing endocrine cells of the pancreas are highly refractory to oncogenic transformation, the presence of multiple hits, including pancreatic injury, can trigger their dysplasia and cancer initiation. In a recent study, ablation of the transcription factor Sox9 in acinar cells of *Ptf1a^{CreER};Kras^{G12D};Sox9$^{f/f}$;R26R^{YFP}* mice inhibited KrasG12D-induced transformation and PanIN formation (Kopp et al., 2012). Accordingly, forced expression of Sox9 increased the frequency of PanIN lesions, suggesting a critical role for the induction of Sox9-expression in acinar cells and the subsequent duct-like reprogramming in the generation of PanIN lesions (Kopp et al., 2012).

GEM model	Tumor initiation	Targeted cell type	Lesions (incidence %)			Observations	References
			PanIN	PDAC	MET		
Elastase-TGF-a	Prenatal	Acinar	100	10	No	KrasG12D accelerates progression of mPanIN lesions to PDAC	Wagner et al., 2001
Pdx1-Cre; K-Ras$^{+/LSLG12D}$	Prenatal	Acinar, CAC, ductal, endocrine	100	100	Yes	Impossibility to asses cell of origin	Hingorani et al., 2003
Ptf1a-Cre; K-Ras$^{+/LSLG12D}$	Prenatal	Acinar, CAC, ductal, endocrine	100	100	Yes	Impossibility to asses cell of origin	Hingorani et al., 2003
Elastase-tTA; Tet-O-Cre; K-Ras$^{+/LSLG12Vgeo}$	Prenatal	Acinar	90	10	No	Pancreatitis accelerates PanIN development.	Guerra et al., 2007
Nestin-Cre; K-Ras$^{+/LSLG12D}$	Prenatal	Acinar, acinar precursors	100	No	No	Short survival due to CNS complications. PDAC in the context of pancreatitis.	Carriere et al., 2007
Elastase-tTA; Tet-O-Cre; K-Ras$^{+/LSLG12Vgeo}$ plus caerulein	Postnatal (8 weeks)	Acinar	100	20	No	PanIN development requires pancreatitis.	Guerra et al., 2007
Elastase-CreER; K-Ras$^{+/LSLG12D}$	Postnatal (6 weeks)	Acinar	36	NA	No	Leaky system. Short term study.	De La O et al., 2008
Elastase-CreERT2; K-Ras$^{+/LSLG12D}$	Postnatal (6 weeks)	Acinar	63	No	No	PanIN development does not require pancreatitis.	Habbe et al., 2008
Mist1-CreERT2; K-Ras$^{+/LSLG12D}$	Postnatal (6 weeks)	Acinar	30	No	No	PanIN development does not require pancreatitis.	Habbe et al., 2008
Pdx1-CreER; K-Ras$^{+/LSLG12D}$	Postnatal (8 weeks)	Endocrine	55	Rare	No	The system may target acinar and precursor cells.	Gidekel-Friedlander et al., 2009
proCPA1CreERT2; K-Ras$^{+/LSLG12D}$	Postnatal (3 weeks)	Acinar	10	No	No	PanIN development require pancreatitis in older mice (5e8 weeks): PanIN in 33% mice.	Gidekel-Friedlander et al., 2009
RipCreER; K-Ras$^{+/LSLG12D}$	Postnatal (2e8 weeks)	Insulin expressing cells	0	No	No	Cooperation with pancreatitis	Gidekel-Friedlander et al., 2009

MET (metastasis); NA: not analyzed.

Table 2. Overview of GEMM that develop PanIN lesions. The cell types to which the genetic modifications were targeted were indicated in the column “targeted cell type”. Adapted from Guerra & Barbacid, Molecular Oncology 2013 (Guerra et al., 2013).

GEM model	Lesions	Metastasis	Survival	References
Pdx1-Cre; K-Ras$^{+/LSLG12D}$; Ink4a/Arf$^{lox/lox}$	PanIN and PDAC	Yes	2 m	Aguirre et al., 2003
Pdx1-Cre; K-Ras$^{+/LSLG12D}$; p53$^{R172H/+}$ (KPC)	PanIN and PDAC	Yes	5 m	Hingorani et al., 2005
Pdx1-Cre; K-Ras$^{+/LSLG12D}$; Ink4a/Arf$^{-/-}$	PanIN and PDAC	Yes	5 m	Bardeesy et al., 2006
Pdx1-Cre; K-Ras$^{+/LSLG12D}$; p53$^{lox/lox}$	PanIN and PDAC	No	3 m	Bardeesy et al., 2006
Pdx1-Cre; K-Ras$^{+/LSLG12D}$; p53$^{lox/lox}$; Ink4a/Arf$^{-/-}$	PanIN and PDAC	Yes	2 m	Bardeesy et al., 2006
Pdx1-Cre; K-Ras$^{+/LSLG12D}$; Smad4$^{lox/lox}$	IPMN and PDAC	Yes	9 m	Bardeesy et al., 2006
Ptf1a-Cre; K-Ras$^{+/LSLG12D}$; TGFbIIR$^{lox/lox}$	PanIN and PDAC	Yes	2 m	Ijichi et al., 2006
Elastase-tTA; Tet-O-Cre; K-Ras$^{+/LSLG12Vgeo}$; p53$^{-/-}$	PanIN and PDAC	Yes	3-4 m	Guerra et al., 2007
Ptf1a-Cre; K-Ras$^{+/LSLG12D}$; Elastase-TGF-a	PanIN, IPMN, PDAC	Yes	7 m	Siveke et al., 2007
Ptf1a-Cre; K-Ras$^{+/LSLG12D}$; Smad4$^{lox/lox}$	MCN and PDAC	Yes	8 m	Izeradjene et al., 2007
Pdx1-Cre; K-Ras$^{+/LSLG12D}$; Brca2$^{Tr/D11}$	PanIN and PDAC	NA	NA	Skoulidis et al., 2010
Pdx1-Cre; K-Ras$^{+/LSLG12D}$; p53$^{R270H/+}$; Brca2$^{Tr/þ}$	PanIN and PDAC	NA	<5 m	Skoulidis et al., 2010
Pdx1-Cre; K-Ras$^{+/LSLG12D}$; p53$^{R270H/+}$; Brca2$^{Tr/D11}$	PanIN and PDAC	Yes	2.5 m	Skoulidis et al., 2010
Pdx1-Cre; K-Ras$^{+/LSLG12D}$; Lkb1$^{lox/lox}$	PanIN and PDAC	NA	4.5 m	Morton et al., 2010
Pdx1-Cre; K-Ras$^{+/LSLG12D}$; Notch1$^{lox/lox}$	PanIN (high grade)	No	3 m	Hanlon et al., 2010
Ptf1a-Cre; K-Ras$^{+/LSLG12D}$; Notch2$^{lox/lox}$	MCN, anaplastic, PDAC	No	>12 m	Mazur et al., 2010
Elastase-tTA; Tet-O-Cre; K-Ras$^{+/LSLG12Vgeo}$; p53$^{lox/lox}$	PanIN and PDAC	Yes	3-4 m	Guerra et al., 2011
Elastase-tTA; Tet-O-Cre; K-Ras$^{+/LSLG12Vgeo}$; Ink4a/Arf$^{lox/lox}$	PanIN and PDAC	Yes	3-4 m	Guerra et al., 2011
Pdx1-Cre; K-Ras$^{+/LSLG12D}$; Usp9x$^{þ/lox}$	PanIN and PDAC	NA	NA	Perez-Mancera et al., 2012

m: Months; NA: Not analyzed.

Table 3. Overview of GEMM of PDAC. Adapted from Guerra & Barbacid, Molecular Oncology 2013. (Guerra et al., 2013)

Neuropathy in pancreatic ductal adenocarcinoma

Aside from genetic instability, extensive adaptive alterations in the PDAC microenvironment are another key feature of PDAC biology. In the complex network of multiple cellular actors of the PDAC microenvironment, immune cells were reported to be selectively enriched in the tumor tissue, which is characterized by suppression of $CD8^+$ cytotoxic T lymphocytes and increased infiltration by regulatory T cells (Demir et al., 2013). Cancer-associated myofibroblasts as producers of tumor-associated desmoplasia are widely accepted to modulate tumor growth, with both tumor-growth-promoting (Olive et al., 2009) and -inhibiting (Ozdemir et al., 2014; Rhim et al., 2014) properties reported in the setting of depletion of PDAC-associated myofibroblasts. Pericytes are known to regulate tumor growth in angiogenesis-dependent PDAC subsets over the platelet-derived growth factor (PDGF) signaling (McCarty et al., 2007). The multiple actors of the tumor microenvironment and their modulatory role on tumor growth have been recently and extensively reviewed (Feig

et al., 2012), and there is no doubt on their deciding role on the development and progression of PDAC.

One major actor in the PDAC microenvironment that has not found sufficient resonance in these reviews but is rapidly receiving attention is the nervous system. Nerves have been traditionally and colloquially associated with a potential to impact disease course, e.g. via stress or pain (Demir et al., 2012). However, that the nerves may similarly represent a key microenvironmental factor affecting disease generation and progression is only being recently considered. In PDAC, intrapancreatic nerves undergo prominent plastic alterations, including neural hypertrophy and increased neural density (Figure 5). This hyperinnervation is encountered both within and around the borders of the tumor, and its extent correlates to the severity of pain of PDAC patients (Ceyhan et al., 2009). The exact implication and mechanism behind the generation of these neuroplastic alterations in PDAC remains unclear. Yet numerous expression analyses in PDAC tissues, normal human pancreas, and recent in vitro models showed that neurotrophic factors like nerve growth factor (NGF), glial-cell-derived neurotrophic factor (GDNF) family members GDNF, artemin and neurturin may be key mediators of this process. Furthermore, very recently, other microenvironmental actors like pancreatic stellate cells, especially via the SLIT2/ROBO-signalling, were also reported to mediate the neuroplastic alterations in PDAC (Secq et al., 2015). Interestingly, comparison of patient characteristics with the extent of neuroplasticity in PDAC revealed that the presence of hyperglycemia also correlates to the extent of neuroplastic alterations among PDAC patients (Li et al., 2011). However, mechanistic studies that investigated the impact of high serum glucose levels on the generation of neuroplastic alterations in PDAC are lacking. The time interval for the generation of neuroplasticity in PDAC has only recently been subject to investigation. Here, Stopczynski et al. showed that in the KPC mouse

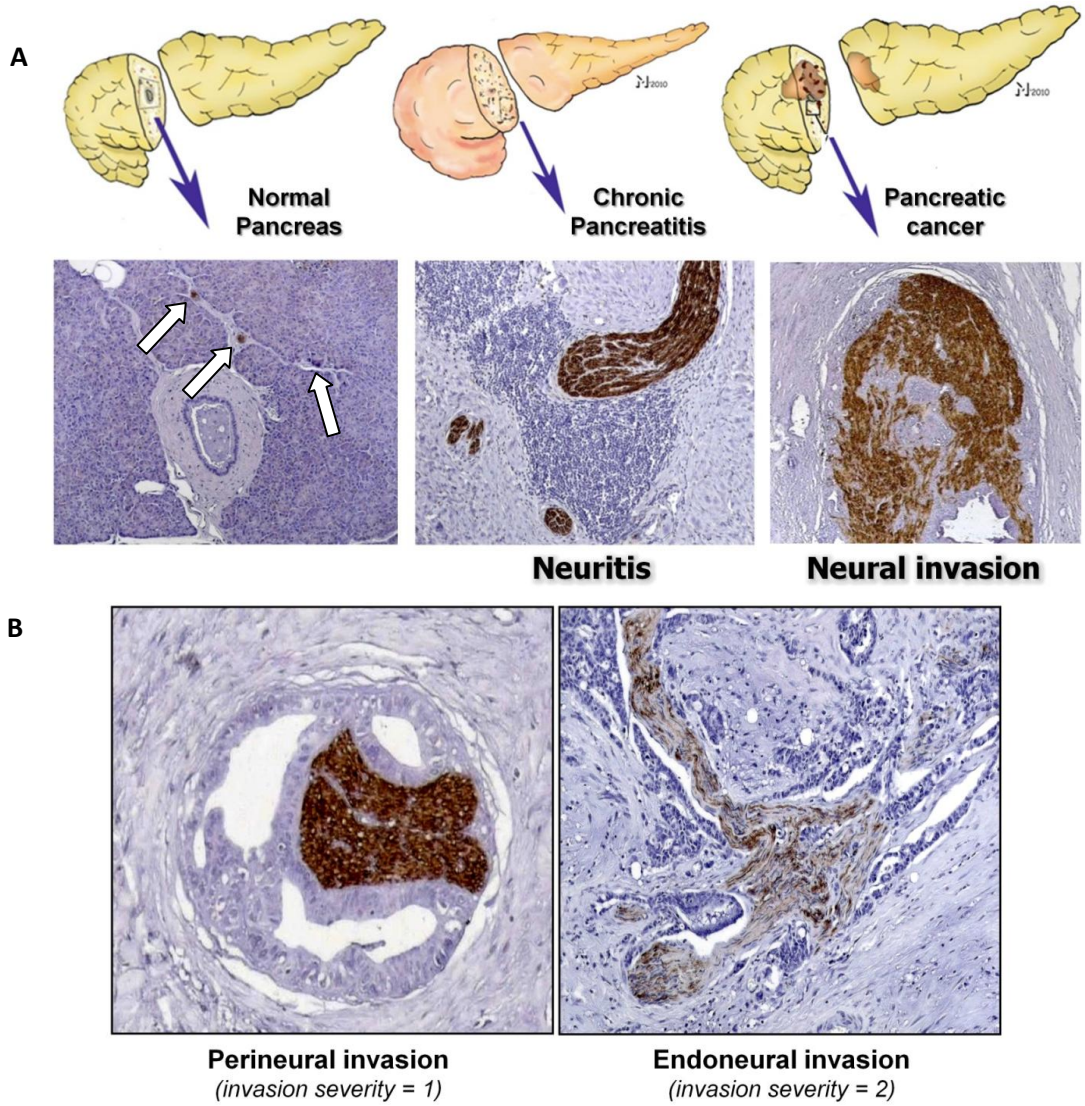

Figure 5. Pancreatic neuropathy. (A) Nerves in the human pancreas can be visualized by immunolabeling with pan-neural markers like protein-gene-product 9.5 (PGP9.5, stained brown on all the images). When compared to nerves in the normal pancreas (white arrows), chronic pancreatitis (CP) and pancreatic cancer (PDAC) tissues contain greater density of nerves that also increase in size (neural sprouting and hypertrophy). In both CP and PCa, a major portion of these nerves are infiltrated by inflammatory cells ("neuritis"). Nerves in PDAC tissues are frequently invaded by cancer cells ("neural invasion"). (B) Neural invasion can manifest in two subtypes: In perineural invasion, cancer cells encircle nerves and are thus encountered along the boundary (epineurium) of nerves. When they penetrate into the interior of nerves, they are encountered between the nerve fiber bundles, which is termed endoneural invasion. Images adapted from Ceyhan et al., Gastroenterology 2009.

model of PDAC, increase in nerve density and particularly in afferent sensory fibers, and augmented expression of neurotrophic factors in the pancreas already occur during the PanIN stage (Stopczynski et al., 2014). From an ultrastructural perspective, electron microscopy of human PDAC specimens previously showed that nerves in PDAC tissues exhibit a distorted architecture, characterized by disruption of the epineurium and perineurium, swelling of axons, and expansion of fiber bundles due to invading cancer cells (Bockman et al., 1994). Therefore, the neuroplasticity in

PDAC seems to be accompanied by prominent neural damage, which is why the nerve alterations in PDAC are also termed “pancreatic neuropathy”. Correspondingly, due to the correlation between the degree of pain and the extent of neuroplasticity, the frequent abdominal and back pain of PDAC patients is increasingly considered as a “neuropathic” type of pain (Demir et al., 2012). That neuropathic pain in PDAC can have an impact on the course of PDAC has been shown in large case studies in which PDAC patients with increasing severity of pain were found to have a reduced overall survival (Ceyhan et al., 2009; D'Haese et al., 2014). Therefore, the extent of neuropathy in PDAC can be assumed to have a role not only during the pathogenesis and within the tumor microenvironment, but to also possess a major clinical relevance.

Neural invasion in pancreatic ductal adenocarcinoma

Besides lymphatic, haematogenous, and locally invasive spread, PDAC cells frequently employ invasion into nerves as an additional mode of dissemination. Though neural invasion (NI) is not specific for PDAC, recent studies comparing its frequency in several gastrointestinal (GI) cancers showed that the frequency of PDAC reaches 100% in true ductal adenocarcinoma cases, thereby surpassing all other GI cancers like colorectal (30%), gastric (38%), esophageal (36-65%) and liver cancer (6-58%) (Liebig et al., 2009; Liebl et al., 2014). While NI has been frequently reported to be in association with local recurrence in PDAC (Bakst et al., 2012), increasing number of systematic literature reviews and meta-analyses show that it also significantly impacts overall survival (Garcea et al., 2008; Zhang et al., 2013). The severity of NI can be quantitatively expressed by means of categorical scoring systems as “0 = no NI or mere epineural association”, “1 = perineural invasion”, and “2 = endoneural invasion” (Ceyhan et al., 2009; Ceyhan et al., 2010). Interestingly,

beyond its presence, also its increasing severity, i.e. endoneural invasion, was also reported to be associated with poor overall survival (Ceyhan et al., 2009; Liebl et al., 2014). Specific therapeutic approaches targeting NI in PDAC in the clinical setting are largely lacking, yet oncoloytic neurotropic viruses or local radiation have been reported to successfully eradicate cancer cells along nerves in the experimental/preclinical setting (Gil et al., 2007; Bakst et al., 2012).

The pathogenesis of NI in PDAC and yet in any cancer remains not fully understood. Initially, NI was attributed to the presence of a low-resistance physical space below the epineurium of nerves, termed the “perineural space”, that would facilitate cancer cell spread long nerves. In this context, perineural lymphatic vessels have been postulated to enable cancer cell access into nerves, yet there is controversy on the true existence of such perineural lymphatic vessels (Larson et al., 1966; Bakst et al., 2012). More recent studies collectively suggested that neurotrophic factors or ligands that were put forward as potential mediators of neuroplasticity in PDAC are secreted from nerves and can build a chemoattractive gradient between cancer cells and nerves. These neurotrophic factors including NGF, GDNF family of ligands and pleiotrophin thus have additional chemoattractive capacity and thereby mediate the “neurotropism” of PDAC cells. Importantly, this neurotropism could be reproduced in an increasing number of co-culture models or migration assays in which PDAC cells were confronted with dorsal root ganglia (DRG) neurons either in Boyden chamber assays (Gohrig et al., 2014) or in suspension within extracellular matrix solutions (Dai et al., 2007; Ceyhan et al., 2008; Gil et al., 2010). Inhibition of these neurotrophic-neurotropic-chemotactic ligands or their receptors led to attenuation of NI in these models.

In addition to this neurotropism, cancer cell-associated adhesion molecules like CD74 and MUC-1, pro-survival genes like MALT1 and TRAF, Schwann cell-

associated cell surface proteins like myelin-associated glycoprotein (MAG), the adrenergic neurotransmitter norepinephrine over STAT3 phosphorylation, and the neuronal chemokines fractalkine or CXCL12/CXCR4 have all been implicated in the generation of NI in PDAC (Marchesi et al., 2008; Demir et al., 2010; Guo et al., 2013; Xu et al., 2014).

Studies that tried to investigate NI in *in vivo* models of PDAC, i.e. in genetically engineered mouse models of PDAC, are widely lacking. In the only study that dealt with innervation and NI in the KPC mouse model of PDAC, Stopczynski et al. analyzed the distribution tdTomato-labeled PDAC cells in the DRG and spinal cord of KPC mice (Stopczynski et al., 2014). Here, they could convincingly show that cancer cells are readily encountered within the pancreas-innervating DRG and the corresponding spinal cord segments of KPC mice. However, this study did not show any evidence of intrapancreatic NI (that is the foremost defining feature of neuropathy in PDAC), and it was unclear whether this detection of tdTomato-labeled PDAC cells was simply due to the extensive and invasive local tumor growth that unavoidably resulted in a more or less unspecific invasion of the retropancreatic DRG and spinal cord. Nonetheless, this study also showed that the exploratory behavior of these animals in a 50x50cm open field diminished over time as the pancreatic tumor progressed (Stopczynski et al., 2014). Critically dissected, this study made the first effort toward describing NI in the most common GEMM of PDAC, although the most characteristic and specific features of NI as seen in human PDAC could not be convincingly demonstrated.

Schwann cells and pancreatic cancer

In the study of neuropathy and NI in PDAC, glia cells of the peripheral nervous system, i.e. the Schwann cells (SC), have not yet been investigated. From a

theoretical perspective, for cancer cells to invade the axons and to progressively grow along the peri- or endoneurium, they must get in close contact with the SC that enwrap the axons (Figure 6). Independent of the myelination status, all nerves in the human organism contain SC, with somatic nerves containing a greater number of myelinating SC when compared to the presence of non-myelinating SC in predominantly autonomic or sensory nerves (Bockman et al., 1994). SC are key actors in the process of nerve regeneration after neural damage that results in the so-called Wallerian degeneration of axonal structures at the distal end of axotomy (Scholz et al., 2007). Neural damage results in the activation of SC, which is characterized by increased proliferation of SC and secretion of pro-inflammatory and neurotrophic factors from SC that chemoattract immune cells and contribute to re-growth of proximal axonal ends toward the periphery (Scholz et al., 2007).

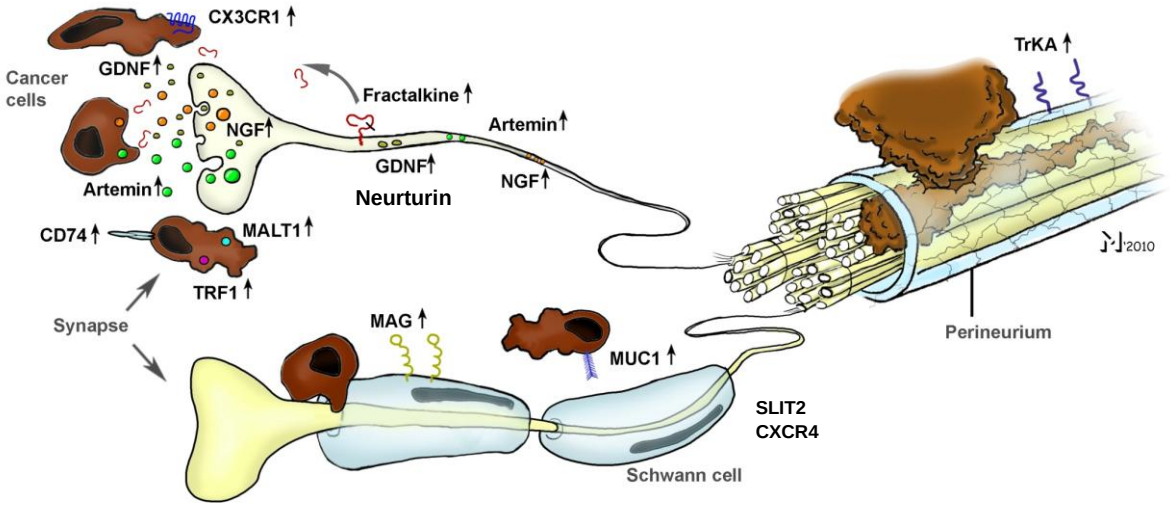

Figure 6. Neuron-cancer cell-Schwann cell interactions. Neurons secrete neurotrophic factors (e.g. NGF, GDNF, Artemin) that bind to their corresponding receptors on cancer cells and chemoattract cancer cells toward nerves. On the other hand, cancer cells are also rich sources of neurotrophic factors like GDNF, artemin or neurturin that can exert trophic effects on nerves. Schwann cells can bind to cancer cells via MAG and MUC1. Axon guidance molecules like SLIT2, or the CXCR4 receptor on Schwann cells can modulate the growth and migration of Schwann cells toward cancer cells. Image adapted from Demir et al., Cancers 2010.

In the light of the already demonstrated neural damage, neuropathy, and growth of cancer cells between nerve fibers in PDAC, it is imperative to assume that SC may acquire an activated state in PDAC. Toward this end, though, there are hardly any

studies that specifically investigated the role of SC in PDAC or in any cancer. This question is particularly important when one considers the obligatory presence of SC in nerves, and the unexceptional presence of nerves in all GI organs. In a study on the role of the epithelial surface antigen and transmembrane mucin MUC1 in PDAC, Swanson et al. discovered the myelin-associated glycoprotein (MAG) as a counter-receptor for MUC1 (Swanson et al., 2007). Inhibition of either of these two molecules could inhibit the adhesion between PDAC cells and SC (Swanson et al., 2007). Beyond adhesion, SC were recently shown to increase the transwell migration rate of human PDAC cell lines, a process that was partly dependent on the CXCR4 chemokine receptor (Xu et al., 2014). In another study, this migration of PDAC cells toward SC in the transwell setting was inhibited by addition of the axon guidance molecule SLIT2 into the culture medium of these cells (Gohrig et al., 2014). Obviously, researchers have become more aware of the possibility that SC may interact with cancer cells in PDAC, but the study of this interaction seems to be at its first footsteps, and the potential role of SC in pancreatic neuropathy and NI remains unclear.

NF-kappaB signaling and pancreatic cancer

Dysregulation of transcription or uncontrolled activation of survival pathways is characteristic for PDAC. The nuclear factor kappa-light-chain-enhancer of activated B cells (NF-kappaB) was identified as a cellular homologue of the v-*rel* oncogene, which is why NF-kappaB family members have been regarded as pleiotropic transcription factors that can function as oncogenes (Wang et al., 1999). The five NF-kappaB/Rel proteins include NF-kappaB2 (p52/p100), NF-kappaB1 (p50/p105), c-Rel, RelA/p65, and RelB. All these proteins serve as dimeric transcription factors that control gene transcription related to multiple biological processes such as cellular

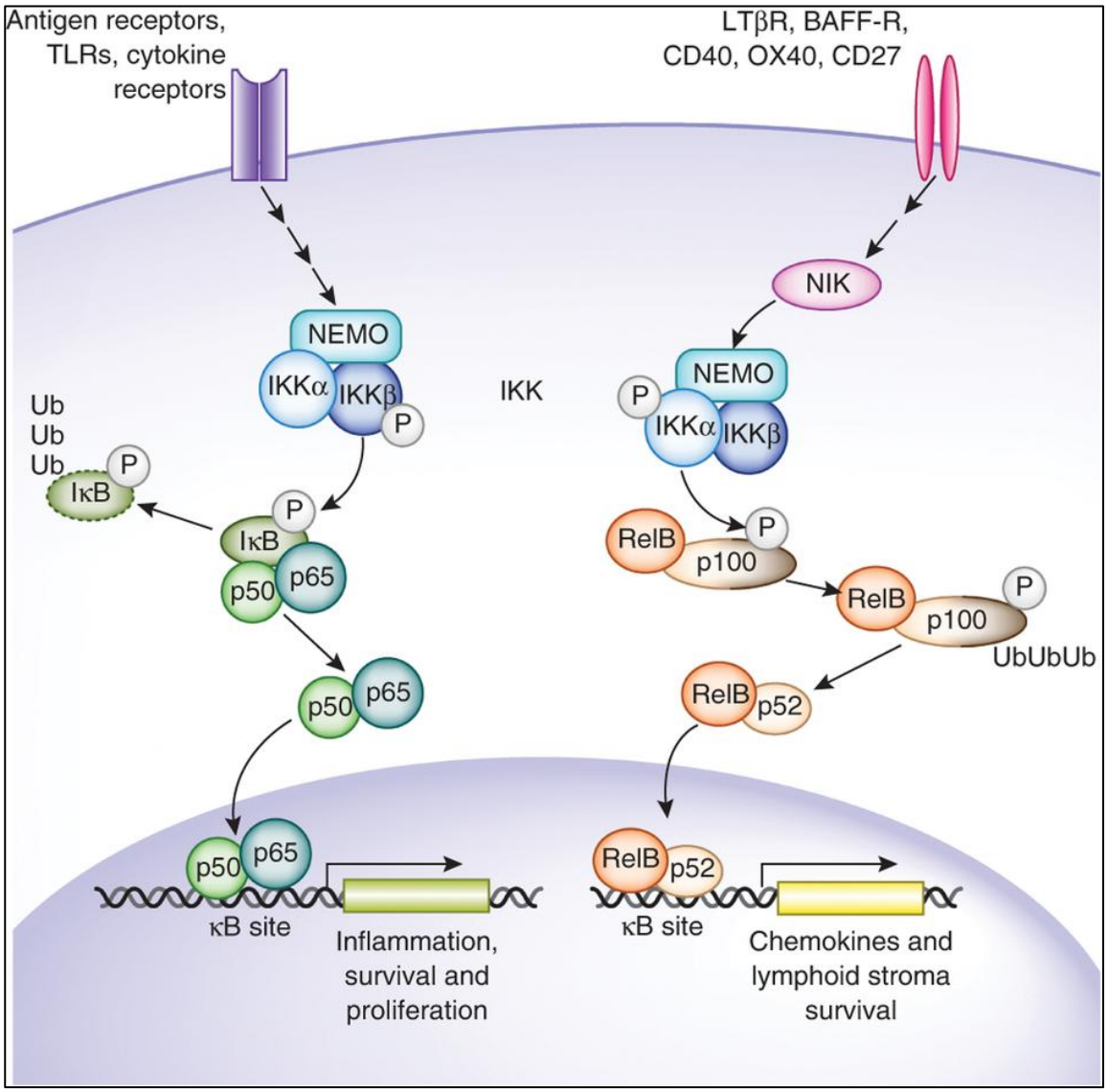

Figure 7. The canonical and non-canonical NF-kappaB signaling pathway (Gerondakis et al., 2014). Left: in the canonical NF-kappaB pathway, IKKβ-mediated phosphorylation of IκB results in ubiquitination (Ub) of IκB and proteasome-induced degradation, leading to the mobilization of the p50/p65 (RelA) complex into the nucleus for transcription. The ligands of the non-canonical pathway activate IKKα, which phosphorylates p100 (NF-κB2), triggering its proteosomal processing to p52 and the nuclear translocation of the active p52-RelB dimers. Image source: Gerondakis et al. Nat Immunol 2014.

stress response, inflammation, immunity, cancer, autoimmune diseases, and B cell development (Hayden et al., 2008). In the classical (or canonical) pathway (Figure 7), NF-κB/Rel proteins [e.g. NFkappaB1(p50)/RelA(p65)] are bound and inhibited by inhibitor of kappaB (IkappaB) proteins (Figure 7). For NFkappaB-activation, the IkappaB protein needs to be degraded by the activation of the IkappaB kinase (IKK). IKK is composed of the catalytic IKKα and IKKβ subunits and NF-κB essential modulator NEMO (IKK gamma). In the presence of activating signals, IKK

phosphorylates two serine residues in the IkappaB regulatory domain, which results in the ubiquitination of IkappaB and its degradation in the proteasome. Thereby, the freed NF-κB/Rel complex is phosphorylated and translocates to the nucleus where it drives target gene expression (Hayden et al., 2008).

In the alternative (or noncanonical) NF-κB pathway, activation of membrane receptors like lymphotoxin-beta-receptor, CD27, CD40, OX40 or BR3, activates the NF-kappaB-inducing kinase (NIK), which in turn activates IkappaB kinase alpha complexes that phosphorylate C-terminal residues in the NF-kappaB2(p100)/RelB complex in the cytoplasm (Figure 7). Phosphorylation of NF-kappaB2(p100)/RelB leads to its ubiquitination and proteasomal processing to the active, translocation- and transcription-capable NF-kappaB2(p52)/RelB (Razani et al., 2011).

Studies on the impact of NF-kappaB/p65 signaling in PDAC have concentrated on its effects on PDAC cell growth and proliferation. In one of the first studies, Wang et al. showed that RelA, the p65 subunit of NF-kappaB, was constitutively active in approximately 67% of PDAC cases but not in normal pancreatic tissues. Similarly, constitutive RelA activity was present in the majority of human PDAC cell lines (Wang et al., 1999). In another analysis on further subunits of the NFkappa-B signaling, Chandler et al. detected increased expression of both cytoplasmic (I kappa B-alpha, p50, p52, p65) and nuclear (p50, p52, p65, c-Rel) NF-kappa B subunits PANC-1 and BxPC-3 PDAC cell lines when compared to FHS 74 intestinal cells (Chandler et al., 2004). At the functional level, NFkappa-B silencing via small-interfering RNA (siRNA) or via a selective inhibitor of IKK disrupted the resistance of PDAC cells to tumor necrosis factor-related apoptosis-inducing ligand (TRAIL)-induced apoptosis (Khanbolooki et al., 2006). Furthermore, blockade of NF-kappaB reversed the constitutive expression of sonic hedgehog (Shh) mRNA in pancreatic cancer cells and inhibited their proliferation (Nakashima et al., 2006). In a

corresponding study, Shh was confirmed as an NF-kappaB target gene that promotes NF-kappaB-mediated resistance to apoptosis and tumor growth in vivo (Kasperczyk et al., 2009). Moreover, in two independent studies, silencing of the RelA/p65 subunit was shown to increase gemcitabine sensitivity of human PDAC cell lines (Pan et al., 2008; Kong et al., 2010). Intrapancreatic expression of N-myc downstream regulated gene 1 (NDRG1)/Cap43 was reported to be a favorable prognostic factor in PDAC (Hosoi et al., 2009). Hosoi et al. could show that the NDRG1/Cap43-mediated suppression of NF-kappaB signaling was due to decreased IKK beta expression and IkappaB-alpha phosphorylation (Hosoi et al., 2009). The activity of NFkappa-B signaling was shown to be modulated by the action of the transforming growth factor-beta (TGF-beta), since TGF-beta induced IkappaB-alpha phosphorylation, nuclear translocation of p65 and suppression of the tumor suppressor PTEN (Chow et al., 2010). Collectively, there is ample evidence on the constitutive activation of NFkappa-B signaling in PDAC, which seems to promote enhanced growth, apoptotic and chemotherapeutic resistance. Correspondingly, therapeutic targeting of NFkappa-B signaling was postulated as a potential approach to limit PDAC progression (Chow et al., 2010), a possibility that has not yet been investigated in GEMM of PDAC.

Aims of the study

Neuropathy and neural invasion (NI) are defining characteristics of human PDAC that are present in nearly all PDAC patients and exert an ominous impact on both local recurrence and overall survival rates. In an era of GEMM of PDAC that made unique contributions toward our understanding of carcinogenesis, tumor suppressors, tumor-associated-inflammation, tumor-host interactions, tumor metabolomics, and tumor microenvironment in PDAC, there is no single GEMM of PDAC that has yet been shown to harbor NI or neural alterations that even resemble those in human disease. For a disease like human PDAC for which no major progress has yet been made toward improved prognosis, it is crucial to develop in vivo models that more effectively recapitulate the human disease.

The present study demonstrates a novel GEMM of PDAC, the Ela-TGFalpha;trp53$^{\Delta/\Delta}$, p65$^{\Delta/\Delta}$ (TPAC) model of PDAC, that, owing to the knockout of the p65 subunit of the NFkappa-B signaling, and in simultaneous comparison with the KC, KPC and TPC (Ela-TGFalpha;trp53$^{\Delta/\Delta}$) models of PDAC, was for the first time detected to exhibit human-PDAC-like NI. Toward this end, this study pursued the following aims:

- Histopathological analysis and quantification of neural density, neural size, neuritis and NI in KC, KPC, TPC and TPAC mice models (immunostaining and densitometry)
- Functional characterization of the neuroplastic and neuroinvasive features of cancer cells derived from these models via:
    - ✓ *3D migration assays using mouse DRG neurons*
    - ✓ *Neuroplasticity assays with supernatants of the mouse cancer cells applied on mouse DRG neurons*

- Comparison of glial (Schwann cell) chemoattraction toward these cancer cell subtypes via:
    - ✓ *a novel 3D Schwann cell outgrowth assay*
    - ✓ *Histopathological quantification of Schwann cell-cancer cell associations in GEMM of PDAC*
- Preliminary comparison of the abdominal mechanosensitivity (via von Frey filaments) and pain-associated behavior of KC, TPC and TPAC mice
- Transcriptional profiling of the primary mouse cancer cells (KC, KPC, TPC and TPAC)
    - ✓ *Affymetrix-chip-based microarray expression analysis*
    - ✓ *RT^2 Profiler RNA Array*

Via this approach that combines detailed histopathological, several *in vitro* functional, transcriptional analyses and *in vivo* pain phenotyping, the present study shall provide the first comparative data on the tumor innervation pattern in GEMM of PDAC, on the *in vivo* role of glia in the generation of NI, and the first clues on why the TPAC model of PDAC may be superior to the remaining GEMM of PDAC in the study of neuropathy and NI in PDAC.

Materials & Methods

Reagents

Product	Company	City, Country
0,25 % Trypsin-EDTA	Gibco, Invitrogen	Paisley, UK
Antibiotics Penicilline and Streptomycine	PAA Laboratories GmbH	Pasching, Austria
Aqua dest.	Braun	Melsung, Germany
B 27-Supplement	Gibco Invitrogen	Paisley, UK
Collagenase Type II	Worthington	Lakewood, NJ; USA
Collagenase Type VIII	Sigma Aldrich	Taufkirchen, Germany
Dulbeco`s Modified Eagle Medium (DMEM) (high Glucose)	PAA Laboratories GmbH	Pasching, Austria
ECM gel	Sigma Aldrich	Taufkirchen, Germany
Fetal bovine serum	PAA Laboratories GmbH	Pasching Austria
Formaldehyde 4%	Carl Roth GmbH	Karlsruhe, Germany
HBSS (Hank`s BSS)	Promo Cell	Heidelberg, Germany
HEPES Buffer Solution	PAA Laboratories GmbH	Pasching, Austria
Human Schwann Cell Medium	ScienCell	California, USA
L-Glutamine	Gibco Invitrogen	Paisley, UK
Liberase	Roche Diagnostics	Mannheim, Germany
MEM (Minimal Essential Medium)	Promo Cell	Heidelberg, Germany
Metronidazol	Merck Pharma	Darmstadt, Germany
Nerve growth factor (NGF), recomb. human	Acris	Herford, Germany
Neurobasal Medium	Gibco Invitrogen	Paisley, UK
PBS	PAA Laboratories GmbH	Pasching, Austria
Poly-D-Lysine Hydrobromide	Sigma Aldrich	Taufkirchen, Germany
Refobacin	Merck Pharma	Darmstadt, Germany
RPMI 1640	PAA Laboratories GmbH	Pasching, Austria
Tris	Carl Roth GmbH	Karlsruhe, Germany
Tween-20	Carl Roth GmbH	Karlsruhe, Germany

Consumables

Product	Company	City, Country
Cell culture flasks 25 und 75 cm^2	Greiner	Frickenhausen, Germany
Cell culture plate, 24-well	Greiner	Frickenhausen, Germany
Cover slips 13mm	Nunc	Roskilde, Denmark
Cryo-Tube	Nunc	Roskilde, Denmark
Injection cannulas, Sterican	Braun	Melsungen, Germany
Parafilm	Pechiney, Plastic Packaging	Chicago, USA
Petri dish 100x20mm	Greiner	Frickenhausen, GER
Petri dish 35x10mm	BD Falcon	Franklin Lakes, USA
Pipette tips	Star Lab	Ahrensburg, Germany

Pipettes	Eppendorf	Wesseling-Erzdorf, Germany
PP-tubes 15 ml und 50 ml	Greiner	Frickenhausen, Germany
Reaction tubes (1,5ml)	Eppendorf	Wesseling-Erzdorf, Germany
Syringe filters	Nalgene	Rochester, USA
Syringes	Braun	Melsungen, Germany
von Frey filaments	Stoelting	Wood Dale, IL, USA

Devices & Software

Product	Company	City, Country
Axio Vision Software	Zeiss	Jena, Germany
Centrifuge 5424	Eppendorf	Wesseling-Erzdorf, Germany
Centrifuge, Multifuge 3SR+	Thermo Science	Bonn, Germany
CO_2 Module	Zeiss	Jena, Germany
Computer	Dell	Frankfurt am Main, Germany
Graph Pad	GraphPad Software Inc.	California, USA
Image J	National Institute of Health	Maryland, USA
Incubator, Hera cell 150	Thermo Science	Bonn, Germany
Keyence BioRevo BZ-9000	Keyence	Neu-Isenburg, Germany
Microscope Observer Z1	Zeiss	Jena, Germany
Microscope, Axiovert 40 CFL	Zeiss	Jena, Germany
Neubauer Hemocytometer	Marienfeld Superior	Lauda-Königshofen, Germany
Pipetboy, IBS	Integra Biosciences	Fernwald, Germany
Semi-sterile work bench	Hera guard, Thermo Science	Bonn, Germany
Stereomicroscope SMZ 1500	Nikon	Düsseldorf, Germany
Sterile hood	Hera Safe, Thermo Science	Bonn, Germany
Temperature Module	Zeiss	Jena, Germany
Water bath Aqualine AL 18	Lauda	Lauda-Königshofen, Germany

Kits

Product	Company	City, Country
RT² Profiler™ PCR Array Mouse Neurotrophins & Receptors	SABiosciences/Qiagen	Hilden, Germany
Extract-N-Amp™ Tissue PCR Kit	Sigma Aldrich	Taufkirchen, Germany
RNEasy Mini Kit	Qiagen	Hilden, Germany

Mice and husbandry

The analysis of neuropathy and neuroplasticity in the GEMM of PDAC was carried out on the following four “core” mouse models:

KC model: These mice were generated by crossing the Pt1fa/p48-Cre$^{ex1/+}$ line that expresses the Cre recombinase in the Exon 1 of the Ptf1a/p48 gene under the control of this pancreas-specific promoter) to the LSL-Kras^{G12D} mouse line. The gene that expresses the Cre recombinase is located within the exon 1 of the pancreas transcription factor 1 (Ptf1a). Ptf1 is a heterotrimeric protein complex that functions as a transcriptional regulator and is responsible for the correct development of the ventral pancreatic bud in the early stages of pancreatic organogenesis. The Pt1fa/p48-Cre$^{ex1/+}$ and LSL-Kras^{G12D} mouse lines on their own do not exhibit any phenotype that differs from their background C57BL/6J mice. The crossing of these mouse lines generates the Pt1fa/p48-Cre$^{ex1/+}$;LSL-Kras^{G12D} mouse line (“KC”) that, as initially described by Hingorani et al. (Hingorani et al., 2003), develops PanIN lesions in at least around 30% of the pancreatic tissue by around 4-5 months of age. These mice, albeit in a low frequency (i.e. 6-8% around 8-10 months of age), can spontaneously progress to invasive cancer (Hingorani et al., 2003). For the present analysis, the pancreatic tissue, together with the neighboring duodenum and spleen were removed and fixed in 4% paraformaldehyde from KC mice between 250-400 days of age. For an overview of the mouse line characteristics, please refer to Table 4.

KPC model: To generate KPC mice, LSL-Kras^{G12D} knock-in (Jackson et al., 2001), Ptf1a-Cre (Nakhai et al., 2007) and Trp53$^{fl/fl}$ (Jonkers et al., 2001) strains were interbred to obtain Ptf1a-Cre;LSL-Kras^{G12D};Trp53$^{fl/fl}$ mice. In Trp53$^{fl/fl}$ mice, the exons 2-10 of the Trp53 gene are flanked by loxP-sites, which allows the excision of this

functional region by Cre-mediated recombination. Hence, these mice differ from the initial description of KPC mice by Hingorani et al. in the Cre-mediated excision of a functional Trp53 exonal sequence (Cre-mediated knockout) as opposed to the Cre-mediated excision of the STOP cassette in front of the mutated (LSL-Trp53$^{R172H/+}$) Trp53 knockin allele in the original study (Hingorani et al., 2005). Due to this modification, these Ptf1a-Cre;LSL-Kras^{G12D};Trp53$^{fl/fl}$ mice more rapidly develop invasive PDAC and exhibit a median survival time of around 61.5 days as opposed to 25 weeks among Ptf1a-Cre;LSL-Kras^{G12D};LSL-Trp53$^{R172H/+}$ mice (Bardeesy et al., 2006). In the current study, mice between 49 and 61 days of age were utilized. For an overview of the mouse line characteristics, please refer to Table 4.

TPC model: The TPC model is based on the Ela-TGFalpha transgenic mice (Sandgren et al., 1990; Wagner et al., 1998; Greten et al., 2001) in which the epidermal growth factor receptor ligand transforming growth factor alpha (TGFalpha) is transgenically expressed under the control of the pancreatic elastase promoter. For the current study, Ela-TGFalpha mice were interbred with Trp53$^{fl/fl}$ mice and then to Ptf1a-Cre$^{ex1/+}$ mice to generate Ela-TGFalpha;Trp53$^{\Delta/\Delta}$ (TPC) mice. This constellation creates pancreas-specific Cre-mediated homozygous knockout of the Trp53 gene with simultaneous pancreatic overexpression of TGFalpha. These mice demonstrate in ca. 66% of cases undifferentiated pancreatic cancer and in around 25% of cases PDAC. They show a 100% tumor incidence and exhibit a median survival time of ca. 300-310 days (versus 445 days for Ela-TGFalpha mice). For the current study, TPC mice between 193 and 339 days of age were utilized. Further details on the cancer cell-specific histology and survival kinetics of TPC mice can be found in the corresponding doctoral thesis by Dr. Marina Lesina (Lesina, 2013). For an overview of the mouse line characteristics, please refer to Table 4.

TPAC model: In order to study the role of NFkappaB-signaling in PDAC, it is necessary to develop GEMM of PDAC in which selected components of the NFkappaB signaling pathway are conditionally altered. For this purpose, a novel GEMM of PDAC was developed in which the RelA/p65 subunit that controls the transcription of several downstream genetic targets in the canonical NFkappaB pathway has been conditionally knocked when compared to the TPC model. Here, Ela-TGFalpha mice were interbred with $Trp53^{fl/fl}$ mice, Ptf1a-$Cre^{ex1/+}$ mice and RelA/$p65^{fl/fl}$ mice to generate Ela-TGFalpha;$Trp53^{\Delta/\Delta}$;$p65^{\Delta/\Delta}$ mice. In these mice, the exons 7 to 10 of the *rela* gene are flanked by two loxP sites. Excision of these gene regions results in disruption in the RelA-homology-domain, distorts the nuclear localization signal (NLS), and abolishes the ability of RelA/p65 to bind to IkappaBalpha. Hence, the deleted RelA/p65 protein is not able to heterodimerize with p50 or to translocate into the nucleus. RelA/$p65^{fl/fl}$ mice do not per se exhibit any phenotype. The median survival time of these TPAC mice was reported to be around 360 days (Lesina, 2013). Interestingly, pancreas-specific truncation of the RelA/p65 gene led to emergence of a ductal pancreatic cancer phenotype, with 75% of all tumors appearing like PDAC (as opposed to 25% among TPC mice). Correspondingly, TPAC mice were reported to bear a higher E-cadherin expression and a lower Vimentin-immunoreactivity than TPC mice (Lesina, 2013). Overall, TPAC mice can be regarded as better differentiated, more ductal-like mouse PDAC when compared to TPC mice (Lesina, 2013). The age of the mice utilized in this study was between 316 and 689 days, with a tumor incidence of 100%.

In addition to these four GEMM of PDAC that represented the “core” models in this study, three additional mouse models were available that served as valuable controls for the histopathological analysis of neuropathy and NI:

KPAC model: These mice were generated by interbreeding Ptf1a-Cre, LSL-Kras^{G12D}, Trp53$^{fl/fl}$ and RelA/p65$^{fl/fl}$ mice. In these mice, pancreas-specific excision of the loxP-flanked exons 7 to 10 of the RelA/p65 gene results in additional specific knockout of the p65 function when compared to KPC mice. Similar with the differentiation-inducing effects of RelA/p65 in TPAC mice, KPAC mice exhibit a more ductal-cancer-like phenotype than KPC mice and a correspondingly somewhat longer median survival time of 82 days. For the current study, mice between the ages of 74 and 86 days were utilized.

Ela-LTαβ model: The analysis of neuropathy and NI in GEMM of PDAC raised the question whether a potential precursor of PDAC, i.e. chronic pancreatitis (CP), can also be detected to be associated with neuropathy in GEMM. Indeed, human CP tissues show a very similar neuropathy like in PDAC, characterized by neural hypertrophy, increased neural density, and neural inflammation (“neuritis”). To date, GEMM of CP are very few in number, although efforts to generate novel GEMM of CP are clearly visible. In this context, one of the first GEMM of CP was reported by Seleznik et al. who generated a transgenic mouse model of autoimmune chronic pancreatitis that is characterized by overexpression of the lymphotoxin signaling ligands lymphotoxin α and β under the control of the pancreatic elastase promoter (“Ela-LTαβ mice” (Seleznik et al., 2012)). Lymphotoxin signaling constitutes a member of the TNF family and is regarded as a key regulator of lymphoid architecture, high endothelial venules, angiogenesis, and lymphangiogenesis (Lu et al., 2014). The first discovered lymphotoxin protein, LTα, is a member of the TNF family of ligands and is secreted as a homotrimeric molecule that binds to the TNF receptors (Lu et al., 2014). LTα can also be encountered in a membrane-bound form within a heterotrimer together with LTβ (termed LTα/β) (Lu et al., 2014). Importantly,

LTα/β binds selectively to the lymphotoxin-beta receptor (LTβR) (Lu et al., 2014). Although immune cells were long believed to be the only source of LT, some parenchymal cells, such as hepatocytes, were also detected to express LT under pathological conditions (Seleznik et al., 2012). Seleznik et al. detected overexpression of LTαβ in human autoimmune pancreatitis tissues (Seleznik et al., 2012). The corresponding overexpression of LTαβ specifically in the murine pancreas resulted in focal infiltrating immune cells foci within the pancreas, acinar-ductal-metaplasia, acinar cell proliferation around 12-22 months of age and occurrence of organized B- and T-cell zones around 6 months of age (Seleznik et al., 2012). Therefore, this model presents a recently generated inflammatory model of CP that served as an additional control in this study. These mice were obtained from the research group of Professor Rolf Graf (Zürich).

KPC-electro model: Current GEMM of PDAC have the limitation that they either harbor cancer-driving mutations from the embryonic step onwards, or to generate PDAC in the adult stage, there is need for additional chronic tissue inflammation. Beyond these features that strongly contradict the human situation, these GEMM develop multifocal PDAC as opposed to the localized core tumor in the human setting. Hence, these models are not suitable for surgical interventions. To circumvent these limitations, Gürlevik et al. recently developed a new transposon-based mouse model with localized acinar-to-ductal metaplasia (ADM) that progresses to overt PDAC (Gürlevik et al., submitted). Here, the investigators performed in situ electroporation of a Cre-expressing plasmid into the pancreatic tail of LSL-$Kras^{G12D}$;$Trp53^{fl/fl}$ mice via a small upper abdominal laparotomy (KPfl mice). In a second approach, they co-electroporated two plasmids, one encoding an SB13 transposase that mediates stable incorporation of the $Kras^{G12V}$-oncogene from the

second plasmid into the genome of the acinar cells (Pfl mice). The Kpfl mice have a longer survival span between 63 to 105 days (median survival of 84 days) as opposed to the Pfl mice that merely survive between 29 and 37 days. As a special feature, the tumors that develop in these mice can be surgically resected to achieve an R0 status. Hence, these mice represent a unique and more human-like opportunity to study the impact of different perioperative, neoadjuvant or adjuvant chemo-/radiotherapeutic strategies in a GEMM of PDAC. To accelerate metastasis, the investigators additionally electroporated a myrAkt2 (constitutively active Akt2 after myristoylation at the N-terminus) transposon together with the Cre recombinase into the pancreatic tail of LSL-Kras^{G12D};trp53$^{fl/fl}$ mice, generating KPfl+Akt2 mice. For the current study, the analyzed mice were 6-8 week old KPfl+Akt2 mice and are herein termed “KPC-electro”.

Mouse line	Genotype	Number (n)	Age range	Age distribution	Median survival
KC	Ptf1a-Cre$^{ex1/+}$;LSL-Kras^{G12D}	10	250-400 days	2 mice <250 d 3 mice 250-400 d 5 mice >400d	467 days
KPC	Ptf1a-Cre$^{ex1/+}$;LSL-Kras^{G12D}; Trp53$^{fl/fl}$	10	49-61 days	2 mice 49-50 d 5 mice 51-54 d 3 mice 54-61 d	61.5 days
TPC	Ela-TGFalpha;Trp53$^{\Delta/\Delta}$	12	193-339 days	2 mice 150-200 d 3 mice 201-250 d 2 mice >250 d	300 days
TPAC	Ela-TGFalpha;Trp53$^{\Delta/\Delta}$;p65$^{\Delta/\Delta}$	15	316-689 days	3 mice 300-350 d 5 mice 350-400 d 4 mice 400-450 d 3 mice >450 d	360 days
KPAC	Ptf1a-Cre$^{ex1/+}$;LSL-Kras^{G12D}; Trp53$^{\Delta/\Delta}$;p65$^{\Delta/\Delta}$	7	70-86 days	2 mice 70-75 d 3 mice 76-85 d 2 mice >85 d	82 days
KPC-electro	prPGK-Cre plasmid electroporated into LSL-Kras^{G12D};Trp53$^{fl/fl}$ mice	8	42-56 days		42 days after electroporation
Ela-LTαβ	Ela-LTαβ$^{tg/+}$	8	6 mo-1 year	2 mice at 6 mo 6 mice at 1 year	

Table 4. Genotypic, age, number and survival characteristics of the analyzed mice.

A total of 73 mice were analyzed. Mice were bred in cooperation with the research group of PD Dr. Hana Algül (Department of Internal Medicine II, Technische Universität München) in the central animal facility of Klinikum rechts der Isar and in accordance with the regulations of the governmental commission for animal protection of the Government of Upper Bavaria (Regierung Oberbayern).

Tissue processing, immunohistochemistry, immunofluorescence

After collection of the mouse pancreas, the tumor was cut into pieces and 1) fixed in 4% paraformaldehyde for subsequent paraffin embedding, 2) snap-frozen for RNA collection, and 3) digested in liberase and type VIII collagenase for cancer cell isolation. For the morphometric analysis of nerve density and size, from each mouse, two 3 µm sections from the main tumor that were at least 10 consecutive sections apart (i.e. 30 µm apart) were subject to immunohistochemistry and subsequent histomorphometric analysis. The immunolabeling of murine intrapancreatic nerves was performed via a specific antibody against the pan-neural marker protein-gene-product 9.5 (PGP9.5; DAKO, Hamburg, Germany). Here, after deparaffinization and dehydration, sections were subject to heat-mediated antigen retrieval and blocking of unspecific labeling with 3% hydrogen peroxide, normal goat serum, and incubated with the primary PGP9.5 antibody overnight. Visualization of immunoreactivity was performed via incubation with horseradish-peroxidase (HRP)-coupled secondary antibodies and subsequent color reaction with the HRP-substrate 3,3'-diaminobenzidine (DAB). All sections were counterstained with hematoxylin to visualize infiltrating cancer cells and inflammatory cells. For the immunofluorescence staining, tissue sections were incubated with primary antibodies overnight in a humid chamber at 4ºC and on the next day with Alexa Fluor® secondary fluorescent

antibodies, as shown previously (Demir et al., 2010). An overview of the utilized antibodies is provided on Table 5.

Antibody	Company	Species	Concentration
Anti-PGP9.5	DAKO, Hamburg, Germany	Rabbit	1:500
Anti-GFAP	DAKO, Hamburg, Germany	Rabbit	1:400
Anti-GFAP	Abcam, Cambridge. UK	Goat	1:100
Anti-S100	Merck-Millipore, Billerica, MA ,USA	Mouse	1:200
Anti-Sox10	Novus Biologicals, Littleton, CO, USA	Rabbit	1:400
Anti-ALDH1L1	Abcam, Cambridge. UK	Rabbit	1:500
Anti-Vimentin	Life Technologies, Darmstadt, Germany	Mouse	1:500
Anti-β-III-Tubulin	Merck-Millipore, Billerica, MA ,USA	Mouse	1:200

Table 5. Primary antibodies.

Histomorphometric analysis

To determine the neural size and neural density in the mouse tumor tissues, all sections were digitally and entirely scanned at high-resolution and 20x magnification via an automated digital epifluorescence microscope (Keyence BioRevo BZ-9000, Neu-Isenburg, Germany). All nerves on each section were measured for their size by means of the freehand selection tool of the ImageJ software (version 1.44p, NIH, USA). Simultaneously, a score for the severity of neural invasion (NI) and neuritis was documented for each nerve. Here, the presence of cancer cells (for NI) or of inflammatory cells (for neuritis) was quantitatively expressed by means of a previously demonstrated categorical scoring system as “0 = no NI or mere epineural association”, “1 = perineural invasion or peri-neuritis”, and “2 = endoneural invasion or endo-neuritis” (Ceyhan et al., 2009; Ceyhan et al., 2010). To calculate nerve density, the number of detected nerves was divided by the total area of the entirely

scanned tissue section and expressed as no. of nerves / mm^2. The mean nerve size was calculated as the average of the size of all individual nerves on each section and was expressed as μm^2. The mean NI or neuritis severity of a tissue was calculated as the mean of all individual NI or neuritis severity scores of each nerve. In the analysis of Schwann cell-PanIN/cancer cell-associations in mouse tissues, the number of invaded precursor or cancer cell sites on each section were counted and proportioned to the total number of precursor and cancer cell clusters per section and expressed as per cent. For all values, the final statistics were calculated after obtaining the mean of the two values from the two analyzed sections from each mouse.

Three-dimensional (3D) migration assay

The comparative analysis of the neurotropism of the mouse cancer cells, i.e. the extent to which they are attracted to neurons, was carried out via a 3D migration assay (Ceyhan et al., 2008; Liebl et al., 2012). In this assay, 50,000 primary cancer cells already isolated from KPC, TPC, TPAC or KC mice were suspended in an extracellular matrix/ECM gel drop (E1270, from Engelbreth-Holm-Swarm (EHS) mouse sarcoma, Sigma-Aldrich, Munich, Germany) and simultaneously confronted in a cross-like geometric matrix (Figure 15) with neurons derived from six lumbar mouse dorsal root ganglia (DRG) neurons. The DRG were collected from the lumbar spinal region of newborn, i.e. 3-7 day-old C57BL/6J pups under stereomicroscopic dissection.

The suspensions containing the mouse cancer cells were pipetted at 1mm distance to each other and connected via an ECM “bridge” that enables generation of a chemoattractive gradient. The ECM gel suspensions were allowed to polymerize for 15 minutes, and the 35 mm dishes containing the polymerized ECM gels were

provided with a 1:1 mixture of Neurobasal medium (supplemented with 100U/mL penicillin and 100µg/mL streptomycin, 2% B-27 and 0.5mM L-glutamine) and cancer cell medium (DMEM, low glucose, supplemented with 5% fetal bovine serum, 100U/mL penicillin and 100µg/mL streptomycin, and 1% non-essential amino acids). At 60 hours after seeding of the assay, the plates were placed in the incubation chamber of a digital time-lapse microscope.

3D Schwann cell outgrowth assay

As SC were increasingly recognized to exhibit a high and specific affinity to malignant cells in our recent investigations, a novel 3-D Schwann cell outgrowth assay was generated that allows live-tracking of primary Schwann cells of the murine sciatic nerve. In this assay, a ca. 5mm segment of the left or right sciatic nerve of C57BL/6J mice was placed at 1mm distance away from a 25µl ECM gel suspension containing the mouse cancer cells, and the cancer cell suspension was connected to the nerve by means of a thin ECM bridge (Figure 18). The nerve segment was placed perpendicular to this connecting bridge so that the exposed Schwann cells at both ends of the nerve segment have the maximum distance to the cancer cell suspension. The assay plates were placed into the digital time-lapse microscope after 24 hours, tracked for up to 7 days and eventually fixed with 4% paraformaldehyde (Carl Roth GmbH, Karlsruhe, Germany) for subsequent immunofluorescence labelling.

Digital time-lapse microscopy

In order to analyze the extent of chemoattraction between murine cancer cells and neurons, or between SC and murine cancer cells, digital time-lapse microscopy

analysis of cell migration was performed for an observation interval of 12 to 24h via a Zeiss observer D1 system (Carl Zeiss, Munich, Germany), equipped with a CO_2 incubation chamber, an AxioCam camera and a plan-neoluar 10x/0.3 PH1 M27 objective. The obtained videos were then converted to avi.-format for subsequent analysis via the ImageJ software (version 1.44p, NIH, USA). On each image sequence, 30 cancer cells or SC at each front were randomly selected and tracked via “manual tracking” plug-in of the ImageJ software, as previously demonstrated (Liebl et al., 2012). This plugin generates numeric data that can be translated into four main morphometric parameters of cell migration in the “chemotaxis and migration tool” (Ibidi, München, Germany). This tool yields the three main morphometric parameters: 1) the *Euclidean distance* (µm), which is the linear distance, i.e. net displacement, of the migrating cells, 2) the *velocity* of migrating cells (µm/min), and 3) the *forward-migration index*/*FMI*, which corresponds to the proportion of the Euclidean distance to the total accumulated migration distance of a cell. Hence, increasing FMI corresponds to a more targeted (linear) migration.

In vitro neuroplasticity assay

Simulation of neuroplasticity, which is a hallmark of pancreatic neuropathy, was recently achieved within an *in vitro* assay in which DRG neurons were treated with supernatants of PDAC cell lines or with tissue extracts from human PDAC or CP tissues (Demir et al., 2010). These treated DRG neurons exhibited increased neurite density, enhanced neurite branching, and perikaryonal hypertrophy under the influence of PDAC or CP tissue extracts or after exposition to PDAC cell line supernatants (Demir et al., 2010). In the present study, DRG neurons were obtained after collagenase II- and trituration-mediated dissociation of DRG from 3-7 day-old C57BL/6J pups. The DRG cells were seeded at a density of 10,000 cells/13mm

coverslip placed in each well of a 24-well plate and supplied with Neurobasal medium (supplemented with 100U/mL penicillin and 100µg/mL streptomycin, 2% B-27 and 0.5mM L-glutamine). The coverslips were coated with poly-D-lysine hydrobromide (40 mg/m^2, Sigma Aldrich, Taufkirchen, Germany) prior to seeding of the neurons. After 24 hours of seeding, the medium of the neurons was discarded and supplied with Neurobasal medium containing the murine PDAC cell supernatants derived from two different mice per each mouse line (KC, KPC, TPC, TPAC) at a protein concentration of 100µg/ml. After incubation of the murine DRG cells with the supernatant-containing medium for 48 hours, the cells were fixed with 4% paraformaldehyde and immunostained with anti-beta-III-tubulin primary and Alexa Fluor® 488 secondary antibodies. For the quantification of neuroplasticity, the four densest regions on each coverslip were photomicrographed on the Keyence BioRevo BZ-9000 microscope. A 50x50 µm grid was placed on each image, and the number of neurites that intersect the horizontal lines on each grid were counted. The neurite density was calculated as the average number of intersecting neurites per 50x50 µm unit area on each image. The mean neurite density induced by each GEMM of PDAC was obtained after averaging the neurite densities of the triplicate coverslips treated with the same murine PDAC cell type.

RT^2 Profiler polymerase chain reaction (PCR) Array

The transcriptional profile of the murine GEMM of PDAC was analyzed within the total RNA of the four core murine PDAC cell types. In the first step, the expression of 84 genes related to neurotrophins and their receptors (for a complete list, please refer to: http://www.sabiosciences.com/rt_pcr_product/HTML/PAMM-031Z.html) the Mouse Neurotrophins and Receptors™ PCR Array was utilized. Total RNA of the primary PDAC cancer cells derived two different mice from each mouse line (KC,

KPC, TPC, TPAC) was extracted according to the instructions of the manufacturer. RT^2 First Strand Kit was used to generate cDNA from total RNA (5.0µg per reverse transcription), and the cDNAs were pipetted together with the RT^2 SYBR Green / Fluorescein PCR master mix onto the Mouse Neurotrophins and Receptors™ PCR Array plates. The PCR plates were analyzed on the Roche LightCycler® 480 system. The statistical comparisons were performed on the data analysis center of the manufacturer (https://www.qiagen.com/us/products/genes%20and%20pathways/data-analysis-center-overview-page/). The changes in the expression profile were considered relevant for a gene if an absolute fold regulation of at least 2-fold was detected after t-test based statistical comparison of the reference group (RNA of PDAC cells derived from KC mice) with the experimental groups (RNA of PDAC cells derived from KPC, TPC or TPAC mice).

Affymetrix GeneChip® Expression Array

To further decipher differentially regulated pathways that may affect neuropathy and NI in GEMM of PDAC, a microarray expression analysis with the mouse PDAC cells was performed. For this purpose, total RNA form at least three different mouse PDAC cell lines derived from each of the four mouse lines (KC, KPC, TPC, TPAC) was isolated with the RNEasy Plus Mini Kit (Qiagen, Hilden, Germany) according to the manufacturer's instructions to obtain at least 900 ng RNA/µl. The samples were analyzed at the "*Kompetenzzentrum für Fluoreszente Bioanalytik"* (Regensburg, Germany) via the Affymetrix GeneChip® Mouse gene 1.0 ST array. The subsequent pathway analysis was performed via the Gene Set Enrichment Analysis (GSEA) v2.1.0 software of the Broad Institute (Cambridge, MA, USA) to include KEGG-based pathway analysis.

Assessment of mechanical abdominal hyperalgesia and open-field behaviour

To compare the impact of tumor growth on the pain sensation of the GEMM, mechanical hypersensitivity was tested via von Frey filaments (Stoelting Co., IL, USA) of increasing tactile stimulus intensity by applying each filament type 10 consecutive times from the bottom of a grid on the abdominal area. The exploratory behaviour of mice was investigated in an open-field white plastic box (50x50x50cm) made of polyvinyl chloride (PVC) that was evenly illuminated. Prior to all hyperalgesia and open-field tests, mice were allowed to accommodate to the experiment room for 3-6 hours, subsequently placed in the open field, and their exploratory behavior was recorded for 2 minutes and 5 consecutive times. These videos were then analyzed for the locomotion path length of the mice via the MTrack2 plugin of the ImageJ software.

Statistical analysis

Statistical analysis was performed using the GraphPad Prism 5 Software (La Jolla, CA, USA). The unpaired t-test or Mann-Whitney U test was applied for two-group analysis depending on the parametric/non-parametric nature of the data. To compare more than two groups, the one-way analysis of variance followed by the Bonferroni's post hoc test or Kruskal-Wallis test followed by the Dunn's test for multiple comparisons was used. Results are expressed as mean ± standard error of the mean (SEM). Two-sided p-values were always computed, and an effect was considered statistically significant at a p-value ≤ 0.05.

Results

Localization of nerves in and around the pancreatic tumor in GEMM of PDAC

The proper analysis of innervation in an organ necessitates the identification of the exact localization, density and quality of nerve fibers in the tissue. Such analyses are widely lacking for the human and mouse pancreas, and even more for the innervation pattern of mouse PDAC. Therefore, in the first part of the study, the pancreatic tumor sections were analyzed in their entirety for the localization and course of nerves in the tissue. In the immunolabeling with the pan neural-marker PGP9.5, nerves could be localized at some typical locations in and around the pancreas. First of all, largest nerve trunks were concentrated around the peripancreatic lymph nodes that lie within the mesentery (Figure 8A-B). From this location on, nerve fibers or smaller nerve trunks were found to penetrate into the pancreatic tissue along few entry sites, usually 2-3 per section, and extend along intrapancreatic, interlobular large septae into the tissue (Figure 8B). Hence, true nerve “trunks” were only visible along these septae that contain blood vessels, or in the proximity of peripancreatic lymphoid structures. This observation represents a major difference from the normal human pancreas in which relatively large nerve trunks are readily encountered within the parenchyma (Ceyhan et al., 2009). Therefore, it seems imperative to include these perilymphoid nerves into the analysis of mouse innervation in any study. Importantly, though, in the present analysis, when tumor-induced neuroplasticity was observed, these altered nerves were predominantly located away from these perilymphoid nerves and detected in the core of the desmoplastic tumor areas (Figure 8C). Therefore, despite the concentration of nerves around peripancreatic lymph nodes in the normal mouse pancreas, a true intratumoral neuroplasticity in GEMM of PDAC seems to exist in the tumor stroma depending on the model.

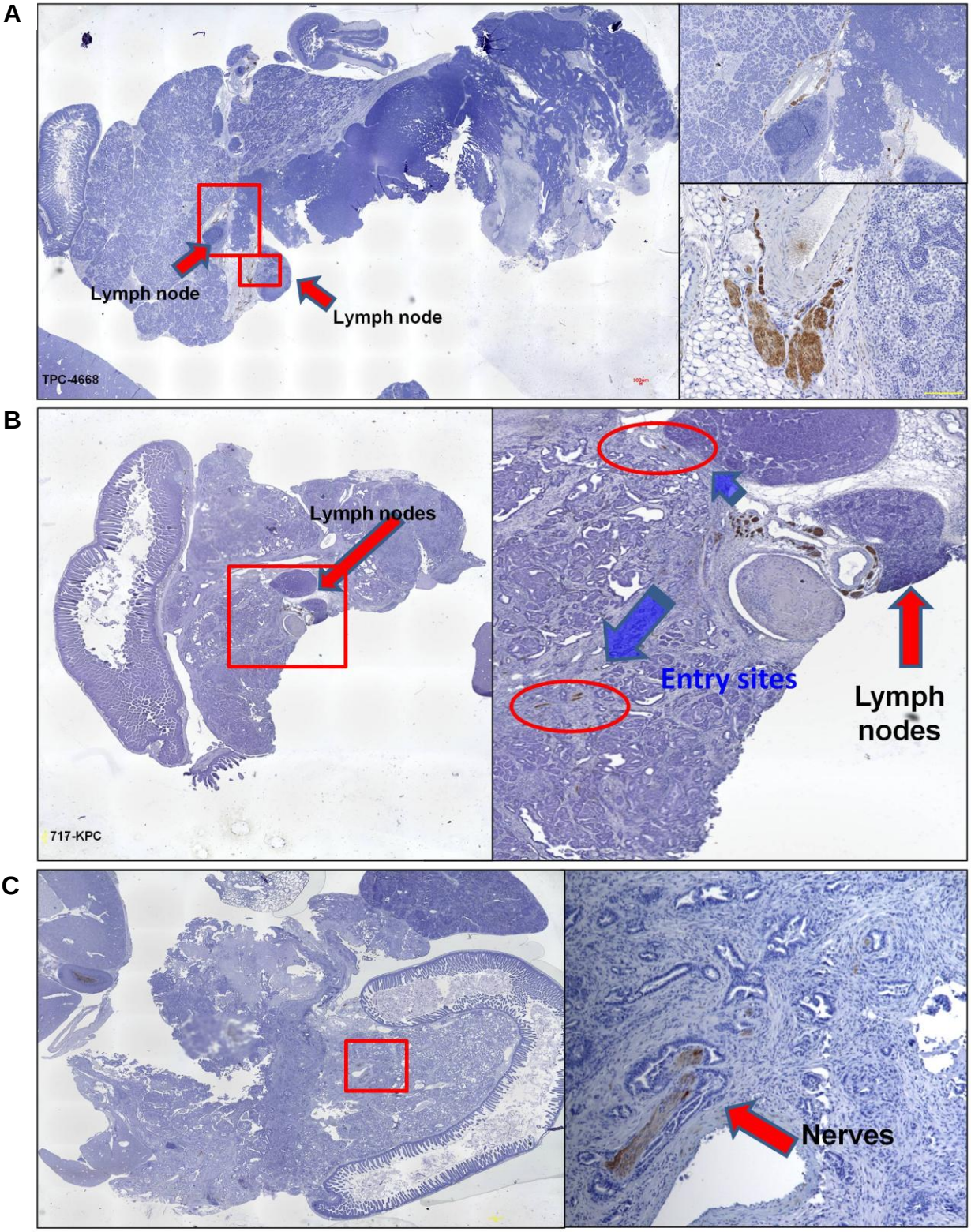

Figure 8. Localization of nerves in the mouse pancreas. (A-B) The mouse pancreas is a "mesenteric type" pancreas that is surrounded by several peripancreatic lymph nodes along its borders. Immunostaining of mouse pancreas with the neural marker PGP9.5 detects the majority of pancreas-innervating nerves around the peripancreatic lymph nodes. In serial sections, smaller caliber nerves are detected to enter the pancreatic parenchyma along few fibrous septae ("entry sites"). (C) In mouse PDAC tissues that harbor true neuropathy, enlarged invaded nerve trunks are detected in the core of tumor, independent of the nerve presence around pancreatic lymph nodes.

Tumor innervation is augmented in all GEMM of PDAC

In the next step, the density and size of all nerves present on each pancreatic tumor section of the analyzed mice were quantified and compared. As the control group, KC mice that are yet in PanIN stage and have not developed overt cancer, have been analyzed. Here, the mean density of nerves per unit area of tumor was prominently increased in KPC (0.79 ± 0.24 nerves per mm^2 tissue), KPAC (0.56 ± 0.17 nerves per mm^2), TPAC (0.38 ± 0.12 nerves per mm^2), and Ela-LTαβ (0.58 ± 0.20 nerves per mm^2) mice when compared to KC mice (0.23 ± 0.17 nerves per mm^2, Figure 9). The nerve density in the KPC-electro and TPC mice tumors was not different from the nerve density of KC mice (Figure 9). The comparison of nerve size in these tumor tissues, though, showed that the mean neural size only in the TPC (5,181 ± 1,382 μm^2), KPC-electro (3,323 ± 1,124 μm^2), and KPAC (3,787 ± 1289 μm^2) mice was somewhat higher than in KC mice (2,107 ± 759 μm^2), however, this difference did not reach statistical significance in the present analysis (Figure 9). Therefore, the tumor models with increased neural density did not exhibit neural hypertrophy, and vice versa, the models with increased mean neural size did not include more nerves in the pancreas.

To express this reciprocal behavior of neural density and size in these GEMM via a single numeric variable, the nerve density and size in the tissues were multiplied and proportioned to the total tissue area to generate a "*total innervation index*". In all analyzed models, except for the Ela-LTαβ chronic pancreatitis model 0.17 ± 0.10 %), the total innervation index was far higher (KPC: 0.84 ± 9.38 %, KPAC: 1.02 ± 0.36 %, KPC-electro; 1.4 ± 0.68 %, TPC: 0.79 ± 0.16 %, TPAC: 0.96 ± 0.37 %) than in KC mice (0.23 ± 0.13%, Figure 9). Hence, the total tumor innervation is enhanced in all GEMM of PDAC when compared to the precursor stage of PDAC or to murine chronic pancreatitis.

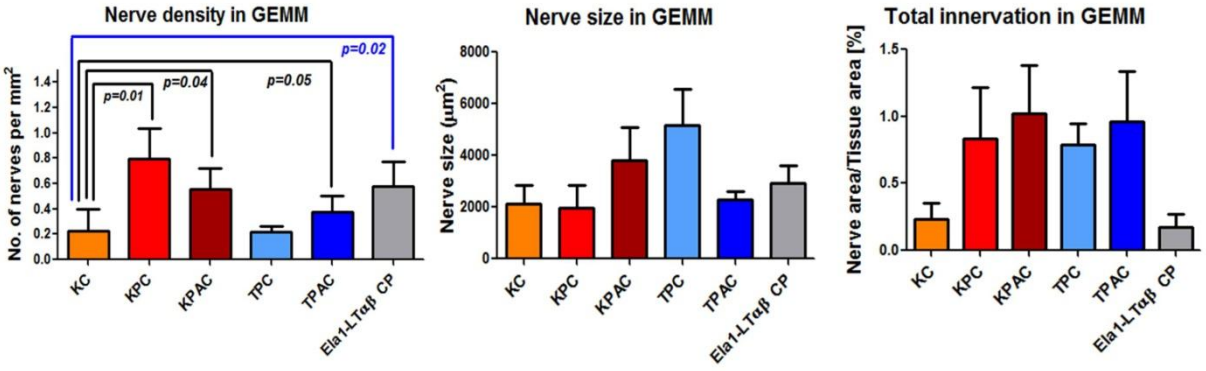

Figure 9. Nerve density and size in GEMM of PDAC. Left: When compared to the preneoplastic KC mice, mice from the KPC, KPAC and Ela1-LTαβ-models exhibit greater nerve density. Middle: Conversely, the remaining models are rather characterized by a greater mean neural size. Right: Hence, when these parameters are multiplied to generate a total innervation index, all GEMM of PDAC, but not the transgenic Ela1-LTαβ model of CP, harbor greater pancreatic innervation when compared to KC mice.

Time course analysis of tumor innervation during carcinogenesis in GEMM of PDAC reveals distinct age-dependent peaks

It is conceivable that the above-depicted tumor hyperinnervation in GEMM of PDAC may be dependent on the age of the mice, or that these alterations may be more pronounced in certain stages of the tumor development in a model-specific manner. Therefore, in the next step, the nerve size and nerve density in these GEMM of PDAC were correlated to the age of the analyzed mice. This analysis yielded distinct and divergent tendencies between these models with regard to the dynamics of tumor innervation. For example, in the KPC model, both the nerve size and density were highest in the earliest analyzed ages between 49-51 days of age (nerve density for 49 days: 2.12 nerves per mm^2, nerve area: 7591.5 μm^2) and rapidly declined toward the end of the life span of these mice around 61 days (nerve density for 61 days: 0.1 nerves per mm^2, nerve area: 621.5 μm^2, Figure 10). In the TPC mice, there were two distinct peaks, detectable around 200 days and 300 days of age, which again rapidly declined toward the end of life in these animals (nerve density for 200 days: 0.68 nerves per mm^2, nerve area: 11,312 μm^2; nerve density for 300 days: 0.79

nerves per mm^2, nerve area: 12,348 µm2; Figure 10). In the TPAC model, there was a single prominent peak in the nerve density toward 570 days of age (nerve density: 2.6 nerves per mm^2, nerve area: 2,967 μm^2, Figure 10), and both the nerve size and density declined in the oldest animals at 689 days of age (nerve density: 0.02 nerves per mm^2, nerve area: 1,551 μm^2, Figure 10). On the other hand, in KC mice, there were two peaks of highest nerve size and density in the life span of animals, one around 230 days (nerve density: 0.14 nerves per mm^2, nerve area: 6,245 μm^2), the other around 500 days of age (nerve density: 0.13 nerves per mm^2, nerve area: 3,279 μm^2, Figure 10). Collectively, these observations suggest that KPC mice exhibit tumor hyperinnervation around 10-20 days before death, and the rapidly invasive overgrowing tumor seems to destruct neural structures in the tumor. In the TPC model, the observed two peaks may be due to the promotion of neural growth via TGFalpha that is secreted from the remaining elastase-containing, transforming acinar cells, followed by a later peak induced by cancer-cell-derived growth factors during overt cancer. In the TPAC model that is characterized by a slower carcinogenesis, the neural growth seems to undergo a progressive evolution in parallel with tumor growth and to eventually succumb to the overgrowing tumor at the end of life. Overall, these observations create an important basis for future identification of the best “neuroplasticity window” in the analysis of innervation in these GEMM models.

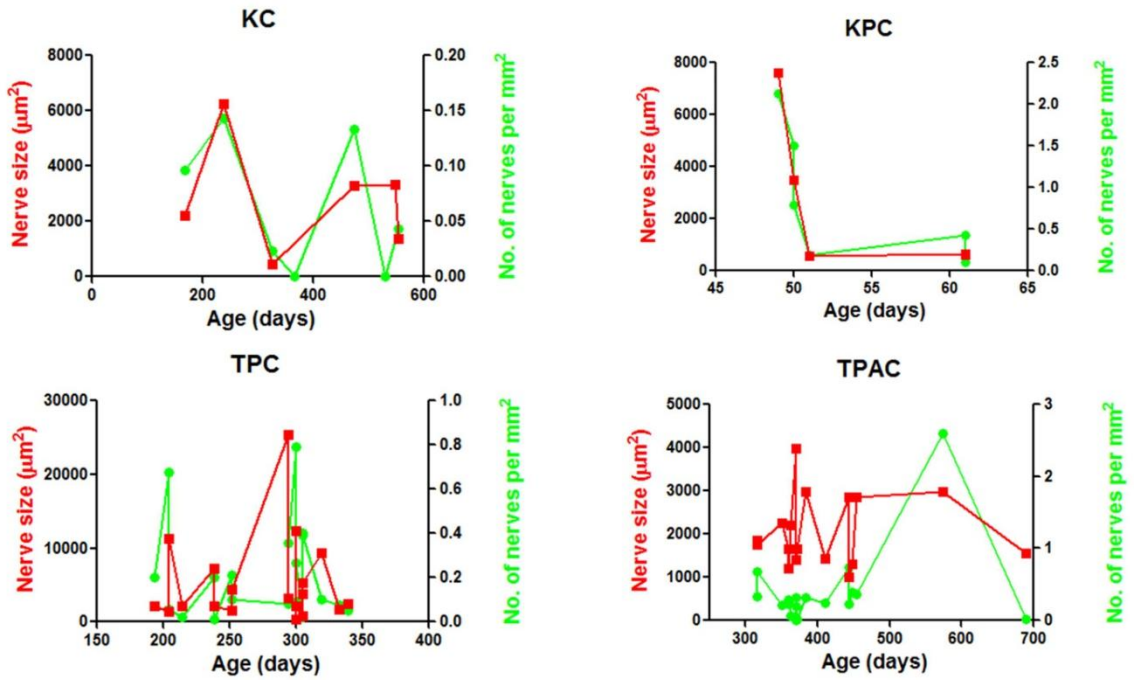

Figure 10. Time course analysis of nerve size and density in the four core GEMM of PDAC. The analysis of nerve density and size in GEMM of PDAC at different ages reveals distinct peaks (KC: 230 and 500 days, KPC: 50 days, TPC: 200 and 300 days, TPAC mice: 570 days) in innervation. In all models, the destructive tumor growth seems to result in rapid decline in tumor innervation toward the end of the life span of these mice.

Current GEMM of PDAC do not harbor true pancreatic neuritis

Pancreatic neuritis represents an insufficiently understood feature of pancreatic neuropathy in PDAC and chronic pancreatitis. It is known to correlate to the presence of pain, and the inflammatory cell population that comprise pancreatic neuritis include cytotoxic T lymphocytes, macrophages, and mast cells, with increased amounts of perineural mast cells among patients with painful disease (Demir et al., 2013). This phenomenon has not yet been even mentioned in any of the studies that made use of GEMM of PDAC. Therefore, all pancreatic nerves in the GEMM of PDAC were analyzed in the present study for the presence of pancreatic neuritis. The human pancreatic neuritis is characterized by a very conspicuous conglomerate of inflammatory cells surrounding nerves (Figure 11A-B). Importantly, one can easily recognize that these inflammatory cell conglomerates do not simply represent a subpopulation or continuation of inflammatory cells that are anyway prevalent in the

tumor tissue, but they are rather a clearly demarcated group of cells that seem to target the nerves. Therefore, in the present study, the presence of such specific “perineural inflammatory cell conglomerates” was searched in the GEMM of PDAC. Although all GEMM harbored quite remarkable amounts of immune cells in the stroma, these immune cells appeared as diffusely tumor-infiltrating cells, detectable nearly in all parts of the tumor tissue, without any predilection for the perineural regions (Figure 11C). In the next step, the severity of immune cell penetration into nerves from these diffusely infiltrating immune cells was quantified. Here, all analyzed models, but particularly the KPC model demonstrated frequent and deep (i.e. endoneural) infiltration of nerves by inflammatory cells, corresponding to higher neuritis severity scores (0.87 ± 0.17) when compared to KC mice (0.27 ± 0.11, Figure 11D). However, none of the models contained nerves that exhibited the perineural immune cell conglomerates that resemble the human pancreatic neuritis in PDAC or chronic pancreatitis.

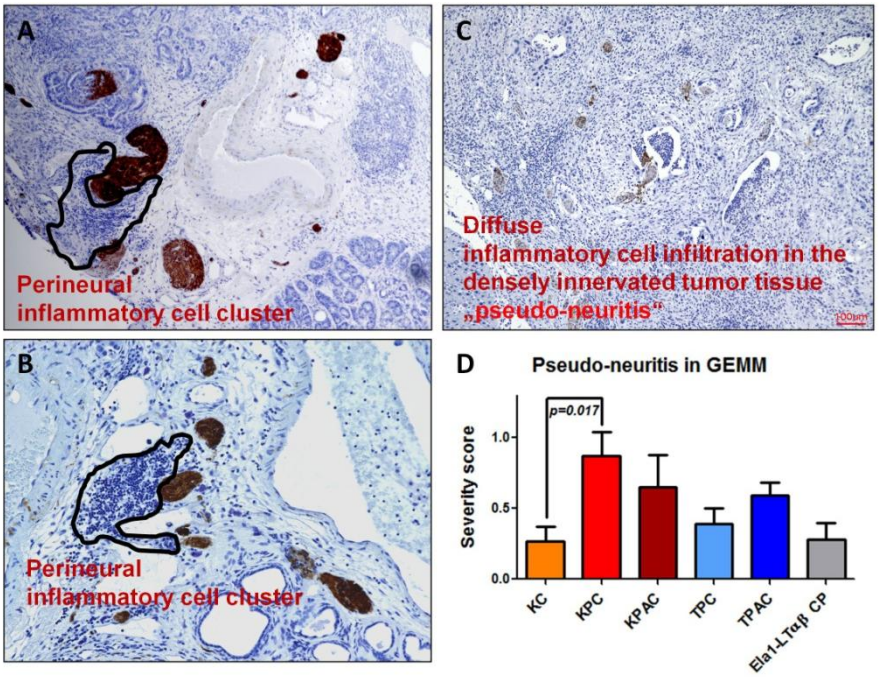

Figure 11. The difference between true pancreatic neuritis and “pseudo-neuritis”. (A-B) Human pancreatic neuritis is characterized by immune cell conglomerates arounds intrapancreatic nerves (demarcated by the black line). In the total of ca. 1,250 nerves analyzed in this study, there were only two nerves that exhibited human-like pancreatic neuritis. Hence, a true pancreatic neuritis seems not to exist in the analyzed GEMM of PDAC. (C) Rather, in all these models, the tumor stroma was diffusely infiltrated by inflammatory cells that were naturally also in the proximity of intrapancreatic nerves. This unavoidable presence of immune cells around nerves in the

inflamed tumor stroma is herein termed “pseudo-neuritis”. (D) The severity of pseudo-neuritis was most pronounced in the KPC model. However, it is questionable, whether such a pseudo-neuritis has relevance for the study of neuropathy in GEMM of PDAC, since a specific spatial association with nerves seems to be absent.

TPAC model of PDAC is the first GEMM that exhibits human-like neural invasion

Human NI assumes a typical conformation. In perineural invasion, cancer cells align along the overwhelming circumference of the epineurium and appear to “tightly encircle” the nerve. The pioneering studies on the KPC model reported to have observed NI in these models, asserting another human-like feature of these models. Yet, in our experience, careful appraisal of the provided images in these publications and the analysis of images provided by personal communication with several research groups working in this field revealed that all these models do not harbor NI that exhibits the above-described conformation of human NI in PDAC. Rather, what these studies put forward as NI are mere epineural associations or the mere presence of cancer cells around the nerves, without any visible encircling activity (Figure 12). In the present study, a two-armed analysis of perineural cancer cell activity was performed. In the first part, the frequency of epineural cancer cell associations was quantified in all GEMM. Indeed, all the GEMM of PDAC exhibited, as opposed to the KC model, frequent presence of cancer cells around nerves (severity score for KPC: 0.45 ± 0.16, for KPAC: 0.35 ± 0.14, for TPC 0.44 ± 0.14, for TPAC 0.50 ± 0.11, for KPC-electro; 0.13 ± 0.07, KC: 0.09 ± 0.04, Figure 12, 13B). However, these cancer cells obviously appeared to not belong to a group of cancer cells that aligned around the nerve in an infiltrative manner, but rather appeared to be more or less occasionally present in the vicinity of nerves.

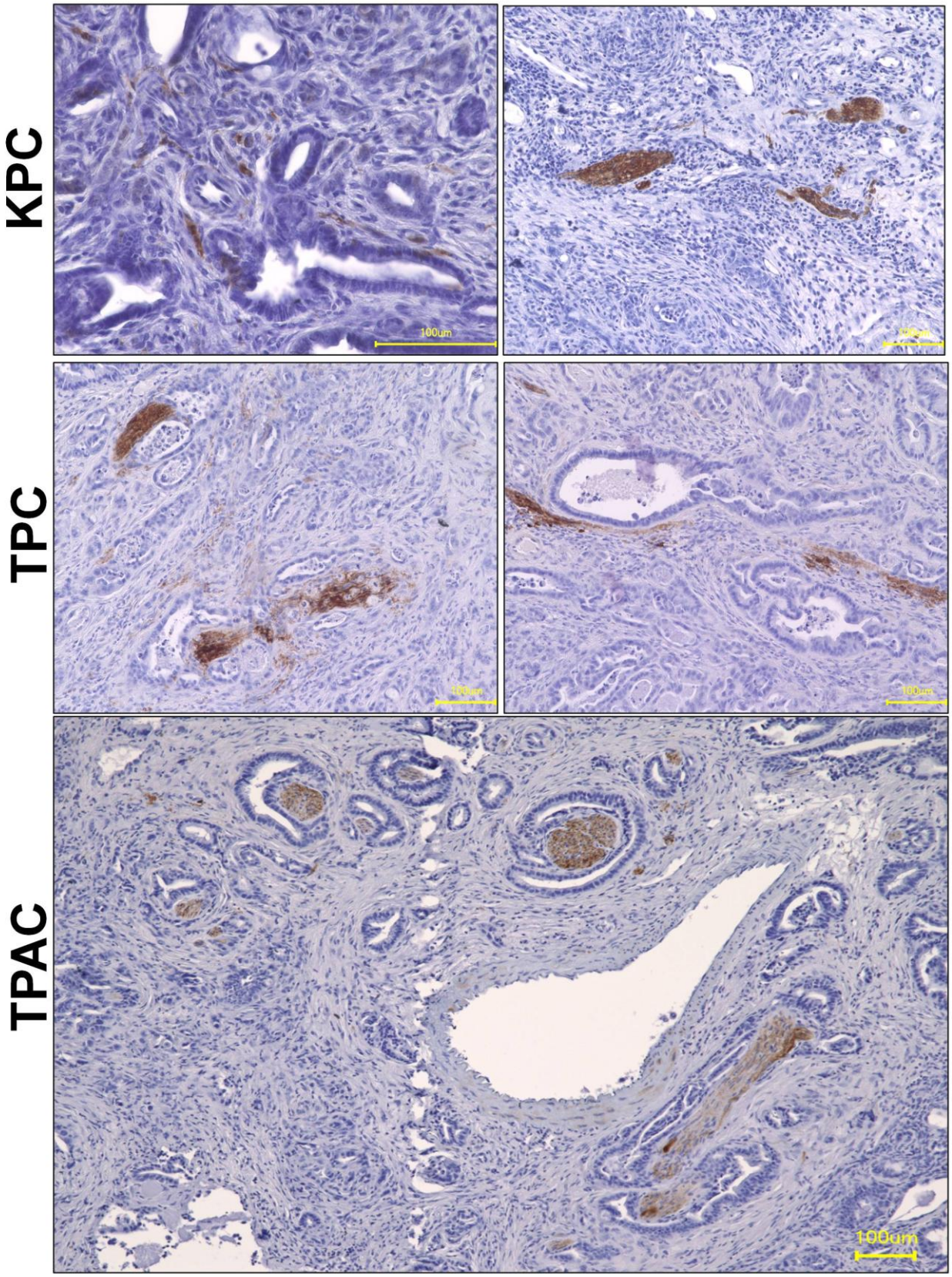

Figure 12. Comparison of neural invasion (NI) morphology in GEMM of PDAC. In the KPC model, PGP9.5 immunostained (brown) nerves are occasionally found to be “in touch” with cancer cells (left), yet frequently to have not contact at all (right). In the TPC model, there are frequent sites of contact between nerves and cancer cells, where cancer cells lie at least on one side on the nerves. However, in the TPAC model, cancer cells literally “embrace” nerves around the majority of their borders, corresponding to true NI.

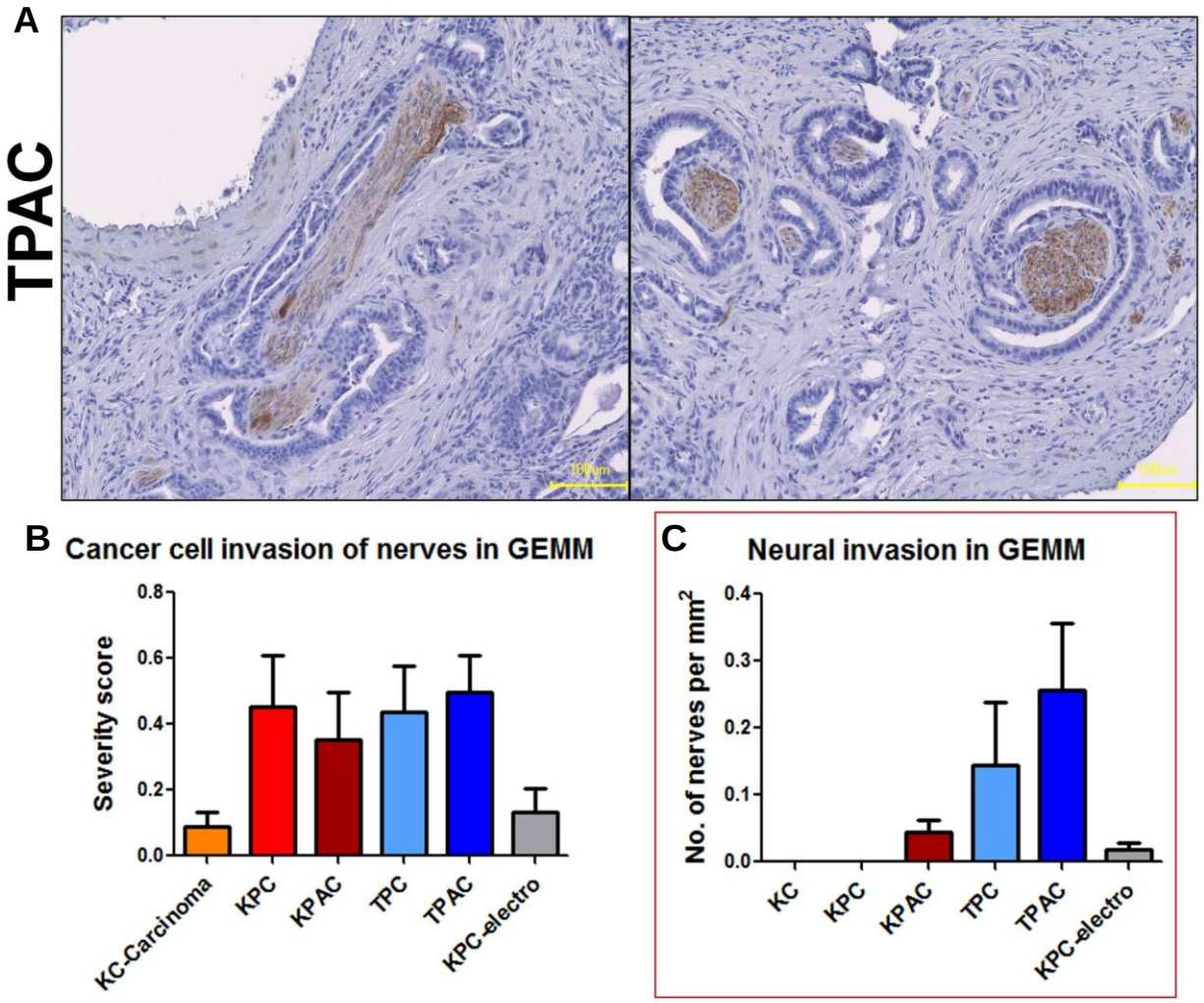

Figure 13. Quantification of unspecific and true neural invasion (NI) in GEMM of PDAC. (A) The TPAC model was herein identified as the only GEMM with true NI, in which cancer cells encircle nerves during NI. (B) In the quantification of tumor infiltration in or around nerves, cancer cells were encountered in or around nerves in all GEMM of PDAC when compared to the KC model. (C) However, when true NI was considered, the TPAC model exhibited the greatest NI severity, followed by the TPC model.

Careful appraisal of the invasion morphology revealed a promising finding for modeling NI in GEMM of PDAC. Whereas a true, human-like NI was not seen in the KC or KPC mice, there were few tissue spots with perineurally invaded nerves in TPC mice (Figure 12). Importantly, though, in 9 out of the 15 analyzed TPAC mice, multiple, prominent sites of true perineural invasion were observed, in which cancer cells appeared to propagate along nerves and not to coincidentally reside due to diffuse cancer cell infiltration (Figure 12, 13A). Therefore, the knockout of the RelA/p65 with the slower tumor progression in this model resulted in the emergence

of true NI in these mice. In accordance with the proposed role of RelA/p65 in this process, analysis of KPAC mice revealed very few sites of true NI as opposed to KPC mice that did not exhibit any true NI at all (Figure 13C). Furthermore, in one of the analyzed KPC-electro mice, there were few intratumoral nerves that resembled human-like NI (Figure 13C). Correspondingly, the quantification of NI severity in the GEMM of PDAC showed remarkably greater NI severity scores for TPAC mice (0.26 ± 0.10) when compared to the remaining mouse models (TPC: 0.14 ± 0.09, KPAC: 0.04 ± 0.02, KPC-electro: 0.02 ± 0.01, KPC: 0.0 ± 0.0, KC: 0.0 ± 0.0, Figure 13C). Hence, possibly as the most important finding of the study, the novel TPAC model was identified to exhibit human-like NI.

The neuro-invasiveness of TPAC mice can be recapitulated in a 3D migration assay

The histological identification of NI in the TPAC model necessitated functional investigation of cancer cells derived from this model for their neuro-invasive ability. A recently described 3D heterotypic migration assay enables the simulation of NI in vitro, since neurotropic cancer cells demonstrate enhanced migration toward DRG neurons in this assay (Ceyhan et al., 2008). For this purpose, DRG neurons from C57BL/6J mice were confronted with the cancer cells from the core GEMM in this study, i.e. with KPC, TPC and TPAC cancer cells, simultaneously in a geometric-matrix-like-conformation (Figure 14). For each GEMM cancer cell type, the migration of the cancer cells facing the murine DRG (“migration front”/MF) and those facing the empty control matrix suspension on the opposite side (“back front”/BF) was quantified and compared via digital time-lapse microscopy. In this analysis, more targeted migration is represented by a greater forward migration index (FMI), and a positive difference between the FMIs of MF versus BF corresponds to a specific targeted

migration. In the present analysis, all the three analyzed major GEMM cells migrated with a greater velocity at their MF than at their BF (KPC-MF: 0.16 ± 0.01 µm/min, KPC-BF: 0.12 ± 0.01 µm/min; TPC-MF: 0.10 ± 0.01 µm/min, TPC-BF: 0.04 ± 0.002 µm/min; TPAC-MF: 0.15 ± 0.01 µm/min, TPAC-BF: 0.11 ± 0.01 µm/min, Figure 14). For the TPC cells (that in vivo exhibited only occasional but still some true NI) and for the TPAC cells (that had pronounced true NI in vivo), the net linear (Euclidean) distance was also greater at the MF than at the BF (TPC-MF: 55.90 ± 5.26 µm, TPC-BF: 28.51 ± 2.32 µm, TPAC-BF: 83.08 ± 9.60 µm, TPAC-MF: 131.1 ± 17.19 µm, Figure 14) as opposed to the similar Euclidean distances of KPC cells at the MF (123.5 ± 6.58 µm) and BF (114.5 ± 12.49 µm). Strikingly, in the analysis of directionality, the difference in the FMIs of MFs versus BFs was greatest for the TPAC cells: Here, KPC cells only demonstrated negative FMI values, i.e. the KPC cells at the migration front migrated away from the neurons (FMI for KPC-MF: -0.12 ± 0.03, KPC-BF: -0.17 ± 0.03). In accordance with the in vivo detection of NI, the TPC and TPAC cells both exhibited positive and greater FMI values at their MF than their BF, where this difference was much more prominent for TPAC cells (TPAC-MF: 0.23 ± 0.03, TPAC-BF: 0.03 ± 0.03; TPC-MF: 0.03 ± 0.003, TPC-BF: -0.12 ± 0.03; Figure 14). As an additional control cell type, cancer cells derived from KC mice that had progressed to overt cancer after 12 months were used in a four-armed simultaneous comparison assay including these KC-carcinoma cells, KPC, TPC and TPAC cells (Figure 15). In this setting, the migration velocity of the four GEMM PDAC cell types toward DRG was comparable (KC-carcinoma: 0.17 ± 0.01 µm/min, KPC: 0.20 ± 0.01 µm/min, TPC: 0.18 ± 0.01 µm/min, TPAC: 0.19 ± 0.01 µm/min, Figure 15). In the comparison of the Euclidean distances, KPC and TPAC cells (as in the previous 3-armed comparison setting) covered longer Euclidean distances when compared to TPC or KC-carcinoma cells (KC-carcinoma: 88.67 ± 9.36 µm, KPC: 122.1 ± 8.53 µm,

TPC: 81.78 ± 8.97 µm, TPAC: 110.2 ± 9.33 µm, Figure 15). Moreover, also in this setting, the FMI of TPAC cells toward DRG exceeded that of all other analyzed GEMM cells (KC-carcinoma: 0.09 ± 0.04, KPC: -0.22 ± 0.05, TPC: 0.09 ± 0.03, TPAC: 0.32 ± 0.03, Figure 15). Hence, in two different 3D migration and neuroaffinity settings using multiple GEMM cells, the current study demonstrated the greater intrinsic neuro-affinity of murine PDAC cells derived from TPAC mice when compared to the other GEMM that largely lacked any neuro-affinity. Therefore, the *in vivo* neuro-invasive ability of TPAC cancer cells was reproducible and attributable to the neuroaffinity of the cancer cells of this GEMM of PDAC.

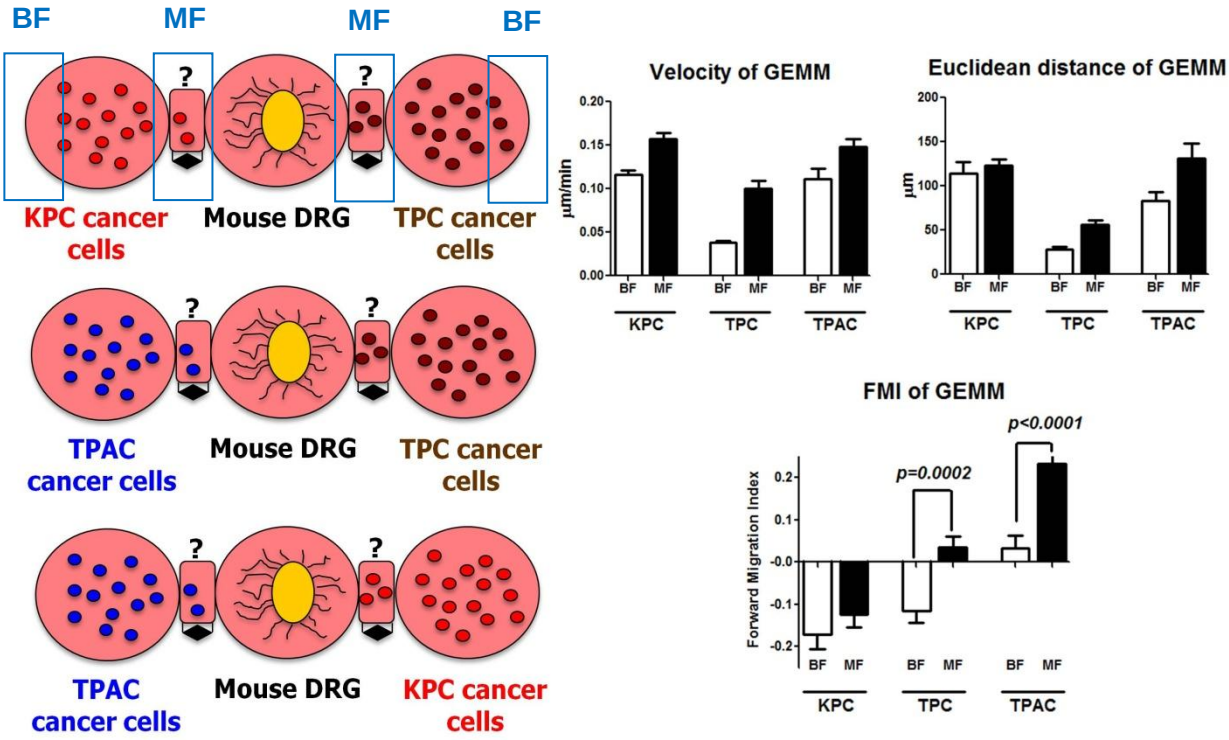

Figure 14. The neuro-invasiveness of GEMM cancer cells in the 3D migration assay. Mouse DRG were dissociated, suspended in an extracellular matrix (ECM) gel and confronted with GEMM cancer cells. The migration of the GEMM cancer cells facing neurons (at the migration front/MF) or an empty gel suspension (back front /BF) was tracked via digital time-lapse microscopy and quantified with the chemotaxis and migration tool of Ibidi. Here, the mean velocity and Euclidean (linear) distance of migration toward DRG neurons did not differ between KPC, TPC and TPAC cancer cells. However, the forward migration index (FMI) that signifies the extent of targeted (non-coincidental) migration toward neurons was greatest at the MF of TPAC cells, followed by TPC cells. Conversely, there was no difference in the FMI of the MF and BF of KPC cells, signifying no neuro-invasiveness.

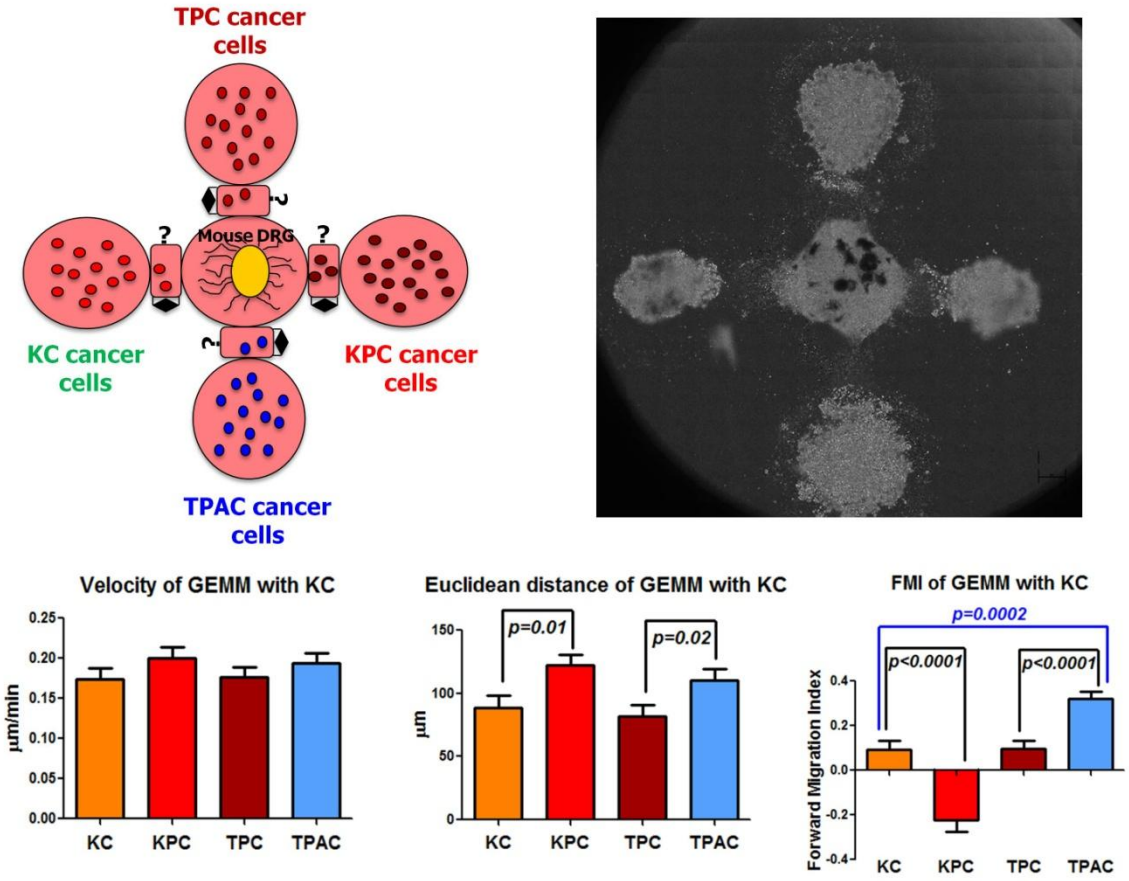

Figure 15. Comparison of the neuro-invasiveness between KC, KPC, TPC and TPAC GEMM cancer cells. As an additional control cell type, cancer cells from KC mice that progressed to overt cancer were used in the 3D migration assay simultaneously with KPC, TPC and TPAC cancer cells. Here, the velocity of migration did not differ between the four cancer cell types. KPC and TPAC cancer cells covered longer Euclidean distances than KC and TPC mice cells. In analogy with the previous analysis, the TPAC cancer cells had the highest FMI, followed by TPC and KC cells. The FMI of KPC cells was, also here, negative.

All GEMM of PDAC have neurotrophic attributes that are in accordance with the tumor hyperinnervation

In order to study neuroplastic alterations in a functional manner, it is essential to develop *in vivo* and *in vitro* tools that model the alterations in the murine models. Therefore, in order to simulate the increase in total innervation of the tumors in the examined models, an in vitro neuroplasticity model was applied, that in a slightly modified version, was shown to model the increased neurite density and neuronal hypertrophy that characterize human pancreatic neuroplasticity (Demir et al., 2010). In the present study, DRG neurons isolated from C57BL/6J mice via a previously

demonstrated technique (Demir et al., 2014) were cultivated in the serum-free supernatants of the four core GEMM cancer cells and quantified for their neurite density. Furthermore, the serum-free normal growth medium of the DRG neurons and the serum-free medium supplied with 10ng/ml NGF were used as negative and positive control, respectively.

The typical neurite density of DRG neurons cultivated in their serum-free normal growth medium in this assay lies around 1.0 neurite per 2500 μm^2 culture area. The positive control NGF induces strong neuronal sprouting with a neurite density that is the double that of the negative control, i.e. around 2.0 neurites per 2500 μm^2. In comparison, the GEMM cancer cell supernatants induced a ca. 50% increase in the neurite density of the murine DRG neurons (Figure 16). Specifically, the neurite density induced by KPC cell line supernatants equaled 1.56 ± 0.15, by TPC was at 1.41± 0.10, and by TPAC reached 1.70 ± 0.23 neurites per 2500 μm^2. On the other hand, supernatants of KC mice that had progressed to carcinoma induced the astonishingly highest neurite density in DRG neurons, reaching 1.93 ± 0.18 neurites per 2500 μm^2 (Figure 16). Although this observation may at first glance contradict the low nerve density of KC mice reported on Figure 9, it should be considered that the histological analysis involved KC mice at PanIN stage, and the cells were derived from the overt cancer of ca. 12 month-old animals. Therefore, the histologically observed hyperinnervation in all GEMM of PDAC correlated to the increased neurite density in this neuroplasticity assay and was reproducible *in vitro* for future functional approaches.

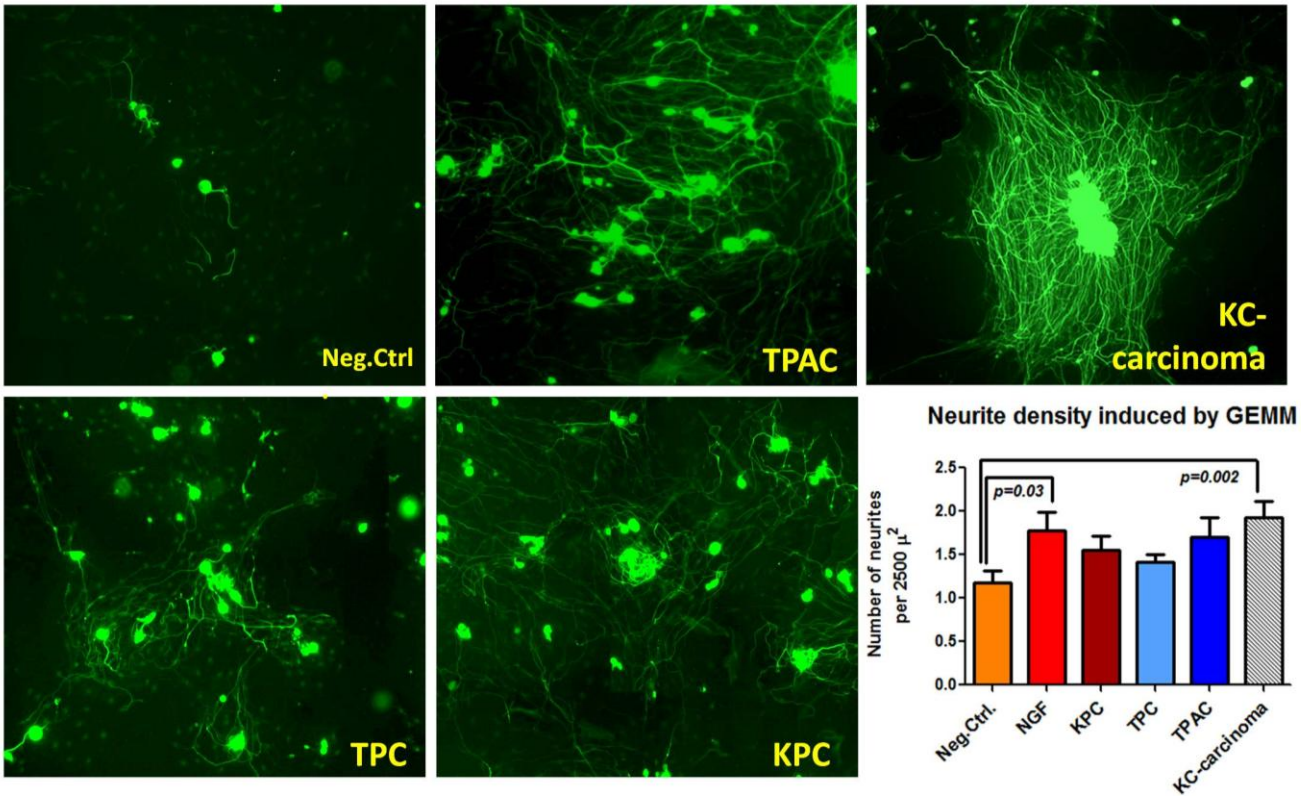

Figure 16. Neuroplastic potential of GEMM PDAC cancer cells. Newborn mouse DRG were treated with the supernatants of KPC, TPC, TPAC, KC-carcinoma cells for 48 hours and compared for their neurite density to DRG neurons kept in their serum-free medium (Neg. Ctlr.) or to neurons treated with recombinant human nerve growth factor (NGF, 10ng/ml). Here, all GEMM PDAC cells resulted in increased neurite density of mouse DRG neurons when compared to the control conditions, and the highest neurite density was induced by KC-carcinoma cell supernatants.

Schwann cell emerge around PanIN lesions during pancreatic carcinogenesis

An important focus of the present study was to analyze the reaction of Schwann cells of peripheral nerves during pancreatic neuropathy and neuroplasticity in GEMM of PDAC. Schwann cells (SC) can be readily identified by several specific markers. Although several studies employed one or two markers to identify these cells, in order to exclude potential labeling of other neural-crest-derived cells, an immunolabeling combining four SC-markers, i.e. GFAP, S100, Sox10, and ALDH1L1 was performed to detect these glial cells with the highest possible certainty. Importantly, myelin-associated markers were not used since pancreatic SC as SC of a visceral organ with non-somatic nerves would be expected to belong to the non-myelinating SC subfamily. In the normal mouse pancreas, immunostaining with these

markers labeled SC only within intrapancretic nerves (Figure 17A). In KC mice that are around 150-200 days of age, SC markers detect a very specific cell population that is only and unexceptionally detected around PanIN lesions (Figure 17B). In KC mice, these cells that are labeled by these glial markers are not detected in any neighboring remaining normal parechymal regions or other cancer-tissue structures (Figure 17B). A similar cell population that is immunolabeled by these four markers was detected in KPC tissues. Here, cells that were labeled by these glial markers were detected to be diffusely distributed in not too high numbers in the tumor stroma (Figure 17C). Correlative labeling of human PDAC tissues revealed that these markers detected either SC that were extending from the distorted and enlarged intratumoral nerves lacking their defined epineural lining into the stroma, or SC that were again detectable in the vicinity of cancer cells (Figure 17D). Hence, these observations revealed the presence of 1) a SC population that is specifically detectable around PanINs in KC mice, and 2) nerve-independent SC (possibly originating from the structurally distorted nerves) diffusely found in tumor stroma. Therefore, the amount of SC around PanINs and PDAC cells was quantified in KC and KPC mice and compared to normal murine pancreas. Here, the proportion of PanIN lesions surrounded by SC in the KC pancreas laid at 78.85 ± 3.59% of all PanIN lesions. The proportion of PDAC cell clusters surrounded by SC in KPC mice was around 43.15 ± 13.72% in KPC mice. Conversely, no SC were detected around pancreatic acini or ductal cells in the normal C57BL/6J pancreas (Figure 17A). Overall, these resulted suggested that SC seem to emerge around PanIN and cancer cells during pancreatic carcinogenesis, suggesting a potential “carcinotropism” of SC.

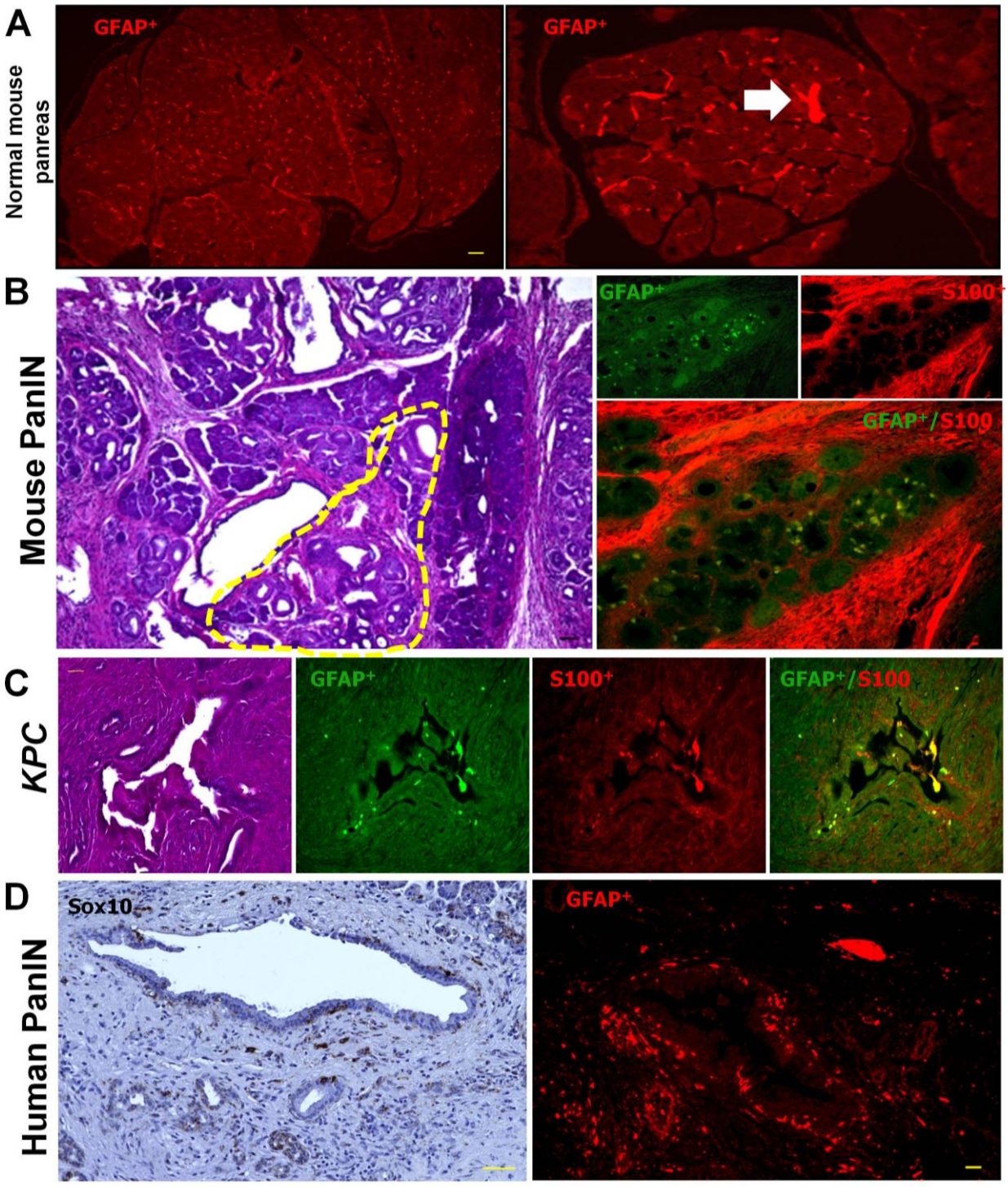

Figure 17. Schwann cells emerge around PanIN and cancer cells in murine and human PDAC. (A) In the normal mouse (C57BL/6J) pancreas, immunolabeling with the glial marker GFAP detects glia cells either in large nerve trunks (white arrow) or in the interlobular septae. (B) In KC mice that develop PanIN lesions, GFAP/S100 labeled putative glial cells are detected specifically within regions that contain PanINs (demarcated by the yellow dashed line) and not in normal pancreatic regions. (C) In KPC mice with overt cancer, GFAP/S100 labeled cells are detected in association with these cancer clusters. (D) In analogy, early precursors like PanIN-I lesions in human tissues contain Sox10+ or GFAP positive cells that are in close spatial association with PanIN lesions. The yellow scale bars indicate 50 µm.

A novel 3D Schwann cell outgrowth assay reveals the greatest glial chemoattraction toward TPAC cancer cells

To test the possibility of SC chemoattraction to PDAC cells, a novel 3D SC outgrowth assay was established. Here, a ca. 3mm measuring segment of the C57BL/6J sciatic nerve was explanted and placed perpendicularly on a 35mm dish next to a suspension of extracellular matrix (ECM) containing the cancer cells derived from the GEMM of PDAC in this study (Figure 18). The premise behind this assay is that in the presence of true chemoattraction of SC to cancer cells, SC that grow out of the two transsected ends of the sciatic nerve segment would have to bend their initially vertical growth path toward the cancer cell suspension. Indeed, around 72 hours after the placement of the nerve segment and the cancer cell suspension, the cancer cells that initially migrated vertically out of the nerve segment made a “U turn” toward the cancer cell suspension (Figure 18). This peculiar migration was documented via digital time-lapse-microscopy, and in analogy with the previously described 3D migration assays, quantified for the extent of carcinotropic SC migration toward the different GEMM PDAC cells. SC that migrated out of the sciatic nerve did not differ with regard to their velocity of migration or the travelled Euclidean distance toward the four GEMM cell types (KC-carcinoma-velocity: 0.44 ± 0.05 µm/min, KC-carcinoma-Euclidean distance: 104.6 ± 14.48 µm; KPC-velocity: 0.47 ± 0.07 µm/min, KPC-Euclidean distance: 67.11 ± 9.16 µm; TPC-velocity: 0.41 ± 0.04 µm/min, TPC-Euclidean distance: 96.36 ± 10.33 µm; TPAC-velocity: 0.54 ± 0.07 µm/min, TPAC-Euclidean distance: 106.6 ± 15.75 µm, Figure 18). However, SC migrated toward the TPAC GEMM cancer cells with the by far highest forward migration index (0.33 ± 0.07) when compared to the other GEMM cell types (Figure 18). SC that migrated toward the TPC cells still had a positive migration index (0.10 ± 0.08) as opposed to the negative migration index of SC confronted with KC-carcinoma (-0.13 ± 0.12) or

KPC cells (-0.3 ± 0.04, Figure 18). Thus, the GEMM of PDAC that harbored true invasion contained at the same the cancer cells that most effectively chemoattracted the SC.

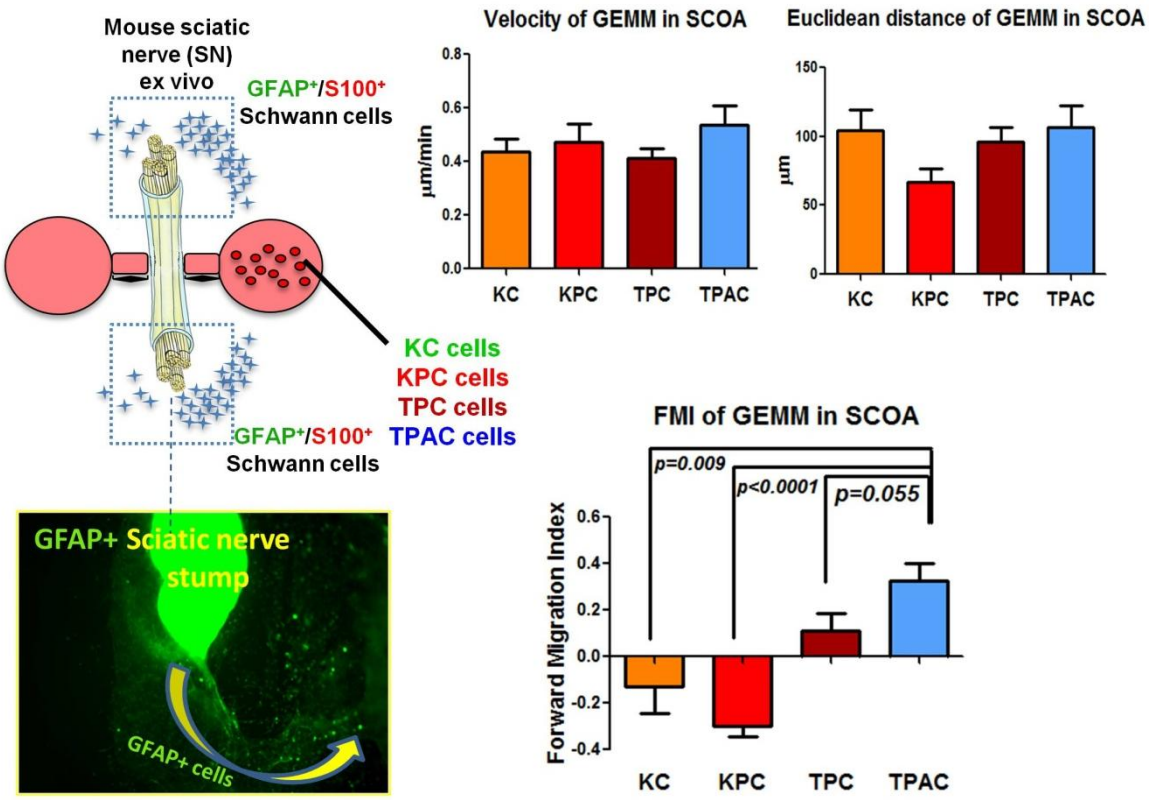

Figure 18. Schwann cell carcinotropism to cancer cells in a novel 3D Schwann cell outgrowth assay (SCOA). Transsected mouse sciatic nerves were placed perpendicular to an ECM gel suspension containing KC-carcinoma, KPC, TPC or TPAC cancer cells. After around 72 hours, resident GFAP/S100 containing Schwann cells within the sciatic nerve were observed to grow out of the transsected sciatic nerve and bent their initially vertical outgrowth direction toward the cancer cell suspension. This carcinotropic Schwann cell migration was tracked via digital time-lapse microscopy and compared for diffent GEMM PDAC cells. Here, the FMI of Schwann cells toward TPAC cells was greater than all other three GEMM PDAC cell types.

TPC mice exhibit less pain and pain-related behavior

Characterization of neuropathy and neuroplasticity in GEMM of PDAC raised the question on the potential correlation of these alterations to the pain sensation in these mouse models. Although pain as an unpleasant experience cannot be directly assessed in animals, assessment of indirect indicators of pain such as the extent of abdominal mechanosensitivity or of exploratory behavior in open fields represent valuable tools that can provide indirect clues. Toward this end, KC, TPC and TPAC

mice were studied by means of von Frey filaments for their abdominal mechanosensitivity, and video-tracked in a defined open field for the length of their locomotion path in a preliminary analysis with a small number of animals (KC: n=4, TPC: n= 2, TPAC: n=2, Figure 19). Here, the mean von Frey score of TPC mice was remarkably smaller (4.14 ± 0.83) than that of KC mice (9.71 ± 1.19) or TPAC mice (8.64 ± 1.22, Figure 19). Correspondingly, TPC mice with obvious less mechanosensitivity covered longer paths in the open field (2.11 ± 0.23 cm per frame) than KC (1.32 ± 0.15 cm per frame) or TPAC mice (1.64 ± 0.12 cm per frame, Figure 19). Hence, TPC mice were identified to bear prominently fewer signs of pain-related alterations than the TPAC mice that have far more NI.

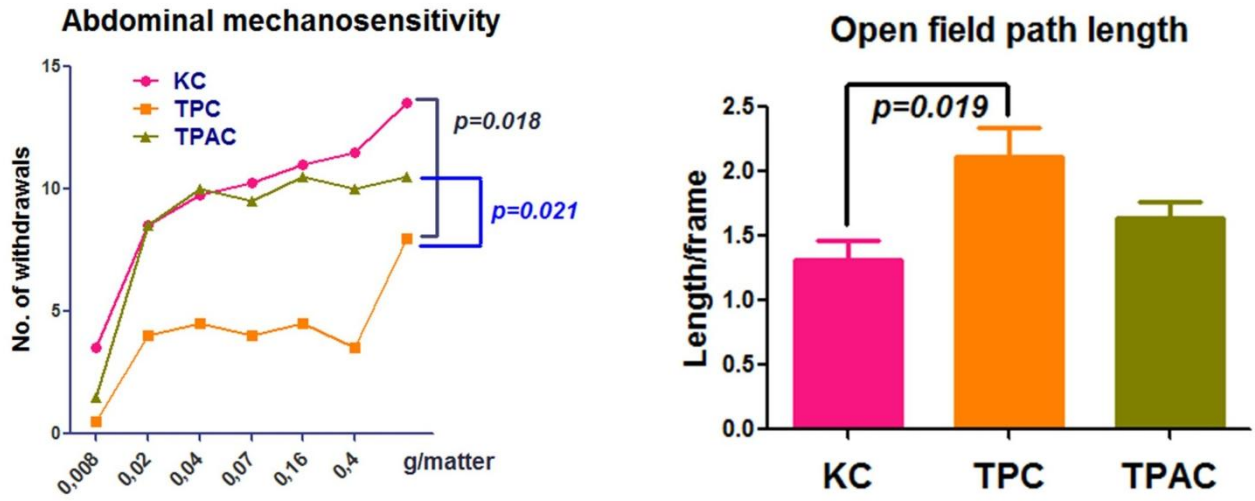

Figure 19. Mechanical hyperalgesia and locomotion in GEMM of PDAC. The two models of PDAC that exhibited NI were compared to KC mice with regard to indicators of abdominal pain. Left: von Frey filaments were applied to the abdomen from the bottom, and the frequency and severity of abdominal retractions were recorded. Right: The GEMM mice were video-tracked in a 50x50x50cm open field for their locomotion for a total of 10 minutes. The average path length per video frame was compared. In both settings, TPC mice exhibited fewer indicators of pain sensation, as evidenced by their lower von Frey scores and longer open field paths.

Transcriptomic comparison of GEMM of PDAC reveals distinct and distinguishing neurotrophin and neurotransmitter signatures

Identification of molecular alterations that are responsible for the observed differences in neuropathy and NI in the analyzed GEMM may shed light on the

mechanism of pancreatic neuropathy in human PDAC. Therefore, a major goal of the present analysis was to perform a wide-scale comparison of the transcriptional products between cancer cells derived from the core models.

For this purpose, whole RNA isolated from three different subsets of cancer cells from each of the four core models (KC, KPC, TPC, TPAC) was used to generate cDNA and analyzed within the Affymetrix Mouse Gene St 1.0 Array. Subsequently, the microarray data were subjected to bioinformatic analysis via the GSEA platform to detect distinct differences in the regulation of molecular pathways (KEGG analysis). In the first part, we aimed at detecting the transcriptomic and pathway regulation differences between the trp53-intact KC-carcinoma cells and the remaining trp53-deficient aggressive GEMM PDAC models (i.e. KPC, TPC and TPAC; Figure 20). Among the significantly regulated 64 gene sets in this KEGG analysis, 60% were, as expected, related to cell growth, cell differentiation and oncogenic pathways, and 22% were related to DNA/RNA biosynthesis and degradation. Interestingly, 5% of all these differentiating gene sets were detected to belong to neural pathways including genes related to neurotrophin signaling and axon guidance. Here, neurotrophin signaling-related genes ranked even 10^{th} among all differentially regulated genes between KC and the remaining GEMM models (“Rest”).

In a subset analysis that involved the comparison of KC to the widely used KPC model, the ranking of differentially regulated pathways revealed that the leading difference among all pathways in the transcriptome was even related to neuroactive ligand receptor interactions (Figure 21). Correspondingly, the 13% of all differtentiating pathways were related to neural signaling and comprised genes that are involved in calcium singnaling, Alzheimer’s or Parkinson’s disease (Figure 21). A very further striking difference between KC and KPC models were differences in the “metabolome”, which comprised 40% of all differences (e.g. propanoate metabolism,

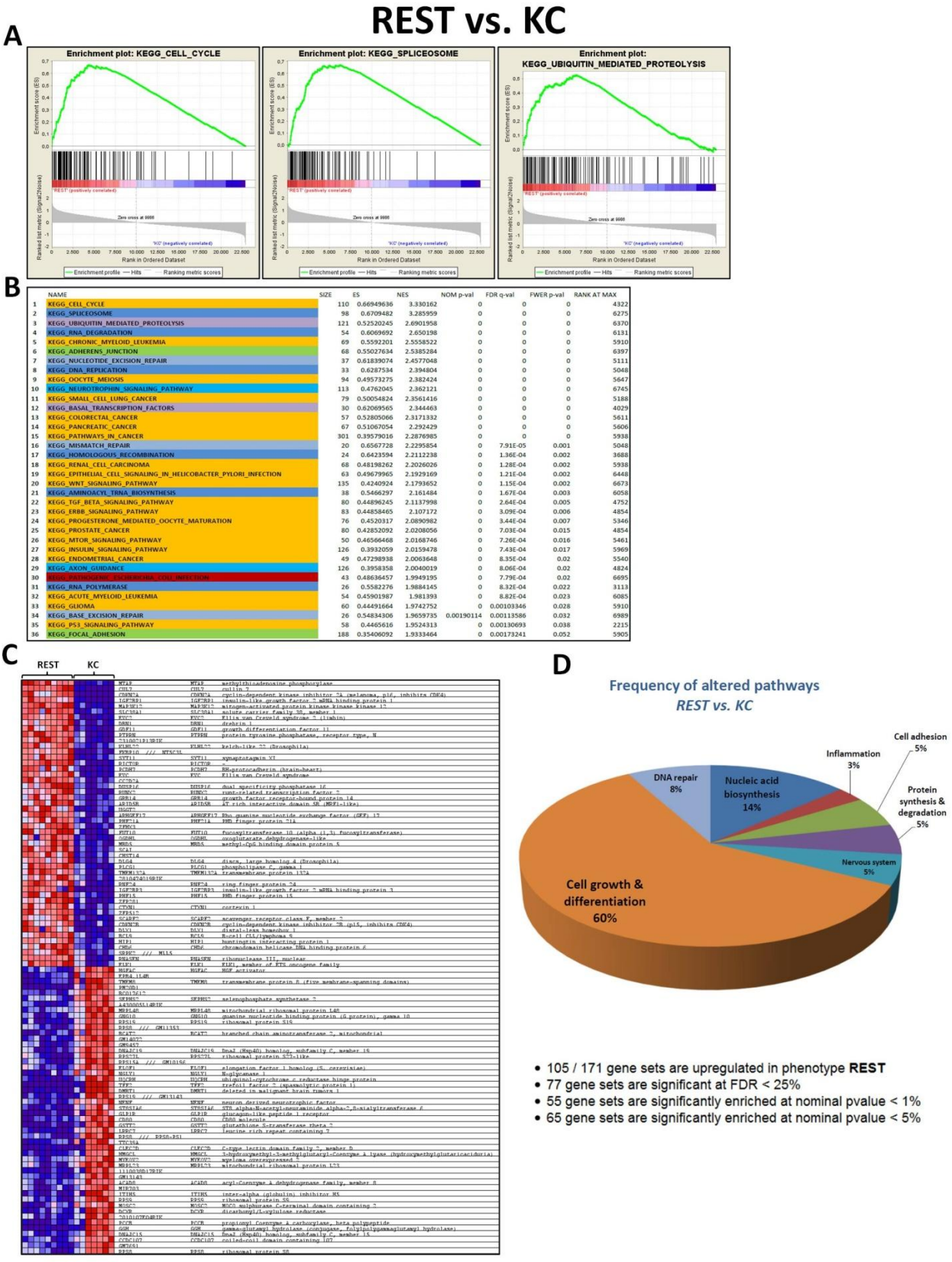

	NAME	SIZE	ES	NES	NOM p-val	FDR q-val	FWER p-val	RANK AT MAX
1	KEGG_CELL_CYCLE	110	0.66949636	3.330162	0	0	0	4322
2	KEGG_SPLICEOSOME	98	0.6709482	3.285959	0	0	0	6275
3	KEGG_UBIQUITIN_MEDIATED_PROTEOLYSIS	121	0.52520245	2.6901958	0	0	0	6370
4	KEGG_RNA_DEGRADATION	54	0.6069692	2.650198	0	0	0	6131
5	KEGG_CHRONIC_MYELOID_LEUKEMIA	69	0.5592201	2.5558522	0	0	0	5910
6	KEGG_ADHERENS_JUNCTION	68	0.55027634	2.5385284	0	0	0	6397
7	KEGG_NUCLEOTIDE_EXCISION_REPAIR	37	0.61839074	2.4577048	0	0	0	5111
8	KEGG_DNA_REPLICATION	33	0.6287534	2.394804	0	0	0	5048
9	KEGG_OOCYTE_MEIOSIS	94	0.49573275	2.382424	0	0	0	5647
10	KEGG_NEUROTROPHIN_SIGNALING_PATHWAY	113	0.4762045	2.362121	0	0	0	6745
11	KEGG_SMALL_CELL_LUNG_CANCER	79	0.50054824	2.3561416	0	0	0	5188
12	KEGG_BASAL_TRANSCRIPTION_FACTORS	30	0.62069565	2.344463	0	0	0	4029
13	KEGG_COLORECTAL_CANCER	57	0.52805066	2.3171332	0	0	0	5611
14	KEGG_PANCREATIC_CANCER	67	0.51067054	2.292429	0	0	0	5606
15	KEGG_PATHWAYS_IN_CANCER	301	0.39579016	2.2876985	0	0	0	5938
16	KEGG_MISMATCH_REPAIR	20	0.6567728	2.2295854	0	7.91E-05	0.001	5048
17	KEGG_HOMOLOGOUS_RECOMBINATION	24	0.6423594	2.2112238	0	1.36E-04	0.002	3688
18	KEGG_RENAL_CELL_CARCINOMA	68	0.48198262	2.2026026	0	1.28E-04	0.002	5938
19	KEGG_EPITHELIAL_CELL_SIGNALING_IN_HELICOBACTER_PYLORI_INFECTION	63	0.49679965	2.1929169	0	1.21E-04	0.002	6448
20	KEGG_WNT_SIGNALING_PATHWAY	135	0.4240924	2.1793652	0	1.15E-04	0.002	6673
21	KEGG_AMINOACYL_TRNA_BIOSYNTHESIS	38	0.5466297	2.161484	0	1.67E-04	0.003	6058
22	KEGG_TGF_BETA_SIGNALING_PATHWAY	80	0.44896245	2.1137998	0	2.64E-04	0.005	4752
23	KEGG_ERBB_SIGNALING_PATHWAY	83	0.44858465	2.107172	0	3.09E-04	0.006	4854
24	KEGG_PROGESTERONE_MEDIATED_OOCYTE_MATURATION	76	0.4520317	2.0890982	0	3.44E-04	0.007	5346
25	KEGG_PROSTATE_CANCER	80	0.42852092	2.0208056	0	7.03E-04	0.015	4854
26	KEGG_MTOR_SIGNALING_PATHWAY	50	0.46566468	2.0168746	0	7.26E-04	0.016	5461
27	KEGG_INSULIN_SIGNALING_PATHWAY	126	0.3932059	2.0159478	0	7.43E-04	0.017	5969
28	KEGG_ENDOMETRIAL_CANCER	49	0.47298938	2.0063648	0	8.35E-04	0.02	5540
29	KEGG_AXON_GUIDANCE	126	0.3958358	2.0040019	0	8.06E-04	0.02	4824
30	KEGG_PATHOGENIC_ESCHERICHIA_COLI_INFECTION	43	0.48636457	1.9949195	0	7.79E-04	0.02	6695
31	KEGG_RNA_POLYMERASE	26	0.5582276	1.9884145	0	8.32E-04	0.022	3113
32	KEGG_ACUTE_MYELOID_LEUKEMIA	54	0.45901987	1.981393	0	8.82E-04	0.023	6085
33	KEGG_GLIOMA	60	0.44491664	1.9742752	0	0.00103346	0.028	5910
34	KEGG_BASE_EXCISION_REPAIR	26	0.54834306	1.9659735	0.00190114	0.00113586	0.032	6989
35	KEGG_P53_SIGNALING_PATHWAY	58	0.4465616	1.9524313	0	0.00130693	0.038	2215
36	KEGG_FOCAL_ADHESION	188	0.35406092	1.9333464	0	0.00173241	0.052	5905

Figure 20. Gene set enrichment analysis (GSEA) and KEGG pathway analysis of the trp53-deficient GEMM PDAC cancer cells versus KC cancer cells. (A) Enrichment plots of the pathways that exhibited strong enrichment in the KPC, TPC, TPAC (termed “rest”) cancer cells when compared to KC cancer cells. (B) Rank list of the pathways that contain the significantly enriched gene sets in the REST group when compared to KC cells. (C) Heat map of the 50 most einriched genes in the REST versus KC group. (D) Pie chart of the biological pathway families that were enriched in the REST vs. KC cells.

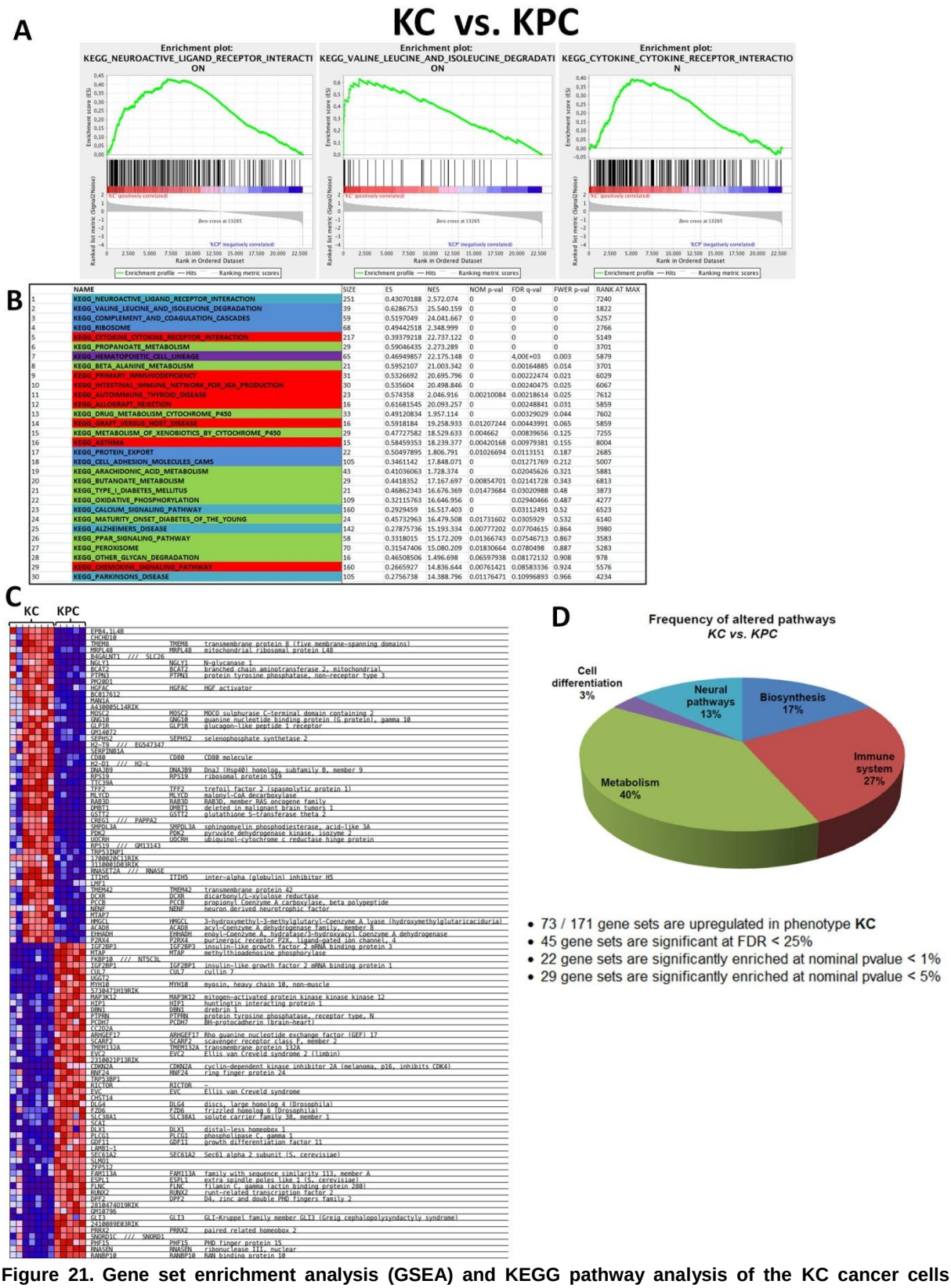

	NAME	SIZE	ES	NES	NOM p-val	FDR q-val	FWER p-val	RANK AT MAX
1	KEGG_NEUROACTIVE_LIGAND_RECEPTOR_INTERACTION	251	0.43070188	2.572.074	0	0	0	7240
2	KEGG_VALINE_LEUCINE_AND_ISOLEUCINE_DEGRADATION	39	0.6286753	25.540.159	0	0	0	1822
3	KEGG_COMPLEMENT_AND_COAGULATION_CASCADES	59	0.5197049	24.041.667	0	0	0	5257
4	KEGG_RIBOSOME	68	0.49442518	2.348.999	0	0	0	2766
5	KEGG_CYTOKINE_CYTOKINE_RECEPTOR_INTERACTION	217	0.39379218	22.737.122	0	0	0	5149
6	KEGG_PROPANOATE_METABOLISM	29	0.59046435	2.273.289	0	0	0	3701
7	KEGG_HEMATOPOIETIC_CELL_LINEAGE	65	0.46949857	22.175.148	0	4,00E+03	0.003	5879
8	KEGG_BETA_ALANINE_METABOLISM	21	0.5952107	21.003.342	0	0.00164885	0.014	3701
9	KEGG_PRIMARY_IMMUNODEFICIENCY	31	0.5326692	20.695.796	0	0.00222474	0.021	6029
10	KEGG_INTESTINAL_IMMUNE_NETWORK_FOR_IGA_PRODUCTION	30	0.535604	20.498.846	0	0.00240475	0.025	6067
11	KEGG_AUTOIMMUNE_THYROID_DISEASE	23	0.574358	2.046.916	0.00210084	0.00218614	0.025	7612
12	KEGG_ALLOGRAFT_REJECTION	16	0.61681545	20.093.257	0	0.00248841	0.031	5859
13	KEGG_DRUG_METABOLISM_CYTOCHROME_P450	33	0.49120834	1.957.114	0	0.00329029	0.044	7602
14	KEGG_GRAFT_VERSUS_HOST_DISEASE	16	0.5918184	19.258.933	0.01207244	0.00443991	0.065	5859
15	KEGG_METABOLISM_OF_XENOBIOTICS_BY_CYTOCHROME_P450	29	0.47727582	18.529.633	0.004662	0.00839656	0.125	7255
16	KEGG_ASTHMA	15	0.58459353	18.239.377	0.00420168	0.00979381	0.155	8004
17	KEGG_PROTEIN_EXPORT	22	0.50497895	1.806.791	0.01026694	0.0113151	0.187	2685
18	KEGG_CELL_ADHESION_MOLECULES_CAMS	105	0.3461142	17.848.071	0	0.01271769	0.212	5007
19	KEGG_ARACHIDONIC_ACID_METABOLISM	43	0.41036063	1.728.374	0	0.02045626	0.321	5881
20	KEGG_BUTANOATE_METABOLISM	29	0.4418352	17.167.697	0.00854701	0.02141728	0.343	6813
21	KEGG_TYPE_I_DIABETES_MELLITUS	21	0.46862343	16.676.369	0.01473684	0.03020988	0.48	3873
22	KEGG_OXIDATIVE_PHOSPHORYLATION	109	0.32115763	16.646.956	0	0.02940466	0.487	4277
23	KEGG_CALCIUM_SIGNALING_PATHWAY	160	0.2929459	16.517.403	0	0.03112491	0.52	6523
24	KEGG_MATURITY_ONSET_DIABETES_OF_THE_YOUNG	24	0.45732963	16.479.508	0.01731602	0.0305929	0.532	6140
25	KEGG_ALZHEIMERS_DISEASE	142	0.27875736	15.193.334	0.00777202	0.07704615	0.864	3980
26	KEGG_PPAR_SIGNALING_PATHWAY	58	0.3318015	15.172.209	0.01366743	0.07546713	0.867	3583
27	KEGG_PEROXISOME	70	0.31547406	15.080.209	0.01830664	0.0780498	0.887	5283
28	KEGG_OTHER_GLYCAN_DEGRADATION	16	0.46508506	1.496.698	0.06597938	0.08172132	0.908	978
29	KEGG_CHEMOKINE_SIGNALING_PATHWAY	160	0.2665927	14.836.644	0.00761421	0.08583336	0.924	5576
30	KEGG_PARKINSONS_DISEASE	105	0.2756738	14.388.796	0.01176471	0.10996893	0.966	4234

Figure 21. Gene set enrichment analysis (GSEA) and KEGG pathway analysis of the KC cancer cells versus KPC cancer cells. (A) Enrichment plots of three pathways that ranked among the top five enriched pathways in KC cancer cells when compared to KPC cells. Please note that the leading pathway that was altered in KC cells was the neuroactive ligand and receptor family. (B) Rank list of the pathways that contain the significantly enriched gene sets in the KC cells when compared to KC cells. (C) Heat map of the 50 most einriched genes in the KC versus KPC group. (D) Pie chart of the biological pathway families that were enriched in the KC vs. KPC cells.

beta-alanine metabolism, drug metabolism over cytochrome p450 or oxidative phosphorylation). Hence, the most striking difference in the transition from KC to the trp53-deficient KPC model was related to neural signaling and metabolic processing (Figure 21).

In the current study, TPAC model was identified to be the first GEMM of PDAC with human-like NI, which is why it was of particular interest to detect cancer cell-derived transcriptomic differences between the TPAC and the more widely used KPC model (Figure 22). This KEGG pathway analysis revealed a remarkable concentration of transcriptomic difference in metabolic pathways. Indeed, 67% of all 46 significantly different gene sets were related to metabolism, including lysosomal pathways, drug metabolism over cytochrome p450, peroxisomal pathways, propanoate metabolism, fatty acid metabolism and several other metabolic pathways. Furthermore, 10% of the differentiating gene sets were related to cell adhesion, and 3% to neural pathways (Figure 22). Moreover, the most significantly enriched gene in TPAC cells (when compared to KPC cells) was CXCL15 (Figure 22). Hence, this analysis revealed that the overwhelming difference between the biological behavior of the neuro-invasive TPAC cells versus KPC GEMM cancer cells lies in the metabolomic profile of these cells.

In the present study, although not at the same extent as TPAC cells, also the TPC model of PDAC and TPC cancer cells were detected to exhibit some NI. Therefore, in the subsequent step, we aimed at detecting the transcriptomic difference between the TPAC and TPC models that could account for enhanced neuro-invasiveness (Figure 23). Very similar to the analysis of TPAC versus KPC, also the comparative KEGG pathway analysis revealed that the leading gene

expression differences (among the 20 significantly upregulated pathways) are related to metabolic regulation (50% of all differences). Indeed, TPAC cells had a

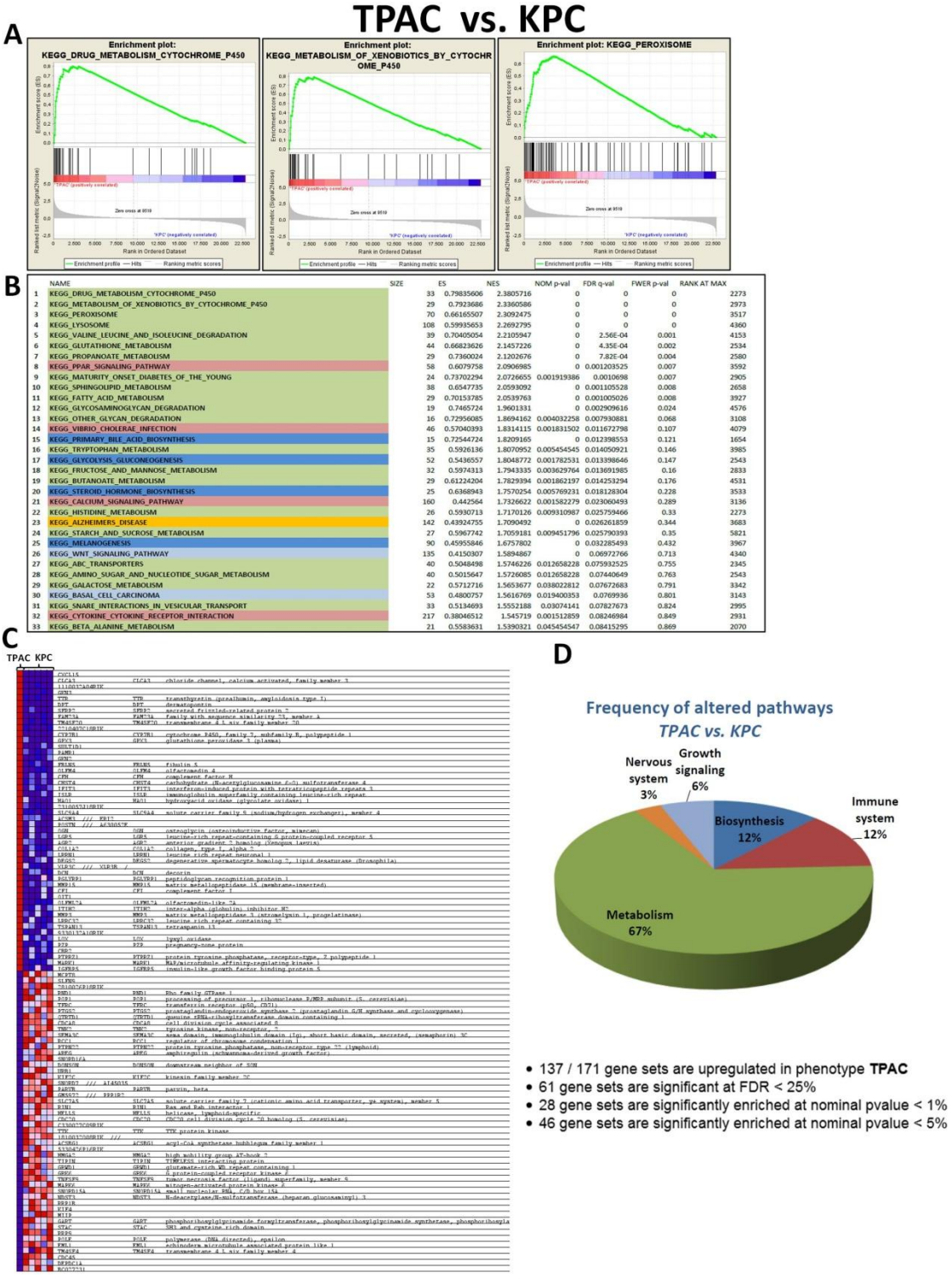

	NAME	SIZE	ES	NES	NOM p-val	FDR q-val	FWER p-val	RANK AT MAX
1	KEGG_DRUG_METABOLISM_CYTOCHROME_P450	33	0.79835606	2.3805716	0	0	0	2273
2	KEGG_METABOLISM_OF_XENOBIOTICS_BY_CYTOCHROME_P450	29	0.7923686	2.3360586	0	0	0	2973
3	KEGG_PEROXISOME	70	0.66165507	2.3092475	0	0	0	3517
4	KEGG_LYSOSOME	108	0.59935653	2.2692795	0	0	0	4360
5	KEGG_VALINE_LEUCINE_AND_ISOLEUCINE_DEGRADATION	39	0.70405054	2.2105947	0	2.56E-04	0.001	4153
6	KEGG_GLUTATHIONE_METABOLISM	44	0.66823626	2.1457226	0	4.35E-04	0.002	2534
7	KEGG_PROPANOATE_METABOLISM	29	0.7360024	2.1202676	0	7.82E-04	0.004	2580
8	KEGG_PPAR_SIGNALING_PATHWAY	58	0.6079758	2.0906985	0	0.001203525	0.007	3592
9	KEGG_MATURITY_ONSET_DIABETES_OF_THE_YOUNG	24	0.73702294	2.0726655	0.001919386	0.0010698	0.007	2905
10	KEGG_SPHINGOLIPID_METABOLISM	38	0.6547735	2.0593092	0	0.001105528	0.008	2658
11	KEGG_FATTY_ACID_METABOLISM	29	0.70153785	2.0539763	0	0.001005026	0.008	3927
12	KEGG_GLYCOSAMINOGLYCAN_DEGRADATION	19	0.7465724	1.9601331	0	0.002909616	0.024	4576
13	KEGG_OTHER_GLYCAN_DEGRADATION	16	0.72956085	1.8694162	0.004032258	0.007930881	0.068	3108
14	KEGG_VIBRIO_CHOLERAE_INFECTION	46	0.57040393	1.8314115	0.001831502	0.011672798	0.107	4079
15	KEGG_PRIMARY_BILE_ACID_BIOSYNTHESIS	15	0.72544724	1.8209165	0	0.012398553	0.121	1654
16	KEGG_TRYPTOPHAN_METABOLISM	35	0.5926136	1.8070952	0.005454545	0.014050921	0.146	3985
17	KEGG_GLYCOLYSIS_GLUCONEOGENESIS	52	0.5436557	1.8048772	0.001782531	0.013398646	0.147	2543
18	KEGG_FRUCTOSE_AND_MANNOSE_METABOLISM	32	0.5974313	1.7943335	0.003629764	0.013691985	0.16	2833
19	KEGG_BUTANOATE_METABOLISM	29	0.61224204	1.7829394	0.001862197	0.014253294	0.176	4531
20	KEGG_STEROID_HORMONE_BIOSYNTHESIS	25	0.6368943	1.7570254	0.005769231	0.018128304	0.228	3533
21	KEGG_CALCIUM_SIGNALING_PATHWAY	160	0.442564	1.7326622	0.001582279	0.023060493	0.289	3136
22	KEGG_HISTIDINE_METABOLISM	26	0.5930713	1.7170126	0.009310987	0.025759466	0.33	2273
23	KEGG_ALZHEIMERS_DISEASE	142	0.43924755	1.7090492	0	0.026261859	0.344	3683
24	KEGG_STARCH_AND_SUCROSE_METABOLISM	27	0.5967742	1.7059181	0.009451796	0.025790393	0.35	5821
25	KEGG_MELANOGENESIS	90	0.45955846	1.6757802	0	0.032285493	0.432	3967
26	KEGG_WNT_SIGNALING_PATHWAY	135	0.4150307	1.5894867	0	0.06972766	0.713	4340
27	KEGG_ABC_TRANSPORTERS	40	0.5048498	1.5746226	0.012658228	0.075932525	0.755	2345
28	KEGG_AMINO_SUGAR_AND_NUCLEOTIDE_SUGAR_METABOLISM	40	0.5015647	1.5726085	0.012658228	0.07440649	0.763	2543
29	KEGG_GALACTOSE_METABOLISM	22	0.5712716	1.5653677	0.038022812	0.07672683	0.791	3342
30	KEGG_BASAL_CELL_CARCINOMA	53	0.4800757	1.5616769	0.019400353	0.0769936	0.801	3143
31	KEGG_SNARE_INTERACTIONS_IN_VESICULAR_TRANSPORT	33	0.5134693	1.5552188	0.03074141	0.07827673	0.824	2995
32	KEGG_CYTOKINE_CYTOKINE_RECEPTOR_INTERACTION	217	0.38046512	1.545719	0.001512859	0.08246984	0.849	2931
33	KEGG_BETA_ALANINE_METABOLISM	21	0.5583631	1.5390321	0.045454547	0.08415295	0.869	2070

Figure 22. Gene set enrichment analysis (GSEA) and KEGG pathway analysis of the TPAC cancer cells versus KPC cancer cells. (A) Enrichment plots of three pathways that ranked among the top five enriched pathways in TPAC cancer cells when compared to KPC cells. (B) Rank list of the pathways that contain the significantly enriched gene sets in the TPAC cells when compared to KPC cells. (C) Heat map of the 50 most einriched genes in the KC versus KPC group. (D) Pie chart of the biological pathway families that were enriched in the TPAC vs. KPC cells.

considerably differently regulated glutathione metabolism, xenobiotic metabolism, tyrosine metabolism, glycolysis, histidine, fructose, mannose, sphingolipid and steroid hormone metabolism when compared to TPC cells (Figure 23). The gene with the highest degree of enrichment in TPAC versus TPC cells was MAL2 (mal, T-cell differentiation protein 2). Hence, the key feature that seemed to differentiate TPAC from TPC cancer cells from the perspective of “enrichment” was increased expression of genes related to numerous metabolic pathways.

When we regarded these differences from the opposite side of the spectrum, i.e. the genes that are enriched in the less neuro-invasive TPC cells when compared to TPAC cells, we could detect a very idiosyncratic gene enrichment: Here, 31% of all pathways that were increasingly active in TPC cells were related to inflammation and cytokine signaling, whereas 23% were related to metabolism, and again 23% to growth/trophic signals. (Figure 24). Hence, in TPC cells, the intact NFkappaB transcription factor signaling seems to promote activation of immune system-related responses, at the same time sustaining the differential metabolic or growth-associated signaling signature of these cells.

Based on the prominent alterations in neural pathways and on the frequently reported link between neurotrophic factors and NI and neuroplasticity in human PDAC, in the final step of the study, a more focused expression array on neural molecules was performed with the GEMM PDAC cells. Here, the cDNA of these GEMM PDAC cells was used to compare these four models with regard to the expression from a set of 84 genes related to neurotrophic factor signaling within a RT^2 Profiler PCR array. In the first analysis, the cancer cells of the trp53-deficient and thus more aggressive models KPC, TPC and TPAC were compared to KC cancer

A

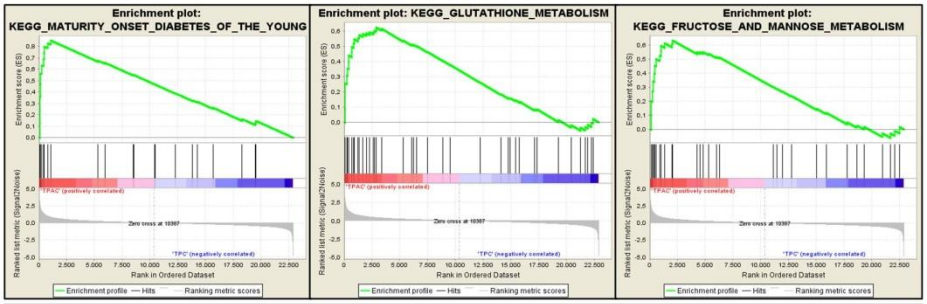

B

	NAME	SIZE	ES	NES	NOM p-val	FDR q-val	FWER p-val	RANK AT MAX
1	KEGG_MATURITY_ONSET_DIABETES_OF_THE_YOUNG	24	0.85073555	2.4092388	0	0	0	1051
2	KEGG_GLUTATHIONE_METABOLISM	44	0.62253064	2.0181694	0	0.003468067	0.007	2901
3	KEGG_FRUCTOSE_AND_MANNOSE_METABOLISM	32	0.63197446	1.8948294	0.001858736	0.02153301	0.061	2046
4	KEGG_HISTIDINE_METABOLISM	26	0.64063203	1.8274286	0	0.03441649	0.128	2921
5	KEGG_SPHINGOLIPID_METABOLISM	38	0.57190394	1.8074318	0.001788909	0.034419093	0.157	3525
6	KEGG_STEROID_HORMONE_BIOSYNTHESIS	25	0.6440711	1.8046125	0.007130125	0.02985083	0.164	3018
7	KEGG_HEMATOPOIETIC_CELL_LINEAGE	65	0.5197438	1.7720928	0.001683502	0.037837602	0.238	1310
8	KEGG_METABOLISM_OF_XENOBIOTICS_BY_CYTOCHROME_P450	29	0.59025455	1.7363237	0.008849558	0.048785776	0.324	3251
9	KEGG_PENTOSE_PHOSPHATE_PATHWAY	24	0.6145124	1.7222588	0.005309735	0.051345617	0.373	2644
10	KEGG_TRYPTOPHAN_METABOLISM	35	0.5676878	1.7196183	0.003521127	0.04690276	0.378	3647
11	KEGG_LEUKOCYTE_TRANSENDOTHELIAL_MIGRATION	108	0.45528454	1.6962656	0	0.053437743	0.447	2150
12	KEGG_TIGHT_JUNCTION	115	0.4466766	1.6917872	0.00166113	0.051120717	0.462	1477
13	KEGG_CELL_ADHESION_MOLECULES_CAMS	105	0.4465153	1.6709884	0.003149606	0.057317026	0.533	1239
14	KEGG_O_GLYCAN_BIOSYNTHESIS	28	0.5693942	1.664826	0.009469697	0.056478947	0.552	1030
15	KEGG_DRUG_METABOLISM_CYTOCHROME_P450	33	0.535267	1.6389766	0.003442341	0.065786235	0.635	2729
16	KEGG_GLYCOLYSIS_GLUCONEOGENESIS	52	0.4945406	1.6271468	0.010186757	0.06751881	0.668	1523
17	KEGG_RIBOSOME	68	0.4578669	1.6036876	0.007130125	0.07976694	0.743	6875
18	KEGG_NICOTINATE_AND_NICOTINAMIDE_METABOLISM	23	0.57636243	1.6033872	0.014260249	0.07538688	0.744	2064
19	KEGG_INOSITOL_PHOSPHATE_METABOLISM	52	0.47702157	1.5561275	0.010016695	0.10421144	0.848	3441
20	KEGG_TERPENOID_BACKBONE_BIOSYNTHESIS	15	0.60388243	1.5507737	0.03250478	0.10315168	0.862	3466
21	KEGG_PEROXISOME	70	0.4472005	1.5393016	0.016638935	0.107746236	0.885	2823
22	KEGG_PATHOGENIC_ESCHERICHIA_COLI_INFECTION	43	0.4784825	1.5223991	0.026929982	0.116578475	0.911	3431
23	KEGG_LYSINE_DEGRADATION	41	0.47991666	1.5068485	0.017857144	0.127734	0.937	5217
24	KEGG_OLFACTORY_TRANSDUCTION	25	0.5097665	1.4775319	0.05283019	0.15294166	0.971	1084
25	KEGG_N_GLYCAN_BIOSYNTHESIS	41	0.4692046	1.4749271	0.044483986	0.1497725	0.972	2558
26	KEGG_JAK_STAT_SIGNALING_PATHWAY	134	0.38527736	1.459002	0.013846153	0.16086785	0.979	2134
27	KEGG_ABC_TRANSPORTERS	40	0.45518944	1.4366304	0.041666668	0.18090415	0.987	1664
28	KEGG_WNT_SIGNALING_PATHWAY	135	0.36600208	1.4006691	0.02511774	0.22057502	0.996	3306

C

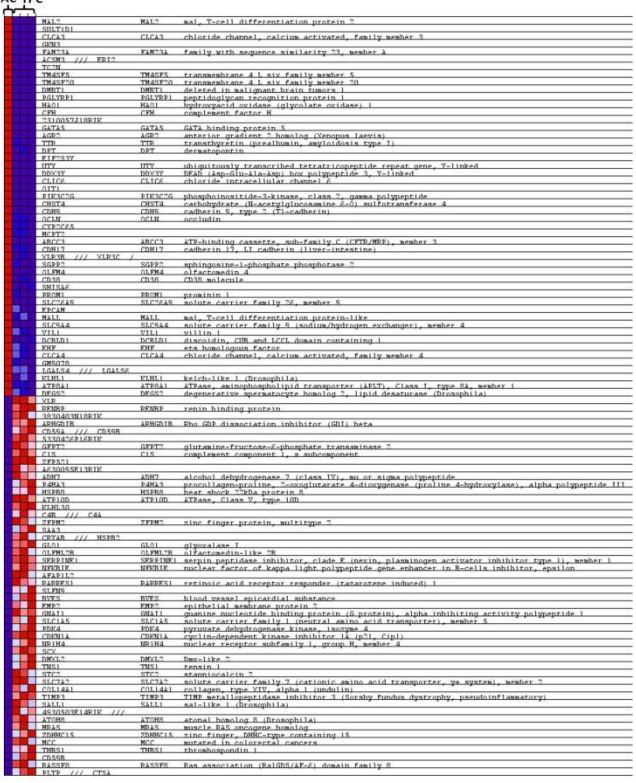

D

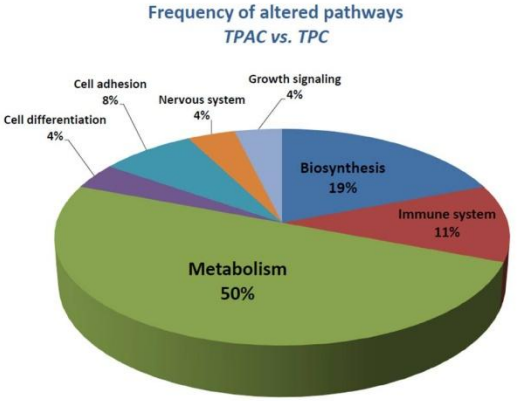

- 100 / 171 gene sets are upregulated in phenotype **TPAC**
- 28 gene sets are significant at FDR < 25%
- 16 gene sets are significantly enriched at nominal pvalue < 1%
- 27 gene sets are significantly enriched at nominal pvalue < 5%

Figure 23. Gene set enrichment analysis (GSEA) and KEGG pathway analysis of the TPAC cancer cells versus TPC cancer cells. (A) Enrichment plots of three pathways that ranked among the top five enriched pathways in TPAC cancer cells when compared to TPC cells. (B) Rank list of the pathways that contain the significantly enriched gene sets in the TPAC cells when compared to KPC cells. (C) Heat map of the 50 most enriched genes in the TPAC versus TPC group. (D) Pie chart of the biological pathway families that were enriched in the TPAC vs. TPC cells.

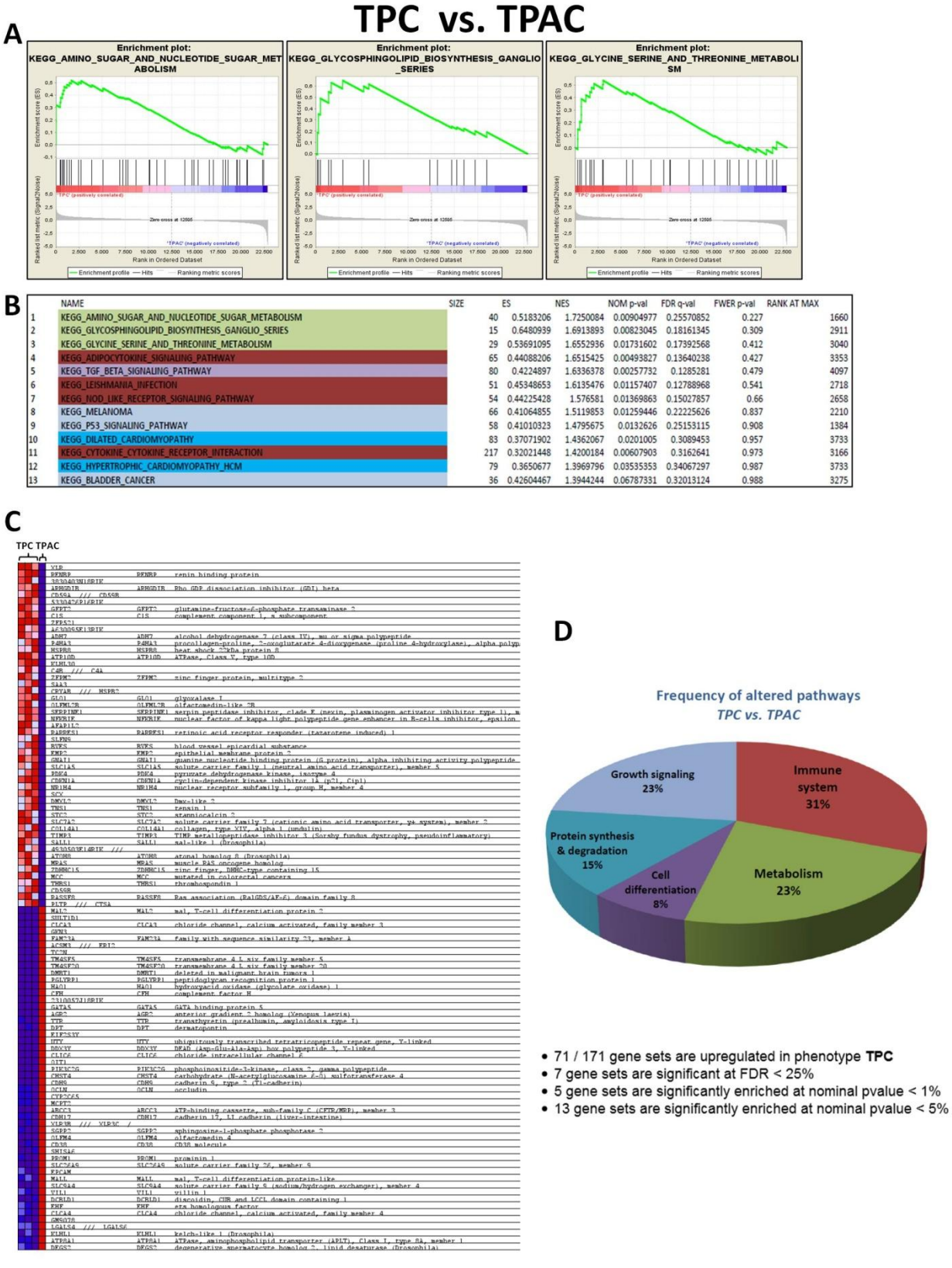

	NAME	SIZE	ES	NES	NOM p-val	FDR q-val	FWER p-val	RANK AT MAX
1	KEGG_AMINO_SUGAR_AND_NUCLEOTIDE_SUGAR_METABOLISM	40	0.5183206	1.7250084	0.00904977	0.25570852	0.227	1660
2	KEGG_GLYCOSPHINGOLIPID_BIOSYNTHESIS_GANGLIO_SERIES	15	0.6480939	1.6913893	0.00823045	0.18161345	0.309	2911
3	KEGG_GLYCINE_SERINE_AND_THREONINE_METABOLISM	29	0.53691095	1.6552936	0.01731602	0.17392568	0.412	3040
4	KEGG_ADIPOCYTOKINE_SIGNALING_PATHWAY	65	0.44088206	1.6515425	0.00493827	0.13640238	0.427	3353
5	KEGG_TGF_BETA_SIGNALING_PATHWAY	80	0.4224897	1.6336378	0.00257732	0.1285281	0.479	4097
6	KEGG_LEISHMANIA_INFECTION	51	0.45348653	1.6135476	0.01157407	0.12788968	0.541	2718
7	KEGG_NOD_LIKE_RECEPTOR_SIGNALING_PATHWAY	54	0.44225428	1.576581	0.01369863	0.15027857	0.66	2658
8	KEGG_MELANOMA	66	0.41064855	1.5119853	0.01259446	0.22225626	0.837	2210
9	KEGG_P53_SIGNALING_PATHWAY	58	0.41010323	1.4795675	0.0132626	0.25153115	0.908	1384
10	KEGG_DILATED_CARDIOMYOPATHY	83	0.37071902	1.4362067	0.0201005	0.3089453	0.957	3733
11	KEGG_CYTOKINE_CYTOKINE_RECEPTOR_INTERACTION	217	0.32021448	1.4200184	0.00607903	0.3162641	0.973	3166
12	KEGG_HYPERTROPHIC_CARDIOMYOPATHY_HCM	79	0.3650677	1.3969796	0.03535353	0.34067297	0.987	3733
13	KEGG_BLADDER_CANCER	36	0.42604467	1.3944244	0.06787331	0.32013124	0.988	3275

Figure 24. Gene set enrichment analysis (GSEA) and KEGG pathway analysis of the TPC cancer cells versus TPAC cancer cells. (A) Enrichment plots of three pathways that ranked among the top five enriched pathways in TPAC cancer cells when compared to TPC cells. (B) Rank list of the pathways that contain the significantly enriched gene sets in the TPC cells when compared to TPAC cells. Here, please note that the major enriched gene classes all belonged to extracellular matrix modeling and adhesion processes. (C) Heat map of the 50 most einriched genes in the TPC versus TPAC group. (D) Pie chart of the biological pathway families that were enriched in the TPC vs. TPAC cells.

cells. Here, more than 30 targets were identified to be at least 2-fold up- or downregulated in the KPC, TPC and TPAC mice when compared to KC mice (Figure 25). As an internal control, the expression of *trp53* was found to be downregulated between 200 to 1000 times in KPC, TPC and TPAC cells when compared to KC cells (KPC: -1221-fold, TPC: -201-fold, TPAC: -852-fold, Figure 25A-C). In comparison of KPC vs. KC, the five most prominently upregulated hits were Gfralpha2 (1102-fold), NGF (272-fold), Fgfr1 (270-fold), Artemin (167-fold), and ciliary-neurotrophic-factor/CNTF-receptor (30-fold), whereas there was strong downregulation in the expression of nuclear factor receptor subfamily 1, group I, member2 (Nr1i2, -51-fold) and of Fas receptor (-17-fold, Figure 25A).

In the comparison of TPC versus KC, the five upregulated hits were Gfralpha2 (392-fold), Fgfr1 (384-fold), Artemin (310-fold), Trophinin (191-fold), and NGF (189-fold), whereas there was prominent downregulation in the expression of metallothionein 3 (MT3, -12-fold) and nuclear factor receptor subfamily 1, group I, member2 (Nr1i2, -9-fold, Figure 25B).

In the same type of comparison between TPAC versus KC mice, the upregulated hits very much resembled the preceding comparisons, with the leading hits for upregulated genes including NGF (376-fold), Fgfr1 (224-fold), Artemin (126-fold), Neuropeptide Y/NPY (95-fold) and GDNF (62-fold). The two most downregulated hits were metallothionein 3 (-6.7-fold) and corticotropin-releasing factor-binding protein (CRHBP, -5-fold, Figure 25C).

In the second step, the leading question was which neuro-molecular signature can help to differentiate the neuro-invasive TPAC and the partially neuro-invasive TPC from the non-neuro-invasive KPC model. Here, the RT^2 Profiler PCR array-based comparison of the expression of the 84 gene-set between TPAC and KPC cells yielded a prominent upregulation in the expression of Fos (33-fold), NPY (31-

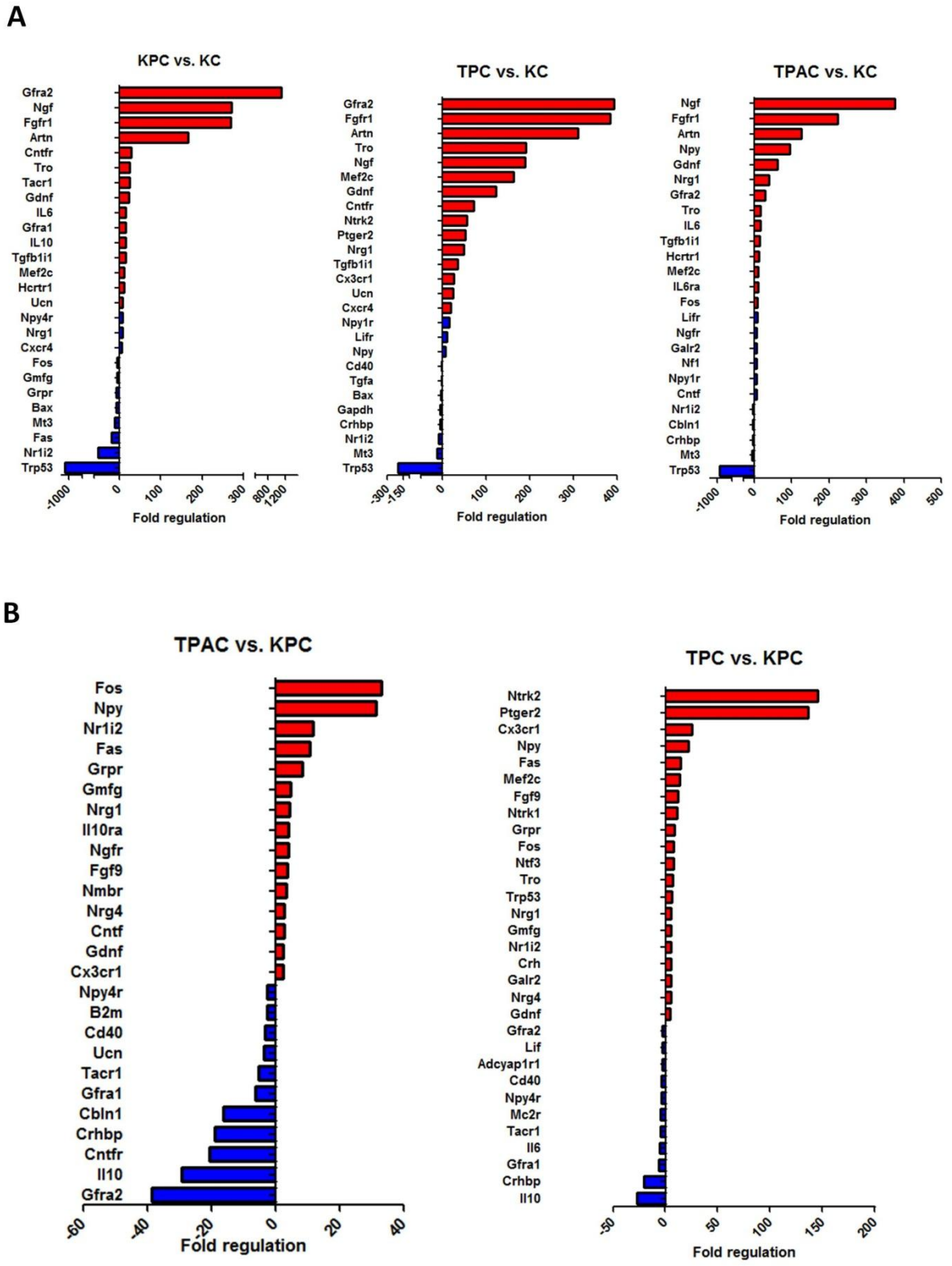

Figure 25. RT^2 Profiler Array results for mouse neurotrophic factor and receptor signaling. (A) Comparative expression of the most up- (red) or downregulated (blue) targets in KPC, TPC and TPAC cells when compared to KC carcinoma cells. (B) In the second step, the neurotrophic factor and receptor expression in the neuro-invasive TPAC and less neuro-invasive TPC cells was compared to the non-neuro-invasive KPC cells. All depicted targets were at least 2-fold up- or downregulated.

fold), Nr1i2 (12-fold), Fas (11-fold) and gastrin-releasing-peptide-receptor (GRPR, 8.5-fold), whereas there was a prominent downregulation in the expression of Gfralpha2 (-39-fold), interleukin-10 (IL-10, -29-fold), CNTFR (-21-fold) and CRHBP (-19-fold) (Figure 25D). Interestingly, the comparison of the same gene set between TPC versus KPC showed a very strong upregulation of the BDNF receptor NTRK2 (neurotrophic factor receptor kinase 2, also known as TrkB, 145-fold), prostaglandin E2 receptor (PTGER2, 136-fold), the CX3CR1 receptor (25-fold), NPY (22-fold) and Fas (14-fold). In this comparison, the most strongly downregulated targets were IL-10 (-27-fold), CRHBP (-20-fold), GFRalpha1 (-6-fold), IL-6 (-5-fold) and tachykinin receptor 1 (Tacr1, neurokinin receptor 1/NKR1, -5-fold, Figure 25E). Therefore, regarding these results collectively, GEMM PDAC cells that are derived from the trp53-deficient aggressive models seem to harmoniously upregulate the expression of a defined panel of a neurotrophic factors and their receptors, particularly NGF, Fgfr1, Artemin, GFRalpha2, and CNTFR, and to downregulate MT3 and Nr1i2. However, once invasive, the neuro-invasive murine cancer cells seem to be characterized by increased expression of NPY, Fos, Fas and CX3CR1, and suppression of IL-10 and CRHBP.

Discussion

The present study was designed to analyze the most common GEMM of PDAC with regard to neuropathy and especially NI in PDAC. Here, we characterize a novel GEMM of PDAC, the TPAC model of PDAC, that, to our knowledge, was for the first model found to exhibit human-like true NI. In the first step, murine PDAC innervation was dissected microanatomically and quantified for nerve density and size in the GEMM of PDAC. This analysis showed that all GEMM of PDAC bear a hyperinnervation of the tumor when compared to the precursor stages, and this hyperinnervation could be simulated in an *in vitro* neuroplasticity assay as increased neurite density of DRG neurons. The TGFalpha-based models, especially in the simultaneous pancreatic depletion of RelA/p65, were identified to harbor human-like NI, whereas none of the models exhibited human-like pancreatic neuritis. The human-like NI in the TPAC model could be modeled as increased neuro-affinitiy of TPAC cells to neurons, and as increased Schwann cell chemoattraction to cancer cells *in vitro* and *in vivo.* Pain sensation in these GEMM was variable and least in the TPC model of PDAC. At molecular level, the knockout of the trp53 in the KPC, TPC, TPAC models resulted in the upregulation of distinct neurotrophic factors and receptors including Gfralpha2, NGF, Fgfr1, and Artemin, whereas the TGFalpha-based models differed from the KPC model in the altered cell metabolism and in the increased activation of NPY and Fos signaling. Overall, these observations offer several key concepts that are likely to broaden our understanding of neuropathy in PDAC and also raise important questions on the pathomechanism of NI in PDAC.

The analysis of neuropathy and NI in murine models of PDAC requires thorough understanding of the anatomy of mouse pancreatic innervation. To this end, an essential feature of mouse pancreas is that is located within the mesentery and

thus considered a “mesenteric” type pancreas from an anatomical standpoint (Dintzis, 2012). This is in sharp contrast with the human or e.g. porcine pancreata that are compact organs with large lobules and evenly distributed intralobular islets (Dintzis, 2012). Accordingly, in the present study, mouse pancreatic nerves were found to be localized around the pancreatic borders and to enter the organ at 2-3 entry sites located near peripancreatic, mesenteric lymph nodes. Importantly, the parenchyma, and especially intralobular septae nearly never contain nerve “trunks” that include several nerve fiber bundles. In the human pancreas, though, nerve trunks containing multiple nerve fibers are readily encountered between acinar clusters in intralobular septae. Thus, in the study of neuropathy and NI in GEMM of PDAC, we should consider that we are dealing with anatomically quite different organs with regard to gross anatomy of innervation. Furthermore, due to its mesenteric localization, the pancreas of the mouse is an intraperitoneal organ as opposed to the retroperitoneal human pancreas. Therefore, when studying the size and distribution of nerves in any given mouse model, one does not have available intraparencyhmal control nerve trunks. In this context, in order to identify neural hypertrophy or increased neural density, it may be better to determine the size and density or the peripancreatic nerve trunks lying directly adjacent to peripancreatic lymph nodes. It is conceivable that tissue hyperinnervation would start from these perilymphoid nerves that lie at the pericapsular nerve entry sites. However, another possibility would be emergence of relatively large nerve trunks within the core of the tumor or toward more interior of the pancreas. Indeed, in the analysis of the nerve density and size, the current study revealed the presence of multiple large nerve trunks in the main tumor mass that, in the examples of the TPAC and TPC models, were frequently invaded by PDAC cells. Therefore, first of all, the present study

provided an histomorphological overview and a road map for analyzing innervation in GEMM of PDAC.

The functional implications of the spatial proximity between nerves and lymphoid tissue around the pancreas are yet unclear. It is imaginable that nerves and inflammatory cells may be affecting each other's function in this spatial vicinity. However, it is overall unlikely that the encapsulated peripancreatic lymph nodes would necessarily communicate with the epineurium-covered nerve trunks that do not seem to sprout nerve endings to these lymph nodes based on our immunhistochemical stainings. Still, there is increasing evidence for a direct neuro-immuno crosstalk between nerves and lymph nodes due to targeting of specific immune cell populations within lymph nodes by e.g. sympathetic nerve fibers (Downing et al., 2000; Nance et al., 2007). Huang et al. could demonstrate that sympathetic, norepinephrine or NPY-containing nerve fibers from the superior cervical ganglion physically terminated around S100-containing cells in the cervical lymph nodes (Huang et al., 2013). While the functional consequences of this interaction are not yet understood, it is likely that the nervous system interacts with certain cell subtypes within lymph nodes. Yet, as the study by Huang et al. demonstrates, this interaction seems to be primarily mediated by nerve endings that stem from distant ganglia.

A major finding of this study was the demonstration of tumor hyperinnervation in malignant murine pancreatic disease when compared to the KC model that only contains the PanIN precursor lesions. Generally speaking, all the GEMM of PDAC seem to simulate the increased tumor innervation in PDAC that is typical for human disease. Yet in human PDAC, the neural density and size behave concordantly and are both augmented in the tumor tissue. In the present study, although the total innervation index of all models was clearly higher than the KC model, neural density

and size seemed to behave oppositely, i.e. increasing neural density was associated with smaller neural size. The mechanism behind this discordant behavior of neural size and density remains unclear. It is imaginable that increase in neural size and density in the murine PDAC may be not parallel but rather sequential events, that would be simultaneously encountered only in the latest stages of tumor progression. Indeed, looking at the dynamic behavior of neural size and density over time in the present analysis, the TPAC model built a simultaneous peak of neural density and size only in the older animals. In the oldest animals that were toward to end of their life span, all models tended to lose the tumor innervation, most likely due to the destructive growth of the locally invasive tumor. On the other hand, in a recent study on the innervation density of the pancreas in the KC model, Stopczynski et al. showed that the beginning of neuroplasticity in Kras-based models like the KC model dates back to the pre-invasive, PanIN stage (Stopczynski et al., 2014). Here, the extracellular matrix surrounding the PanIN lesions was shown to exhibit a prominently enhanced fine fiber innervation when compared to the normal pancreatic parenchyma (Stopczynski et al., 2014). Hence, it seems that tumor hyperinnervation occurs not during the whole, but a rather broad phase of carcinogenesis between the pre-invasive and pre-final stage.

Emergence of tumor hyperinnervation in GEMM of PDAC underlines the concept that pancreatic carcinogenesis is associated with a trophic tumor microenvironment for nerves, a concept that has been repeatedly shown to hold true for human PDAC (Zhu et al., 1999; Ceyhan et al., 2006; Ceyhan et al., 2010). This trophic microenvironment seems to be created by increased expression and release of neurotrophic factors from different sources in the tumor tissue. The leading cell types that are responsible for neurotrophic growth in the PDAC stroma are cancer cells (Ceyhan et al., 2006; Ceyhan et al., 2010; Demir et al., 2012), inflammatory

cells that e.g. secrete NGF (Demir et al., 2013), or stromal cells like pancreatic stellate cells that were shown to induce neuronal plasticity (Demir et al., 2010; Secq et al., 2015). In a comprehensive review on neuroplastic alterations in gastrointestinal cancers, these sources of neuroplasticity and neurotrophism were shown to be similarly encountered in all major GI cancers including PDAC, colon cancer, liver cancer, and gastric cancer (Demir et al., 2013). The functional implications of tumor hyperinnervation can be multifold. It can serve 1) to enhance local surveillance for better detection of noxious alterations or cancer cells during tumor growth, 2) to facilitate tumor spread due to increased availability of large nerve trunks along which cancer cells can spread, 3) to signal more frequent and/or intense pain to the central nervous system, 4) to augment local inflammation due to neuro-immune crosstalk, or 5) to influence tumor growth directly due to growth-modulating properties of neurotransmitters or growth factors like NGF, neurturin, GDNF or artemin released from nerves (Okada et al., 2003; Ceyhan et al., 2006; Ceyhan et al., 2010; Wang et al., 2014). Hence, cancer cells or inflammatory cells can augment neural growth and enhance secretion of trophic factors from nerves that can, as in a vicious cycle, in turn enhance cancer cell growth or sustain local inflammation (Demir et al., 2013). In the present study, the transcriptomic profiling of the primary cancer cells derived from these GEMM of PDAC revealed that the loss of trp53 during pancreatic carcinogenesis rapidly switches the expression profile of cancer to a more “neurotrophic” phenotype with particularly enhanced expression of Gfralpha2, NGF, Fgfr1, and artemin. In accordance with human studies, all these four factors have been shown to be upregulated in human PDAC and to correlate to neuroplasticity, pain or NI in human PDAC (Korc, 2007; Ceyhan et al., 2010; Wang et al., 2014). Therefore, the current GEMM of PDAC seem to successfully model the tumor hyperinnervation that is typical for human PDAC also at molecular level. However, in

human PDAC, the severity of NI is known to correlate to the extent of neuroplasticity in the tumor tissue (Ceyhan et al., 2009). In the present study, though, the TPAC and TPC models as the only truly neuro-invasive models did not exhibit a greater hyperinnervation than e.g. KPC mice. Therefore, based on the results of the present study, increasing NI does not always have to be associated with increased neuroplasticity and vice versa. There seem to exist other molecular mechanisms that favor the emergence of NI independent of neuroplasticity in PDAC. In this regard, the transcriptional profile of the neuro-invasive TPAC and TPC models in comparison to KPC mice provides some important clues, since these neuro-invasive mice did not differ from KPC with regard to the expression of neurotrophic factors, but rather with regard to the increased expression of neuropeptides like NPY or to the expression of the proto-oncogene product Fos. Hence, also at molecular level, neuroplasticity and NI in murine PDAC seem to share divergent and thereby differentiating transcriptional signatures.

Pancreatic neuritis represents a hallmark of pancreatic neuropathy in PDAC and CP (Ceyhan et al., 2009). The presence of pancreatic neuritis was reported to correlate to the severity of pain among patients with CP and PDAC (Di Sebastiano et al., 1997; Di Sebastiano et al., 2000; Ceyhan et al., 2009). Furthermore, immune cells that infiltrate intrapancreatic nerves were shown to upregulate intracellular interleukin-8 (Di Sebastiano et al., 2000). However, analysis of pancreatic neuritis necessitates separate analysis of perineural inflammation from the general tissue inflammation that is very frequent in PDAC tissues (Ceyhan et al., 2009), since perineural inflammatory cell foci in CP and PDAC are clearly marked off from the remaining pancreatic tissue infiltrate (Ceyhan et al., 2009). The impact of the general tumor inflammation has been subject to extensive study in recent years, particularly in association with desmoplastic alterations. Indeed, increased tumor desmoplasia

was recently shown to augment the overall immune cell infiltration and the number of T effector cells (Teff), and to result in decreased amounts of FoxP3$^+$ regulatory T cells (Treg) (Ozdemir et al., 2014; Rhim et al., 2014). Depletion of tumor stroma resulted in reversion of this proportion toward increased amounts of Treg in the PDAC stroma (Ozdemir et al., 2014; Rhim et al., 2014). Yet there are other investigators who reported increased sequestration of CD8$^+$ cytotoxic T cells due to pancreatic stellate cell activation, thereby limiting their contact with tumor cells in the juxtatumoral compartment (Ene-Obong et al., 2013). In a study on the inflammatory cell subtypes in human PDAC, CP and normal human pancreas, Emmrich et al. reported CD8$^+$ cytotoxic T cells to be the most prevalent cell type in the stroma (Emmrich et al., 1998). At this point, it seems imperative to perform studies that compare the immune cell infiltration pattern of the whole pancreatic tumor between human and murine PDAC. Hence, there seem to exist parallels between the types of inflammatory cells in human and murine PDAC. In a study that specifically analyzed perineural inflammatory cell infiltrates in PDAC and CP, we could previously show that pancreatic neuritis lesions are composed of CD8$^+$ cytotoxic T cells, CD68$^+$ macrophages, and mast cells (Demir et al., 2013). Importantly, among PDAC and CP patients with pain, the amount of perineural mast cells was selectively increased, and there were increased amounts of activated versus quiescent mast cells in pancreatic neuritis lesions (Demir et al., 2013). Mast cells were further reported to promote tumor growth in xenograft mice with PDAC or GEMM of PDAC (Chang et al., 2011; Ma et al., 2013), yet to be dispensable for the initiation of pancreatic tumorigenesis (Schonhuber et al., 2014). Therefore, pancreatic neuritis is increasingly recognized to be a clinically relevant type of pancreatic neuro-inflammation, and efforts to target it therapeutically are underway. Yet why such a key feature of pancreatic neuropathy is not encountered in any of the total of seven murine models analyzed in this study

remains unclear. It is conceivable that the overall pronounced tumor inflammation in these mouse models masks the presence of nerve-targeting inflammatory cells in the stroma. Furthermore, although specific perineural inflammatory cell foci were not observed in these murine models, there were inflammatory cells that were in contact with the epi- or perineurium of nerves at several occasions, and the severity of this immune cell penetration into nerves from the population of tissue-infiltrating immune cells was quantified and presented on Figure 11. Therefore, the present analysis primarily shows that the pancreatic neuritis as it is known from the perineural immune cell conglomerates in human PDAC is not encountered in murine PDAC, yet these observations do not exclude neuro-immuno crosstalk in nerves within the stroma of GEMM of PDAC.

The potentially most important finding of this study is the demonstration of a truly neuro-invasive GEMM of PDAC and the mechanistic dissection of the particular neuroaffinity of this model as opposed to the remaining murine PDAC models. There has been a long-standing quest for neuro-invasive murine PDAC models among researchers who had specialized in the field of NI in PDAC, since the traditional models including chemically-induced or xenograft models contained no human-like NI at all (Demir et al., 2012). It is obvious that there is rapidly increasing interest in understanding nerve-cancer interactions in PDAC because these are considered to considerably influence the course of the disease (Stopczynski et al., 2014; Secq et al., 2015). NI was indeed also briefly addressed in one of the two pioneering studies by Hingorani et al. on murine Kras-based PDAC models and was demonstrated to exist as invasion of neural plexus. Yet, based on the provided image in that study, it seems that the investigators observed local continuous tumor growth toward the retroperitoneum in the initial description of the KC model that had progressed to become invasive. However, the provided images in that study merely showed a large,

probably retropancreatic neural plexus that was encased by the non-selectively invading pancreatic tumor. This non-selective tumor growth toward the juxtatumoral neural or also other structures does not correspond to true NI. Indeed, real NI is characterized by the intrapancreatic entry of cancer cells into the nerves that cancer cells use as physical paths of spread from the interior toward the exterior of the organ (Kayahara et al., 2007; Demir et al., 2012). Furthermore, NI can even be encountered in nerves within apparently tumor-free regions of the pancreas as “intrapancreatic, extratumoral perineural invasion”, briefly termed “nex”, (Takahashi et al., 1997). Unfortunately, in the past decade of outstanding achievements related to GEMM of PDAC, NI as a defining feature in the histopathology and the UICC classification of PDAC (Liebl et al., 2014) has not received any attention. In a consensus conference on the histopathological features of GEMM of PDAC by expert GEMM pathologists, NI has even found no mention in the consensus report (Hruban et al., 2006). The results of the presented study and especially the reporting of true NI in a GEMM of PDAC is likely to contribute to increased perception and reporting of this feature in future models.

Despite the identification of differentiating molecular signatures of cancer cells derived from the neuro-invasive TPAC in comparison to the remaining models, the general reasons for the human-like neuroinvasive ability of TPAC cancer cells have yet to be further studied. One distinguishing feature that may guide future research in this direction was the increased incidence of ductal, and less anaplastic, tumors after the depletion of RelA/p65 in the TPAC model. Indeed, the TPAC tumors had a more ductal appearance compared to all other remaining models in this study and a correspondingly longer life span. It is thus imaginable that increased tumor differentiation, in combination with a somewhat longer time-span, i.e. a slower invasive tumor dynamics, may let sufficient time for the generation of NI. In an

anaplastically growing pancreatic tumor, which is relatively rare in the human disease, nerves may get rapidly destructed by the anaplastic cancer cells, and there may be no time for an adaptive neuronal plasticity. Hence, for future studies, it seems useful to generate novel GEMM of PDAC with better tumor differentiation as opposed to rapidly invasive or metastatic tumors.

The possibilities that are intrinsic to such a human-like neuro-invasive model are multifold. In the era of neoadjuvant regimens for managing locally advanced PDAC, such a GEMM of PDAC would allow the study of the impact of neoadjuvant therapy on the degree of NI, on the severity of pain, and on the rate of local recurrence, or on the disease-free, progression-free or overall survival of the animals. It would allow to determine the impact of radiotherapy that was recently reported to limit NI on the clinical course of the disease (Bakst et al., 2012). Furthermore, it would finally enable in vivo mechanistic studies that would aim at in vivo tracking of cancer cells after or before resection of the pancreatic tumor mass. Overall, the TPAC model is likely to serve as a valuable tool for studying NI, for deciphering its mechanism and for developing novel therapeutic strategies that may have higher translational relevance due to the more human-like nature of the model.

The present study also described that glial cells of the peripheral nervous system, i.e. Schwann cells (SC), can assume hitherto unknown and surprising roles in the progression of cancer. During NI, via the interaction of surface receptors like MAG or MUC1, SC were previously reported to undergo a potentially very close spatial interaction with PDAC cells (Swanson et al., 2007). However, it was unknown how SC react to the presence of PDAC cells that are beneath the epi- or perineurium during NI. Another possibility in this context was that the neuroaffinity of PDAC cells may not be directed at the neuronal processes within nerves but rather toward the SC that are located within peripheral nerves. To examine all these possibilities, a

novel heterotypic culture system was established in which transsected sciatic nerves were confronted with PDAC cells. This 3D SC outgrowth assay, together with simultaneous investigations using 3D migration assays in our research group, revealed that SC have a very early and strong affinity to cancer cells that even surpasses the affinity of cancer cells to neurons (Demir et al., 2014). *In vivo*, a compelling observation was the emergence of SC already around PanIN lesions and their persistence into the overt cancer stage as diffusely distributed cells in the tumor stroma. The current study therefore provided substantial evidence for SC as potential initiators of nerve-cancer interactions in PDAC. Furthermore, it introduced the novel concept of “Schwann cell carcinotropism”. This concept implies that, in contrast with the traditional assumption, cancer cells do not migrate actively toward nerves, but that SC as peripheral glia are chemoattracted toward PDAC precursor lesions and lay the ground for NI. This concept implies that following the emergence of the PDAC precursors, interaction of the nervous system with cancer has started. Furthermore, if SC chemoattraction to cancer precursors is the genuine initiator of NI, then NI may even be unavoidable on the background of defined genetic alterations. To further understand the potential contribution of SC to cancer, it is imperative to consider their roles in multiple neurological processes. SC are responsible for serving as a protection for the axons, for facilitating axonal signal transmission and particularly for neural repair after axonal injury (Scholz et al., 2007). Furthermore, recent studies suggested that SC phagocytose synapses and terminal nerve endings during axonal pruning (Smith et al., 2014), and that their decreased capacity for autophagy contributes to initiation of chronic neuropathic pain (Marinelli et al., 2014). Considering these roles of SC related to neural repair, growth promotion, selective clearance of axons, autophagy, and phagocytosis, our findings open up multiple novel possibilities for investigating the role of SC in PDAC and also all other cancers.

In future studies, in vivo approaches that will selectively manipulate SC-intrinsic signaling pathways may further broaden our understanding of the role SC in cancer.

The current study provided some clues for the difference in the extent of pain sensation between various GEMM of PDAC. Pain is an unpleasant experience and coupled to the perception of this unpleased trait by the emotion-generating cortical areas of the brain (Demir et al., 2011). As mice are not able to articulate their emotions, analysis of pain in mouse models of disease relies on the identification of indirect signs of pain sensation. A typical feature of increased pain sensation is cross-activation of mechanosensitive pathways in the presence of high nociceptive activity, which corresponds to allodynia (Sandkuhler, 2009). Therefore, assessment of abdominal allodynia represents one of the most commonly applied methods to assess potential pain sensation in rodents. By using von Frey filaments, the current study found that TPC mice have less abdominal allodynia when compared to KPC or TPAC mice. The mechanism behind these mice of comparable cancer stage remains unclear. The expression analysis from the cancer cells of these models showed that TPC cells actually upregulate important nociceptive receptors like TrkB (Ntrk2) and CX3CR1. Hence, it has to be assumed that cancer-cell derived factors may not be the determinants of pain sensation in these models. Factors released from other players in the tumor microenvironment such as inflammatory cells and especially their subtypes may exert a major impact on the nociceptive activation in these models. Therefore, future studies should aim at the characterization and selective depletion of inflammatory cell subtypes in these GEMM of PDAC and correlate these alterations to the extent of allodynia or other parameters of increased pain sensation, such decreased locomotion, diminished exploratory behavior or grooming.

Identifying the differences in the molecular signature of the core models was one of the key goals of this study. The microarray-based transcriptomic analysis

revealed multiple key differences between the analyzed GEMM. First of all, the loss of trp53 in the TPC, TPAC, or KPC cancer cells was associated with an expected enrichment of genes that belonged to the regulation of growth, cell cycle and cell differentiation. However, in the ranking and KEGG-based pathway analysis of enriched genes, alterations in the neurotrophin signaling ranked among the top ten alterations, and neural pathway genes comprised 7% of all transcriptomic alterations in the trp53-deficient cancer cells versus KC carcinoma cells. Furthermore, in the subanalysis of KC versus KPC cells, the highest ranked altered pathway among all significantly enriched genes was the neuroactive ligand and receptor pathway, surpassing all other differences related to major pathways like cell metabolism, protein biosynthesis or immune-related alterations. These observations suggested that loss of trp53 may generate a genetic signature that may specifically support the growth of nerves or the invasion of cancer cells along nerves. This conclusion from the microarray analysis was strongly supported by the prominent enrichment of neurotrophic factors and receptors like NGF, GFRalpha2 and Artemin in the expression profile of trp53-deficient murine PDAC cells. Therefore, a major transcriptomic feature of trp53-deficient murine PDAC cells seems to be the upregulation of neurotrophic factor and receptors.

The transcriptomic analysis also enabled the comparison of the neuro-invasive TPAC cancer cells with the commonly used KPC cancer cells. Here, there was an overwhelming accumulation of enriched genes in TPAC cells within pathways related to cell metabolism, including lysosomal, peroxisomal pathways, cytochrome p450, and aminoacid biosynthesis. Indeed, 67% of enriched pathways in TPAC versus KPC cells were related to metabolomics. A very similar major difference in the metabolic properties of TPAC cells was additionally detected in the microarray analysis of TPAC versus TPC cells. Also here, around 50% of all enriched gene sets were

related to metabolic alterations, including those within glutathione metabolism, cytochrome p450, tyrosine metabolism and glycolysis. Hence, the defining transcriptomic counterpart for the neuro-invasiveness of TPAC cells, when compared to KPC or TPC cells, seems to be the profoundly different metabolomic profile of TPAC cells, potentially regulated by the RelA/p65. From the perspective of neuroactive signaling, the profiler arrays showed an upregulation of neuropeptide Y (NPY) in the neuro-invasive TPAC and TPC cells when compared to KPC cells. In the biomedical literature, a pro-neuro-invasive role for NPY signaling has not yet been described. However, NPY and its receptors Y1-, Y2-, Y4-, Y5-, and Y6-R were reported to regulate multiple aspects of cancer progression, including cell proliferation, invasion, metastasis, and angiogenesis in neural crest-derived tumors, breast and prostate cancer (Ruscica et al., 2007). It is imaginable that NPY may also contribute to the altered metabolic behavior of TPAC cells. On the other hand, in the analysis of all upregulated pathways, the less neuro-invasive TPC model exhibited an enrichment of genes that are related to extracellular matrix generation, including gylcosaminoglycan synthesis and TGF-beta signaling. Overall, these detailed transcriptomic analyses collectively suggest distinct alterations that clearly distinguish the cancer cells of these GEMM of PDAC from the remaining models and therefore provide important clues for the generation of future, more human-like GEMM of PDAC.

Conclusion

GEMM of PDAC have recently enabled a major advance in our understanding of the pathophysiology of PDAC. Human PDAC is characterized by prominent alterations in pancreatic innervation, including NI, increased neural density, neural hypertrophy and pancreatic neuritis. NI is an independent prognostic factor for the overall, disease-free and progression-free survival in human PDAC and encountered in up to 100% of PDAC cases. Although a hallmark of human PDAC, neuropathy and especially NI have not yet been studied in GEMM of PDAC.

The current study provided the first comparative functional and molecular characterization of the most important GEMM of PDAC. It demonstrates that the tumor hyperinnervation and neuroplasticity as typical features of human PDAC are similarly encountered in the oncogenic Kras-based KPC, and the TGFalpha-overexpression-based transgenic TPC and TPAC models of PDAC. Correspondingly, supernatants of cancer cells derived from these models could induce increased neurite density of cultivated mouse DRG neurons. In contrast with human PDAC, none of the studied GEMM was found to harbor a specific pancreatic neuritis, although tumor nerves were frequently embedded within the large tissue inflammatory deposits that are typical for all GEMM of PDAC. As the key finding of the study, a true human-like NI with perineural lining of cancer cells was solely detected in the TPAC model, yet the overall frequency of NI even in this model remained around 40-50%. The differences in the NI severity of the GEMM of PDAC were recapitulated in a novel 3D migration assay, in which cancer cells from the TPAC model exhibited a much more targeted migration toward murine neurons as analyzed via quantitative digital time-lapse analysis. Furthermore, the current study shed light on a previously unknown reaction of peripheral glia of nerves, i.e. Schwann

cells (SC), during pancreatic carcinogenesis. Here, SC were detected to emerge in the tumor stroma as physically separate cells from the nerves around the PanIN precursor lesions of PDAC. In a novel 3D SC outgrowth assay using explanted murine sciatic nerves, SC were found to specifically migrate toward cancer cells, and the extent of this “carcinotropism” was strongest toward TPAC cells, thus in accordance with the histological high frequency of true NI in this model. As increasing NI severity was previously shown to be linked to pain sensation in PDAC, the GEMM of PDAC were additionally analyzed with regard to the pain sensation of mice. Here, TPC mice with much less NI as opposed to the TPAC mice were observed to exhibit a decreased abdominal mechanosensitivity, implying a more severe pain-induced mechanosensitization in TPAC mice. At the transcriptional level, cancer cells from the TPAC, TPC and KPC models of PDAC were characterized by prominent upregulation of the neurotrophic factor-receptor axis, including GFRalpha2, NGF, Fgf2 and Artemin, when compared to the KC model with intact p53 function. In the comparison of the p53-deficient models, the neuro-invasive TPAC model showed a profoundly altered metabolic profile especially with regard to lysosomal, peroxisomal, and protein biosynthesis, and also enhanced expression of neuropeptide Y (NPY) in cancer cells, which is a co-neurotransmitter within sympathetic nerve fibers.

Overall, the present study showed that GEMM of PDAC feature some of the major characteristics of human pancreatic neuropathy, yet in differing extent based on the genetic alterations that define each model. Due to the depletion of RelA/p65 and thereby of the canonical NFkappaB-signaling in the TPAC model, NFkappaB signaling seems to play a leading role in the generation of neuro-invasive GEMM of PDAC. Similarly, metabolomic differences, differential regulation of ECM synthesis, and NPY upregulation as a distinguishing transcriptomic signature of the neuro-invasive TPAC cells point out toward the mechanisms that may lie behind the unique

neuro-invasiveness of this model. These targets may serve as valuable molecular tools for generating future GEMM of PDAC with greater similarity to human PDAC and thus with higher translational relevance for treating this utmost lethal malignancy.

References

Bakst, R. L., N. Lee, et al. (2012)"Radiation impairs perineural invasion by modulating the nerve microenvironment."PLoS One 7: e39925.

Ballehaninna, U. K. and R. S. Chamberlain. (2011)"Serum CA 19-9 as a Biomarker for Pancreatic Cancer-A Comprehensive Review."Indian J Surg Oncol 2: 88-100.

Bardeesy, N., A. J. Aguirre, et al. (2006)"Both p16(Ink4a) and the p19(Arf)-p53 pathway constrain progression of pancreatic adenocarcinoma in the mouse."Proc Natl Acad Sci U S A 103: 5947-52.

Barton, C. M., S. L. Staddon, et al. (1991)"Abnormalities of the p53 tumour suppressor gene in human pancreatic cancer."Br J Cancer 64: 1076-82.

Bauer, T. M., B. F. El-Rayes, et al. (2013)"Carbohydrate antigen 19-9 is a prognostic and predictive biomarker in patients with advanced pancreatic cancer who receive gemcitabine-containing chemotherapy: a pooled analysis of 6 prospective trials."Cancer 119: 285-92.

Biankin, A. V., N. Waddell, et al. (2012)"Pancreatic cancer genomes reveal aberrations in axon guidance pathway genes."Nature 491: 399-405.

Bockhorn, M., F. G. Uzunoglu, et al. (2014)"Borderline resectable pancreatic cancer: a consensus statement by the International Study Group of Pancreatic Surgery (ISGPS)."Surgery 155: 977-88.

Bockman, D. E., M. Buchler, et al. (1994)"Interaction of pancreatic ductal carcinoma with nerves leads to nerve damage."Gastroenterology 107: 219-30.

Carriere, C., E. S. Seeley, et al. (2007)"The Nestin progenitor lineage is the compartment of origin for pancreatic intraepithelial neoplasia."Proc Natl Acad Sci U S A 104: 4437-42.

Ceyhan, G. O., F. Bergmann, et al. (2009)"Pancreatic neuropathy and neuropathic pain--a comprehensive pathomorphological study of 546 cases."Gastroenterology 136: 177-186 e1.

Ceyhan, G. O., I. E. Demir, et al. (2008)"Neural invasion in pancreatic cancer: a mutual tropism between neurons and cancer cells."Biochem Biophys Res Commun 374: 442-7.

Ceyhan, G. O., S. Deucker, et al. (2009)"Neural fractalkine expression is closely linked to pain and pancreatic neuritis in human chronic pancreatitis."Lab Invest 89: 347-61.

Ceyhan, G. O., N. A. Giese, et al. (2006)"The neurotrophic factor artemin promotes pancreatic cancer invasion."Ann Surg 244: 274-81.

Ceyhan, G. O., F. Liebl, et al. (2010)"The severity of neural invasion is a crucial prognostic factor in rectal cancer independent of neoadjuvant radiochemotherapy."Ann Surg 252: 797-804.

Ceyhan, G. O., K. H. Schafer, et al. (2010)"Nerve growth factor and artemin are paracrine mediators of pancreatic neuropathy in pancreatic adenocarcinoma."Ann Surg 251: 923-31.

Chandler, N. M., J. J. Canete, et al. (2004)"Increased expression of NF-kappa B subunits in human pancreatic cancer cells."J Surg Res 118: 9-14.

Chang, D. Z., Y. Ma, et al. (2011)"Mast cells in tumor microenvironment promotes the in vivo growth of pancreatic ductal adenocarcinoma."Clin Cancer Res 17: 7015-23.

Chow, J. Y., M. Ban, et al. (2010)"TGF-beta downregulates PTEN via activation of NF-kappaB in pancreatic cancer cells."Am J Physiol Gastrointest Liver Physiol 298: G275-82.

Conroy, T., F. Desseigne, et al. (2011)"FOLFIRINOX versus gemcitabine for metastatic pancreatic cancer."N Engl J Med 364: 1817-25.

D'Haese, J. G., M. Hartel, et al. (2014)"Pain sensation in pancreatic diseases is not uniform: the different facets of pancreatic pain."World J Gastroenterol 20: 9154-61.

Dai, H., R. Li, et al. (2007)"Enhanced survival in perineural invasion of pancreatic cancer: an in vitro approach."Hum Pathol 38: 299-307.

Delpu, Y., N. Hanoun, et al. (2011)"Genetic and epigenetic alterations in pancreatic carcinogenesis."Curr Genomics 12: 15-24.

Demir, I. E., A. Boldis, et al. (2014)"Investigation of Schwann cells at neoplastic cell sites before the onset of cancer invasion."J Natl Cancer Inst 106.

Demir, I. E., G. O. Ceyhan, et al. (2010)"Neural Invasion in Pancreatic Cancer: The Past, Present and Future."Cancers 2: 1513-1527.

Demir, I. E., G. O. Ceyhan, et al. (2010)"The microenvironment in chronic pancreatitis and pancreatic cancer induces neuronal plasticity."Neurogastroenterol Motil 22: 480-90, e112-3.

Demir, I. E., H. Friess, et al. (2012)"Nerve-cancer interactions in the stromal biology of pancreatic cancer."Front Physiol 3: 97.

Demir, I. E., K. H. Schafer, et al. (2013)"Neural plasticity in the gastrointestinal tract: chronic inflammation, neurotrophic signals, and hypersensitivity."Acta Neuropathol 125: 491-509.

Demir, I. E., S. Schorn, et al. (2013)"Perineural mast cells are specifically enriched in pancreatic neuritis and neuropathic pain in pancreatic cancer and chronic pancreatitis."PLoS One 8: e60529.

Demir, I. E., E. Tieftrunk, et al. (2011)"Pain mechanisms in chronic pancreatitis: of a master and his fire."Langenbecks Arch Surg 396: 151-60.

Demir, I. E., E. Tieftrunk, et al. (2014)"Simulating pancreatic neuroplasticity: in vitro dual-neuron plasticity assay."J Vis Exp.

Di Sebastiano, P., F. F. di Mola, et al. (2000)"Expression of interleukin 8 (IL-8) and substance P in human chronic pancreatitis."Gut 47: 423-8.

Di Sebastiano, P., T. Fink, et al. (1997)"Immune cell infiltration and growth-associated protein 43 expression correlate with pain in chronic pancreatitis."Gastroenterology 112: 1648-55.

DiMagno, E. P., H. A. Reber, et al. (1999)"AGA technical review on the epidemiology, diagnosis, and treatment of pancreatic ductal adenocarcinoma. American Gastroenterological Association."Gastroenterology 117: 1464-84.

Dintzis, S. M., Liggitt, D. (2012). Comparative Anatomy and Histology: A Mouse and Human Atlas. San Diego, Academic Press, Elsevier.

Downing, J. E. and J. A. Miyan. (2000)"Neural immunoregulation: emerging roles for nerves in immune homeostasis and disease."Immunol Today 21: 281-9.

Emmrich, J., I. Weber, et al. (1998)"Immunohistochemical characterization of the pancreatic cellular infiltrate in normal pancreas, chronic pancreatitis and pancreatic carcinoma."Digestion 59: 192-8.

Ene-Obong, A., A. J. Clear, et al. (2013)"Activated pancreatic stellate cells sequester CD8+ T cells to reduce their infiltration of the juxtatumoral compartment of pancreatic ductal adenocarcinoma."Gastroenterology 145: 1121-32.

Ergul, N., C. Gundogan, et al. (2014)"Role of (18)F-fluorodeoxyglucose positron emission tomography/computed tomography in diagnosis and management of pancreatic cancer; comparison with multidetector row computed tomography, magnetic resonance imaging and endoscopic ultrasonography."Rev Esp Med Nucl Imagen Mol 33: 159-64.

Feig, C., A. Gopinathan, et al. (2012)"The pancreas cancer microenvironment."Clin Cancer Res 18: 4266-76.

Garcea, G., A. R. Dennison, et al. (2008)"Survival following curative resection for pancreatic ductal adenocarcinoma. A systematic review of the literature."Jop 9: 99-132.

Gerondakis, S., T. S. Fulford, et al. (2014)"NF-kappaB control of T cell development."Nat Immunol 15: 15-25.

Gidekel Friedlander, S. Y., G. C. Chu, et al. (2009)"Context-dependent transformation of adult pancreatic cells by oncogenic K-Ras."Cancer Cell 16: 379-89.

Gil, Z., O. Cavel, et al. (2010)"Paracrine regulation of pancreatic cancer cell invasion by peripheral nerves."J Natl Cancer Inst 102: 107-18.

Gil, Z., A. Rein, et al. (2007)"Nerve-sparing therapy with oncolytic herpes virus for cancers with neural invasion."Clin Cancer Res 13: 6479-85.

Gillen, S., T. Schuster, et al. (2010)"Preoperative/neoadjuvant therapy in pancreatic cancer: a systematic review and meta-analysis of response and resection percentages."PLoS Med 7: e1000267.

Goggins, M., M. Schutte, et al. (1996)"Germline BRCA2 gene mutations in patients with apparently sporadic pancreatic carcinomas."Cancer Res 56: 5360-4.

Gohrig, A., K. M. Detjen, et al. (2014)"Axon guidance factor SLIT2 inhibits neural invasion and metastasis in pancreatic cancer."Cancer Res 74: 1529-40.

Greten, F. R., M. Wagner, et al. (2001)"TGF alpha transgenic mice. A model of pancreatic cancer development."Pancreatology 1: 363-8.

Guerra, C. and M. Barbacid. (2013)"Genetically engineered mouse models of pancreatic adenocarcinoma."Mol Oncol 7: 232-47.

Guerra, C., M. Collado, et al. (2011)"Pancreatitis-induced inflammation contributes to pancreatic cancer by inhibiting oncogene-induced senescence."Cancer Cell 19: 728-39.

Guerra, C., A. J. Schuhmacher, et al. (2007)"Chronic pancreatitis is essential for induction of pancreatic ductal adenocarcinoma by K-Ras oncogenes in adult mice."Cancer Cell 11: 291-302.

Guo, K., Q. Ma, et al. (2013)"Interaction of the sympathetic nerve with pancreatic cancer cells promotes perineural invasion through the activation of STAT3 signaling."Mol Cancer Ther 12: 264-73.

Habbe, N., G. Shi, et al. (2008)"Spontaneous induction of murine pancreatic intraepithelial neoplasia (mPanIN) by acinar cell targeting of oncogenic Kras in adult mice."Proc Natl Acad Sci U S A 105: 18913-8.

Hahn, S. A., M. Schutte, et al. (1996)"DPC4, a candidate tumor suppressor gene at human chromosome 18q21.1."Science 271: 350-3.

Hanlon, L., J. L. Avila, et al. (2010)"Notch1 functions as a tumor suppressor in a model of K-ras-induced pancreatic ductal adenocarcinoma."Cancer Res 70: 4280-6.

Hartwig, W., T. Hackert, et al. (2009)"Multivisceral resection for pancreatic malignancies: risk-analysis and long-term outcome."Ann Surg 250: 81-7.

Hartwig, W., C. M. Vollmer, et al. (2014)"Extended pancreatectomy in pancreatic ductal adenocarcinoma: definition and consensus of the International Study Group for Pancreatic Surgery (ISGPS)."Surgery 156: 1-14.

Hayden, M. S. and S. Ghosh. (2008)"Shared principles in NF-kappaB signaling."Cell 132: 344-62.

Herreros-Villanueva, M., E. Hijona, et al. (2012)"Mouse models of pancreatic cancer."World J Gastroenterol 18: 1286-94.

Hidalgo, M. (2010)"Pancreatic cancer."N Engl J Med 362: 1605-17.

Hingorani, S. R., E. F. Petricoin, et al. (2003)"Preinvasive and invasive ductal pancreatic cancer and its early detection in the mouse."Cancer Cell 4: 437-50.

Hingorani, S. R., L. Wang, et al. (2005)"Trp53R172H and KrasG12D cooperate to promote chromosomal instability and widely metastatic pancreatic ductal adenocarcinoma in mice."Cancer Cell 7: 469-83.

Hosoi, F., H. Izumi, et al. (2009)"N-myc downstream regulated gene 1/Cap43 suppresses tumor growth and angiogenesis of pancreatic cancer through attenuation of inhibitor of kappaB kinase beta expression."Cancer Res 69: 4983-91.

Hruban, R. H., N. V. Adsay, et al. (2006)"Pathology of genetically engineered mouse models of pancreatic exocrine cancer: consensus report and recommendations."Cancer Res 66: 95-106.

Hruban, R. H., M. I. Canto, et al. (2010)"Update on familial pancreatic cancer."Adv Surg 44: 293-311.

Huang, J., C. Zhu, et al. (2013)"S100+ cells: a new neuro-immune cross-talkers in lymph organs."Sci Rep 3: 1114.

Iacobuzio-Donahue, C. A., V. E. Velculescu, et al. (2012)"Genetic basis of pancreas cancer development and progression: insights from whole-exome and whole-genome sequencing."Clin Cancer Res 18: 4257-65.

Jackson, E. L., N. Willis, et al. (2001)"Analysis of lung tumor initiation and progression using conditional expression of oncogenic K-ras."Genes Dev 15: 3243-8.

Jones, S., R. H. Hruban, et al. (2009)"Exomic sequencing identifies PALB2 as a pancreatic cancer susceptibility gene."Science 324: 217.

Jones, S., X. Zhang, et al. (2008)"Core signaling pathways in human pancreatic cancers revealed by global genomic analyses."Science 321: 1801-6.

Jonkers, J., R. Meuwissen, et al. (2001)"Synergistic tumor suppressor activity of BRCA2 and p53 in a conditional mouse model for breast cancer."Nat Genet 29: 418-25.

Kanda, M., T. Fujii, et al. (2014)"Pancreatoduodenectomy with portal vein resection is feasible and potentially beneficial for elderly patients with pancreatic cancer."Pancreas 43: 951-8.

Kasperczyk, H., B. Baumann, et al. (2009)"Characterization of sonic hedgehog as a novel NF-kappaB target gene that promotes NF-kappaB-mediated apoptosis resistance and tumor growth in vivo."Faseb J 23: 21-33.

Katz, M. H., R. Marsh, et al. (2013)"Borderline resectable pancreatic cancer: need for standardization and methods for optimal clinical trial design."Ann Surg Oncol 20: 2787-95.

Kayahara, M., H. Nakagawara, et al. (2007)"The nature of neural invasion by pancreatic cancer."Pancreas 35: 218-23.

Khanbolooki, S., S. T. Nawrocki, et al. (2006)"Nuclear factor-kappaB maintains TRAIL resistance in human pancreatic cancer cells."Mol Cancer Ther 5: 2251-60.

Kobayashi, M., S. Mizuno, et al. (2014)"Gemcitabine-based chemoradiotherapy followed by surgery for borderline resectable and locally unresectable pancreatic ductal adenocarcinoma: significance of the CA19-9 reduction rate and intratumoral human equilibrative nucleoside transporter 1 expression."Pancreas 43: 350-60.

Kong, R., B. Sun, et al. (2010)"Downregulation of nuclear factor-kappaB p65 subunit by small interfering RNA synergizes with gemcitabine to inhibit the growth of pancreatic cancer."Cancer Lett 291: 90-8.

Kopp, J. L., G. von Figura, et al. (2012)"Identification of Sox9-dependent acinar-to-ductal reprogramming as the principal mechanism for initiation of pancreatic ductal adenocarcinoma."Cancer Cell 22: 737-50.

Korc, M. (2007)"Pancreatic cancer-associated stroma production."Am J Surg 194: S84-6.

Larson, D. L., A. E. Rodin, et al. (1966)"Perineural lymphatics: myth or fact."Am J Surg 112: 488-92.

Lesina, M. (2013)"Charakterisierung der Funktion des Transkriptionsfaktors RelA/p65 im Ela-TGFα transgenen Mausmodell der pankreatischen Karzinogenese."http://mediatum.ub.tum.de/doc/1116592/1116592.pdf.

Li, J., Q. Ma, et al. (2011)"Relationship between neural alteration and perineural invasion in pancreatic cancer patients with hyperglycemia."PLoS One 6: e17385.

Liebig, C., G. Ayala, et al. (2009)"Perineural invasion in cancer: a review of the literature."Cancer 115: 3379-91.

Liebl, F., I. E. Demir, et al. (2014)"The impact of neural invasion severity in gastrointestinal malignancies: a clinicopathological study."Ann Surg 260: 900-8.

Liebl, F., I. E. Demir, et al. (2012)"The severity of neural invasion is associated with shortened survival in colon cancer."Clin Cancer Res: Nov 12. [Epub ahead of print].

Lopez, N. E., C. Prendergast, et al. (2014)"Borderline resectable pancreatic cancer: definitions and management."World J Gastroenterol 20: 10740-51.

Lu, T. T. and J. L. Browning. (2014)"Role of the Lymphotoxin/LIGHT System in the Development and Maintenance of Reticular Networks and Vasculature in Lymphoid Tissues."Front Immunol 5: 47.

Ma, Y., R. F. Hwang, et al. (2013)"Dynamic mast cell-stromal cell interactions promote growth of pancreatic cancer."Cancer Res 73: 3927-37.

Makohon-Moore, A., J. A. Brosnan, et al. (2013)"Pancreatic cancer genomics: insights and opportunities for clinical translation."Genome Med 5: 26.

Mann, K. M., J. M. Ward, et al. (2012)"Sleeping Beauty mutagenesis reveals cooperating mutations and pathways in pancreatic adenocarcinoma."Proc Natl Acad Sci U S A 109: 5934-41.

Marchesi, F., L. Piemonti, et al. (2008)"The chemokine receptor CX3CR1 is involved in the neural tropism and malignant behavior of pancreatic ductal adenocarcinoma."Cancer Res 68: 9060-9.

Marinelli, S., F. Nazio, et al. (2014)"Schwann cell autophagy counteracts the onset and chronification of neuropathic pain."Pain 155: 93-107.

McCarty, M. F., R. J. Somcio, et al. (2007)"Overexpression of PDGF-BB decreases colorectal and pancreatic cancer growth by increasing tumor pericyte content."J Clin Invest 117: 2114-22.

McGreevy, K., R. W. Hurley, et al. (2013)"The effectiveness of repeat celiac plexus neurolysis for pancreatic cancer: a pilot study."Pain Pract 13: 89-95.

Nakashima, H., M. Nakamura, et al. (2006)"Nuclear factor-kappaB contributes to hedgehog signaling pathway activation through sonic hedgehog induction in pancreatic cancer."Cancer Res 66: 7041-9.

Nakhai, H., S. Sel, et al. (2007)"Ptf1a is essential for the differentiation of GABAergic and glycinergic amacrine cells and horizontal cells in the mouse retina."Development 134: 1151-60.

Nance, D. M. and V. M. Sanders. (2007)"Autonomic innervation and regulation of the immune system (1987-2007)."Brain Behav Immun 21: 736-45.

Neoptolemos, J. P., J. A. Dunn, et al. (2001)"Adjuvant chemoradiotherapy and chemotherapy in resectable pancreatic cancer: a randomised controlled trial."Lancet 358: 1576-85.

Neoptolemos, J. P., D. D. Stocken, et al. (2010)"Adjuvant chemotherapy with fluorouracil plus folinic acid vs gemcitabine following pancreatic cancer resection: a randomized controlled trial."Jama 304: 1073-81.

Okada, Y., G. Eibl, et al. (2003)"Glial cell-derived neurotrophic factor upregulates the expression and activation of matrix metalloproteinase-9 in human pancreatic cancer."Surgery 134: 293-9.

Olive, K. P., M. A. Jacobetz, et al. (2009)"Inhibition of Hedgehog signaling enhances delivery of chemotherapy in a mouse model of pancreatic cancer."Science 324: 1457-61.

Ozdemir, B. C., T. Pentcheva-Hoang, et al. (2014)"Depletion of carcinoma-associated fibroblasts and fibrosis induces immunosuppression and accelerates pancreas cancer with reduced survival."Cancer Cell 25: 719-34.

Pan, X., T. Arumugam, et al. (2008)"Nuclear factor-kappaB p65/relA silencing induces apoptosis and increases gemcitabine effectiveness in a subset of pancreatic cancer cells."Clin Cancer Res 14: 8143-51.

Pasca di Magliano, M., S. Sekine, et al. (2006)"Hedgehog/Ras interactions regulate early stages of pancreatic cancer."Genes Dev 20: 3161-73.

Rad, R., L. Rad, et al. (2015)"A conditional piggyBac transposition system for genetic screening in mice identifies oncogenic networks in pancreatic cancer."Nat Genet 47: 47-56.

Razani, B., A. D. Reichardt, et al. (2011)"Non-canonical NF-kappaB signaling activation and regulation: principles and perspectives."Immunol Rev 244: 44-54.

Redston, M. S., C. Caldas, et al. (1994)"p53 mutations in pancreatic carcinoma and evidence of common involvement of homocopolymer tracts in DNA microdeletions."Cancer Res 54: 3025-33.

Rhim, A. D., P. E. Oberstein, et al. (2014)"Stromal elements act to restrain, rather than support, pancreatic ductal adenocarcinoma."Cancer Cell 25: 735-47.

Roberts, N. J., Y. Jiao, et al. (2012)"ATM mutations in patients with hereditary pancreatic cancer."Cancer Discov 2: 41-6.

Ruscica, M., E. Dozio, et al. (2007)"Relevance of the neuropeptide Y system in the biology of cancer progression."Curr Top Med Chem 7: 1682-91.

Sandgren, E. P., N. C. Luetteke, et al. (1990)"Overexpression of TGF alpha in transgenic mice: induction of epithelial hyperplasia, pancreatic metaplasia, and carcinoma of the breast."Cell 61: 1121-35.

Sandkuhler, J. (2009)"Models and mechanisms of hyperalgesia and allodynia."Physiol Rev 89: 707-58.

Scholz, J. and C. J. Woolf. (2007)"The neuropathic pain triad: neurons, immune cells and glia."Nat Neurosci 10: 1361-1368.

Schonhuber, N., B. Seidler, et al. (2014)"A next-generation dual-recombinase system for time- and host-specific targeting of pancreatic cancer."Nat Med 20: 1340-7.

Secq, V., J. Leca, et al. (2015)"Stromal SLIT2 impacts on pancreatic cancer-associated neural remodeling."Cell Death Dis 6: e1592.

Seleznik, G. M., T. Reding, et al. (2012)"Lymphotoxin beta receptor signaling promotes development of autoimmune pancreatitis."Gastroenterology 143: 1361-74.

Siegel, R., J. Ma, et al. (2014)"Cancer statistics, 2014."CA Cancer J Clin 64: 9-29.

Smith, I. W., M. Mikesh, et al. (2014)"Terminal Schwann cells participate in the competition underlying neuromuscular synapse elimination."J Neurosci 33: 17724-36.

Stopczynski, R. E., D. P. Normolle, et al. (2014)"Neuroplastic changes occur early in the development of pancreatic ductal adenocarcinoma."Cancer Res 74: 1718-27.

Swanson, B. J., K. M. McDermott, et al. (2007)"MUC1 is a counter-receptor for myelin-associated glycoprotein (Siglec-4a) and their interaction contributes to adhesion in pancreatic cancer perineural invasion."Cancer Res 67: 10222-9.

Takahashi, T., H. Ishikura, et al. (1997)"Perineural invasion by ductal adenocarcinoma of the pancreas."J Surg Oncol 65: 164-70.

Tinder, T. L., D. B. Subramani, et al. (2008)"MUC1 enhances tumor progression and contributes toward immunosuppression in a mouse model of spontaneous pancreatic adenocarcinoma."J Immunol 181: 3116-25.

Wagner, M., F. R. Greten, et al. (2001)"A murine tumor progression model for pancreatic cancer recapitulating the genetic alterations of the human disease."Genes Dev 15: 286-93.

Wagner, M., H. Luhrs, et al. (1998)"Malignant transformation of duct-like cells originating from acini in transforming growth factor transgenic mice."Gastroenterology 115: 1254-62.

Wang, K., I. E. Demir, et al. (2014)"The neurotrophic factor neurturin contributes toward an aggressive cancer cell phenotype, neuropathic pain and neuronal plasticity in pancreatic cancer."Carcinogenesis 35: 103-13.

Wang, W., J. L. Abbruzzese, et al. (1999)"The nuclear factor-kappa B RelA transcription factor is constitutively activated in human pancreatic adenocarcinoma cells."Clin Cancer Res 5: 119-27.

Warshaw, A. L., Z. Y. Gu, et al. (1990)"Preoperative staging and assessment of resectability of pancreatic cancer."Arch Surg 125: 230-3.

Wong, G. Y., D. R. Schroeder, et al. (2004)"Effect of neurolytic celiac plexus block on pain relief, quality of life, and survival in patients with unresectable pancreatic cancer: a randomized controlled trial."Jama 291: 1092-9.

Xu, Q., Z. Wang, et al. (2014)"Stromal-derived factor-1alpha/CXCL12-CXCR4 chemotactic pathway promotes perineural invasion in pancreatic cancer."Oncotarget.

Zhang, J. F., R. Hua, et al. (2013)"Influence of perineural invasion on survival and recurrence in patients with resected pancreatic cancer."Asian Pac J Cancer Prev 14: 5133-9.

Zhu, Z., H. Friess, et al. (1999)"Nerve growth factor expression correlates with perineural invasion and pain in human pancreatic cancer."J Clin Oncol 17: 2419-28.

Acknowledgements

The present study was performed during a difficult period of the Department of Surgery at our university. It was a period in which the work load of each person in our department substantially increased, and performance of such studies was only possible with the genuine support of friends, cooperation partners, and colleagues.

In this regard, I first of all would like to thank Dr. Hana Algül and all members of his research group, especially Dr. Marina Lesina, Dr. Magdalena Kurkowski, Dr. Sonja Wörmann, Dr. Nina Diakopoulos who have all the way from the beginning till the end of my PhD period regarded me as part of their research group and family. Without their unique support and patience, this thesis would not have been possible.

I would like express my gratitude to Prof. Mathias Heikenwälder for accepting me as a mentee during my PhD period, for his brilliant ideas and for his always inspiring fascination for research that I felt during each committee meeting.

I am grateful to our chief lab technician Ms. Ulrike Bourquain for her tremendous, endless, patient support in all technical and organizational aspects of this thesis in the past years. The whole research group Ceyhan loves working with you, Ulrike!

Also, I would like to thank Dr. Ö. Cemil Saricaoglu for the rapid assistance he provided during the late-night measurement sessions with neuronal cultures. Thank you so much, Cemil!

Two co-operation partners whom I was delighted to get to know in the past 2 years, i.e. Dr. Engin Gürlevik and Dr. Gitta Seleznik, have provided me with two exceptionally valuable models that have broadened our horizon. Dear Engin, dear Gitta, thank you both very much for sharing your unique expertise with us.

I would like to thank the coordinators of the PhD program, i.e. Dr. Katrin Offe and Dessi Zlatanova, for their superb assistance and patience during the past 3 years. I think all PhD students felt comfortable to know that they will receive rapid and reliable support from Katrin and Dessi in case of any question or concern.

I have worked in my current research field for the past 11 years, and my biggest luck was to have got to know my mentors Professor Helmut Friess and Assoc. Professor Güralp O. Ceyhan, who have provided me with endless support, possibilities, mental and material support, and far beyond all the way from the beginning of my research back in 2004 until today. I am happy to see that I am able to present this work owing to their mentorship and guidance. This thesis is intended to be my best means to thank them from the bottom of my heart.

I would like to thank Dr. Elke Tieftrunk for motivating me to make further progress at each step of my thesis, for thinking of my comfort during the days when I got very tired, for feeling my research fascination together with me in her golden heart.

Finally, I would like to thank my parents Mrs. Zeynep Demir and Dr. Ismail Demir for enduring the difficulty of missing their only child in a foreign country, for their altruistic support and for their endless love.

A wholehearted thank you.